PERFORMANCE ANALYSIS AND SIMULATION OF SATELLITE MOBILE COMMUNICATION SYSTEM OVER COMBINED SCINTILLATION AND MULTIPATH FADING CHANNELS

WANNAREE WONGTRAIRAT

A THESIS SUBMITTED IN PARTIAL FULFILLMENT

OF THE REQUIREMENT FOR THE DEGREE OF

DOCTOR OF ENGINEERING IN ELECTRICAL ENGINEERING

FACULTY OF ENGINEERING

KING MONGKUT'S INSTITUTE OF TECHNOLOGY LADKRABANG

2009

KMITL-2009-EN-D-018-035

หัวข้อวิทยานิพนธ์	การวิเคราะห์สมรรถนะ และการจำลองระบบการสื่อสารเคลื่อนที่ผ่านดาวเทียมภายใต้ช่องสัญญาณการจางหายร่วมกับมัลติพาทเฟดดิง
นักศึกษา	นางสาววรรณรีย์ วงศ์ไตรรัตน์
รหัสประจำตัว	47060007
ปริญญา	วิศวกรรมศาสตรดุษฎีบัณฑิต
สาขาวิชา	วิศวกรรมไฟฟ้า
พ.ศ.	2552
อาจารย์ที่ปรึกษาวิทยานิพนธ์	ผศ.ดร.พรชัย ทรัพย์นิธิ

บทคัดย่อ

ในระบบการสื่อสารเคลื่อนที่ผ่านดาวเทียม ปรากฏการณ์ซินทิลเลชันในชั้นบรรยากาศไอโอโนสเฟียร์ (Ionospheric scintillation) และมัลติพาทเฟดดิงแบบไม่เลือกความถี่ ส่งผลกระทบต่อสมรรถนะของระบบเมื่อสัญญาณมีการส่งผ่านชั้นบรรยากาศไอโอโนสเฟียร์ทั้งในเขตเมืองและในชนบท ปรากฏการณ์ซินทิลเลชันส่งผลให้ค่าอัตราส่วนกำลังสัญญาณต่อกำลังสัญญาณรบกวน (Signal-to-Noise Ratio) ที่ใช้ประโยชน์ได้มีค่าลดลง หรือทำให้ค่าอัตราบิตผิดพลาดมีค่าเพิ่มสูงขึ้น และจะมีความรุนแรงมากขึ้นเมื่อปรากฏการณ์ดังกล่าวเกิดขึ้นร่วมกับมัลติพาทเฟดดิงแบบไม่เลือกความถี่ พารามิเตอร์สำคัญในการประเมินสมรรถนะของระบบสื่อสารดิจิตอลในช่องสัญญาณร่วมดังกล่าว ได้แก่ อัตราบิตผิดพลาดเฉลี่ย (Average bit error probability) และค่าความน่าจะเป็นของสัญญาณที่เกิดการขาดหาย (Outage probability)

วิทยานิพนธ์นี้นำเสนอวิธีการใช้ฟังก์ชันโมเมนเจนเนอเรติง (Moment generating function : MGF) ในการคำนวณหาค่าอัตราบิตผิดพลาดเฉลี่ยและความน่าจะเป็นของสัญญาณที่เกิดการขาดหายของระบบ สำหรับช่องสัญญาณการจางหายของซินทิเลชันแบบเดี่ยว และช่องสัญญาณการจางหายร่วมกับมัลติพาทเฟดดิงบนระบบที่มีการมอดูเลตสัญญาณแบบเอ็มพีเอสเค (M-PSK) และเอ็มคิวเอเอ็ม (M-QAM) ทั้งที่มีและไม่มีเอ็มอาร์ซีไดเวอร์ซิตี (MRC diversity) โดยแสดงในรูปของการคูณกันของ 2 ช่องสัญญาณในรูปแบบจำลองที่เป็นช่องสัญญาณร่วมไรเซียน×ไรเซียน และนาคากามิ-เอ็ม×นาคากามิ-เอ็ม รูปสมการผลลัพธ์ที่ได้แสดงอยู่ในรูปของการอินทิเกรตฟังก์ชันเจอเนอร์รอลไรซ์ไฮเปอร์จีโอเมตริกซ์ (generalized hypergeometric function : ${}_2F_0$) ในช่วงขอบเขตที่จำกัด ซึ่งสามารถใช้โปรแกรมทั่วไปในการคำนวณ จากผลลัพธ์ที่ได้นั้น สมการเอ็มจีเอฟที่ได้จากช่องสัญญาณร่วมนาคากามิ-เอ็ม×นาคากามิ-เอ็มจะมีรูปแบบของสมการที่กระชับกว่าสมการที่ได้จากช่องสัญญาณร่วมไรเซียน×ไรเซียน เนื่องจากรูปของสมการที่ได้จากช่องสัญญาณร่วมไรเซียน

×ไรเซียนนั้นจะมีคู่ของการรวมค่าจากอนุกรมอนันต์ประกอบอยู่ในสมการ นอกจากนี้ ยังสามารถนำสมการเส้นขอบเขตด้านบน (Upper bound) ของอัตราบิตผิดพลาดเฉลี่ยมาใช้เพื่อการคำนวณค่า ซึ่งจะทำให้การคำนวณค่าสามารถทำได้อย่างรวดเร็วและให้ความผิดพลาดน้อยในการคำนวณเชิงเลข จากรูปทั่วไปของสมการเอ็มจีเอฟที่ได้ยังสามารถแสดงให้อยู่ในรูปของช่องสัญญาณเรย์ลี ×ไรเซียน, เรย์ลี×นาคากามิ-เอ็ม, ช่องสัญญาณเรย์ลีคู่, ช่องสัญญาณเรย์ลีเดี่ยว, ช่องสัญญาณไรเซียนเดี่ยว, ช่องสัญญาณนาคากามิ-เอ็มเดี่ยว, และช่องสัญญาณที่ไม่มีการจางหาย เป็นกรณีพิเศษได้อีกด้วย

ผลจากการคำนวณเชิงเลขที่ได้จากการคำนวณค่าตามสมการถูกนำไปเปรียบเทียบกับผลที่ได้จากการจำลองระบบ ค่าที่ได้จากการคำนวณใกล้เคียงกับผลการจำลองระบบ ทั้งในกรณีที่มีการเปลี่ยนค่าดัชนีชินทิเลชัน S_4, ตัวประกอบไรเซียน κ, ตัวประกอบรูปร่างนาคากามิ m, และจำนวนของไดเวอร์ซิตี L ในกรณีที่ค่าดัชนีซินทิเลชันมีค่าน้อย ($S_4 \rightarrow 0$) ค่าของสมการที่ได้จะสามารถแสดงได้ในรูปของช่องสัญญาณการจางหายเดี่ยว

ยิ่งไปกว่านั้น ผลที่ได้จากวิเคราะห์ในวิทยานิพนธ์นี้ยังสามารถนำไปประยุกต์ใช้กับการสื่อสารไร้สายในระบบอื่นๆ เช่น ระบบการสื่อสารที่ภาครับและภาคส่งมีการเคลื่อนที่ (mobile-to-mobile communication system) และระบบการสื่อสารไร้สายแบบหลายอินพุต หลายเอาท์พุต (Multiple-input multiple-output : MIMO) เป็นต้น

Thesis	Performance Analysis and Simulation of Satellite Mobile Communication System over Combined Scintillation and Multipath Fading Channels
Student	Miss Wannaree Wongtrairat
Student ID.	47060007
Degree	Doctor of Engineering
Program	Electrical Engineering
Year	2009
Thesis Advisor	Asst.Prof.Dr.Pornchai Supnithi

ABSTRACT

In satellite mobile communication system, scintillation and multipath flat fading cause degradation of performance when the signals go through the ionosphere as well as urban/rural areas. Scintillation causes reduction of available SNR or increased bit error rate and when combined with flat multipath fading, the degradation becomes more severe. The challenge is to evaluate the performance of the system, in terms of the average bit error probabilities (BEP) and the outage probability.

In this thesis, through the use of the moment generating function (MGF), we derived and computed the average BEP and outage probability for M-ary phase shift keying (M-PSK) and M-ary quadrature amplitude modulation (M-QAM) systems with and without MRC diversity reception over single scintillation fading channel and combined scintillation and multipath fading channel. The expressions are derived for 2 product channel models: the combined Rician×Rician fading channel and Nakagami-m×Nakagami-m fading channel. The results are expressed as a single integration with finite limits in terms of the generalized hypergeometric function ${}_2F_0$, which can be computed using standard commecial software. The derived results of MGF of combined Nakagami-m×Nakagami-m model is expressed in a more compact form than the MGF of combined Rician×Rician since the MGF of the latter has a double summation in the infinite series. Moreover, the upper bound of average BEP is derived with advantages of faster computation and less numerical error. We have shown that the derived BEP considers combined Rayleigh×Rician, Rayleigh×Nakagami-m, double Rayleigh, single Rayleigh, single Rician, single Nakagami-m, and non-fading channels as special cases.

Numerical results are obtained from the derived expressions and compared with simulation results. They show very good agreement for various scintillation indices S_4, Rician factors κ, Nakagami shape factors m, and the number of diversity branches L. For a small scintlllation index ($S_4 \rightarrow 0$), the expression is simplified to a single multipath fading channel.

In addition, the derived results expressions in this thesis find applications in other existing wireless system such as mobile-to-mobile communication system and multiple-input multiple-output (MIMO) wireless communication system.

ACKNOWLEDGEMENTS

Many people have played important roles in the development of this thesis, and I am deeply thankful to them.

First of all, I would like to thank my advisor Asst. Prof. Dr. Pornchai Supnithi who has provided me with all the assistance, suggestions, and encouragement during the research. I would like to express my sincere appreciation to all the support and help given from Assoc.Prof.Nipha Leelaruji and Assoc.Prof.Narong Hemmakorn. Moreover, the valuable comments of the anonymous reviewers and especially Prof.Dr.Sawasd Tantaratana, are also very much appreciated.

Great appreciation must also go to all of my best friends, whom I met at KMITL.

I am extremely thankful to my family for their support and love since I was born. Thank you my beloved mum, beloved father, and my beloved brother for their eternal love, understanding, support, and encouragement. I hope they will be proud of me seeing my achievement of this study.

And never enough thanks go to one who doesn't want to be named but he knows who he is and so do I. Thank you to him who walks beside me, be my best friend, and always gives the sprites for me at all time.

Finally, I am deeply thankful to the dharma from the Buddha which makes me strong and full of high spirits.

Wannaree Wongtrairat

TABLE OF CONTENTS

TABLE OF CONTENTS(to)

TABLE OF CONTENTS(to)

LIST OF TABLES

LIST OF FIGURES

LIST OF FIGURES(to)

NOMENCLATURE

Notation	Description or Name of Function and Reference Citation for Its Definition
α_{comb}	Coefficients of combined fading channel
α_{sc}	Coefficients of ionospheric scintillation
α_{ter}	Coefficients of terrestrial multipath fadings
ASK	Amplitude-shift keying
AWGN	Additive white Gaussian noise
BEP	Bit error probability
CDF	Cumulative distribution function
DPSK	Differentially encoded phase-shift keying
DQPSK	Differentially encoded 4-ary phase-shift keying
EGC	Equal gain combining
$E\{X^n\}$	n-th moment of the RV X
E_b	Average bit energy
$E(A,N,Q)$	Desired error bound over all error term in the outage probability
$erf(x)$	Error function
${}_2F_0(a,b;;z)$	Generalized hypergeometric function [40]
FSK	Frequency-shift keying
$F_X(x)$	CDF of the RVs X
γ	Instantaneous SNR
$\overline{\gamma}$	Average SNR
$\Gamma(p)$	Gamma function
ITS	Intelligent transport system
$I_v\{z\}$	v-th order modified Bessel function of the first kind [37]
κ	Rician factor
$K_\alpha\{\cdot\}$	α-th order modified Bessel function of the second kind [37]
L	L-order MRC receiver diversity
LOS	Line-of-sight
$(\lambda)_n$	Pochhammer symbol
m	Nakagami-m shape factor

Notation	Description or Name of Function and Reference Citation for Its Definition
MGF	Moment generating function
MIMO	Multiple-input, multiple-output
M-PSK	M-ary phase shift keying
M-QAM	M-ary quadrature amplitude modulation
MRC	Maximum-ratio combining
MSK	Minimum-shift keying
MUOS	Mobile user object system
$\mu_{X_1X_2}$	Covariance of the RVs X_1 and X_2
N_0	Noise variance
NLOS	Non line-of-sight
Ω	Average envelope power
PDF	Probability density function
$P_b(E\|\gamma_T)$	Conditional BEP of linear modulation in AWGN channel
P_{out}	Outage probability
$p_X(x)$	PDF of the RV X
$\Phi_\gamma(-s)$	MGF of the instantaneous SNR
$\Psi(a,b;z)$	Confluent hypergeometric function of the second kind [37]
QAM	Quadrature amplitude modulation
$Q(x)$	Gaussian Q function
$Q_m(a,b)$	Generalized Marcum's Q function
r_{comb}	Envelope of combined fading
$r_{sc} = \|\alpha_{sc}\|$	Envelope of scintillation fading
$r_{ter} = \|\alpha_{ter}\|$	Envelope of terrestrial multipath fading
RV	Random variable
$\rho_{X_1X_2}$	Correlation coefficient of two RVs, X_1 and X_2
s^2	Specular power
S_4	Scintillation index
σ_x^2	Variance of the RV X
SC	Selection combining
SNR	Signal-to-noise ratio
TEC	Total electron content

Notation	Description or Name of Function and Reference Citation for Its Definition
UFO	Ultra high frequency follow-on
$\bar{X} = m_X = E\{X\}$	Mean or expected value of the RV X
w_k	Weighting coefficient in MRC diversity system
$W_{\mu,\nu}(z)$	Whittaker-W function [37]

CHAPTER 1

INTRODUCTION

1.1 Literature Review of Scintillation Phenomenon

In many radio links, it is well known that the fading effect is one of the factors that affect system performance. For mobile satellite communications, the signals could be degraded by scintillation and terrestrial multipath fading, which may occur singly or in a combination of both effects. Both phenomena cause signal fluctuations as seen at the receiver. As an example, Mobile User Object System (MUOS) at frequency 225-400 MHz is the next generation of narrowband satellite communications system in UHF-band. This system provides a replacement to the Ultra High Frequency Follow-On (UFO) communication satellite system [1],[2]. The environment of MUOS includes the satellite link degradations, namely, ionospheric scintillation, terrestrial multipath, and perturbation by an additive white Gaussian noise (AWGN) as shown in Figure 1.1.

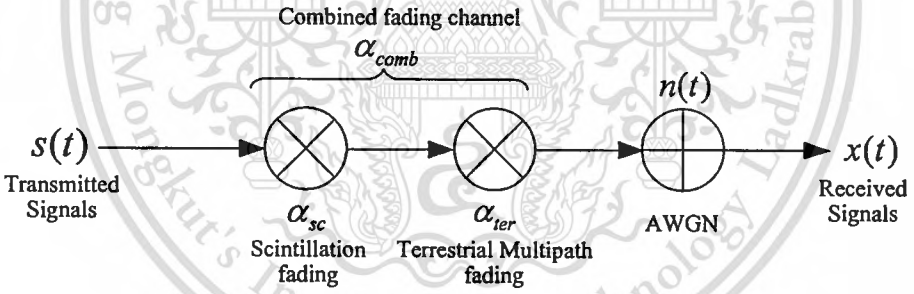

Figure 1.1 Block diagram of combined fading channel in mobile satellite communication system.

Ionospheric scintillation, which manifests itself as an increased noise on radio signal intensity and phase, is caused by small-scale variations and non-uniform electrical charge distribution along the trans-ionospheric propagation path between the transmitter and the receiver. It is well known that the ionospheric scintillation intensity varies with location of earth, time of day, season, and sunspot activity [3]. Severe scintillation effect occurs within about ±20° of the equatorial geomagnetic and the polar region after local sunset in the equinox periods during the

years with maximum sunspot number. The length of solar sunspot cycle averages at approximately 11 years [3] with the last strong scintillation occurred in 2000-2002.

In [4], Shaft delineates statistical characteristics of ionospheric scintillation by using the relationship between scintillation index, Rician factor, and Nakagami shape factor. Subsequently, the statistical model of ionospheric scintillation is typically modeled as Rayleigh, Rician [1],[2],[5], or Nakgami-*m* [6]-[8] distribution function for small-scale fading.

The amplitude distributions of the faded signals due to scintillation and combined scintillation and multipath fading channels in satellite mobile communication system have recently been studied in the literatures [2],[4]-[8]. The probability density functions (PDFs) of the combined ionospheric scintillation and terrestrial multipath fading are formulated in terms of the envelope PDF. The expressions are derived for 2 models: 1) combined Rician×Rician fading [5], and 2) combined Nakagami-*m*×Nakagami-*m* fading. Results show that doubly Rayleigh or combined Rayleigh×Rayleigh fading produces deeper fades than a single Rayleigh fading channel in terms of the envelope PDF.

Phase modulation such as phase shift keying (PSK) and quadrature amplitude modulation (QAM) are almost universally used for satellite link. Most work on the computation of the error probability of *M*-ary PSK (*M*-PSK) and rectangular *M*-ary QAM (*M*-QAM) on radio channels focuses on either scintillation or terrestrial multipath fading channel [9]-[25]. Several researchers have attempted to derive the closed-form expressions for computing the error rate performance of the system. In [9], Lindsey derives the performance characteristics for multi-receivers of binary and *M*-ary signals over single Rician fading channel, but these results are not in closed form. Closed-form solutions presented in [10] are the general results of a symbol error probability for multiphase signaling over a slow frequency-nonselective Rayleigh fading channel. The exact expressions of the error probability for linear modulation in frequency-flat Rician or Rayleigh channel with additive noise are derived in [12].

More recently, the moment generating function (MGF) methods have been suggested by several authors for analyzing the system performance of linear modulation in different fading environments such as [13],[16],[25]. Furthermore, diversity reception methods (e.g. maximum-ratio combining (MRC), selection combining (SC), and equal gain combining (EGC)) have been shown to be an effective and simple method against the performance degradation due to fading channels. Derivation of the performance of *M*-PSK and *M*-QAM systems with MRC diversity reception have been presented by several authors [14],[16]-[25], which appear to have general

and closed-form solutions. However, a few researchers have investigated the effect of combined ionospheric scintillation and multipath fading channels [1],[2],[5].

Recently, combined fading channels such as combined Rayleigh×Rayleigh fading channel and combined Nakagami-*m*×Nakagami-*m* fading channel have gained interest due to its applicability in mobile-to-mobile radio communication channels [26],[27] and multiple-input, multiple-output (MIMO) wireless communication channels [28]-[31]. In mobile-to-mobile communication system, both transmitter and receiver move simultaneously over wireless medium. Examples of such system include intelligent transport system (ITS) and mobile ad hoc networks. The term combined Rayleigh×Rayleigh [28] is also coined to describe the regions around the transmitter and receiver. In the mobile-to-mobile system, the researchers know this combined channel in the name of "*double Rayleigh*" or "*cascaded Rayleigh*" fading. In [31], an upper bound of symbol error rate of *M*-PSK modulation in combined Rayleigh×Rayleigh fading channels with multiple receive antennas and space-time coding are derived by using the MGF method. In MIMO wireless channel, combined fading exist when two rings of scatterers are separated by a large distance, and all propagation paths of the channel travel through the same narrow "pipe" [28]. In [29],[30], the authors consider MIMO communication in combined Rayleigh×Rayleigh and combined Nakagami-*m*×Nakagami-*m* fading and derive the exact expression of bit error probability (BEP) of *M*-PSK and *M*-QAM in the form of *generalized hypergemetric function* ${}_2F_0$.

1.2 Significance of the Research

As few researchers have investigated the effect of combined ionospheric scintillation and multipath fading channels, parameters related to the performance analysis such as the average BEP, the outage probability for such combined fading channel have never been proposed.

In this thesis, we derive the average probability of bit error for some common digital modulation schemes with and without MRC diversity for 2 channels 1) single scintillation fading channels and 2) combined flat scintillation and flat multipath fading channels in the model of combined Rician fading channel and combined Nakagami-*m* fading channel. The combined probability density functions (PDFs) are equivalent to the PDF of combined Rician fading channels and the PDF of combined Nakagami-*m* fading channels while the PDFs of scintillation can be modelled as Rician or Nakagami-*m* distribution. The results are provided in terms of instantaneous signal-to-noise ratio (SNR) per bit and expressed by using the generalized

hypergeometric function ${}_2F_0$. The resulting expressions can be used to predict the error performance for common digital modulation schemes and the outage probability of mobile satellite communication systems. In addition, the results are applicable to other systems, such as mobile-to-mobile communications and MIMO communication systems.

1.3 Objective and Confinement of Thesis

The purpose of this thesis is to analyze the performance of some common modulation schemes in terms of *average* BEP and outage probability over combined ionospheric scintillation and small-scale flat terrestrial multipath fading which appears in land mobile satellite communication system. In order to derive *average* BEP and outage probability in the combined fading channels, the PDF of the *instantaneous* SNR is required. It is thus necessary to convert the envelope PDFs into the SNR PDFs first. The derived BEP generalizes the already available results for the case of Rayleigh, Rician and/or Nakagami-*m* fading channel, and the case of no diversity reception.

In this thesis, we consider the performance analyses for some common modulation schemes over 2 types of combined fading models:

1) Combined Rician×Rician fading channels or a product of two Rician fading channel.
2) Combined Nakagami-*m*×Nakagami-*m* fading channel or a product of two Nakagami-*m* fading channel.

The methods and results are provided in this thesis as follows:

In Chapter 2, we provide a brief overview of the background and characterization of the ionospheric scintillation phenomenon. The PDF in terms of envelopes and instantaneous SNR of the combined ionospheric scintillation and terrestrial multipath fading channels are modelled as 1) combined Rician×Rician fading channel and 2) combined Nakagami-*m*×Nakagami-*m* fading channel. The derived PDF of the instantaneous SNR results is an important element required in the derivation of the average BEP and the outage probability in the next Chapter.

In Chapter 3, we derive the average error probability of single and combined fading channels with and without MRC diversity by using the MGF based approach. The derived MGF results are simplified in terms of the generalized hypergeometric function ${}_2F_0$. In addition, the upper bounds of the error probability and the outage probabilities of both channel models are determined.

In Chapter 4, efforts are made to compute the average BEP and the outage probability of various digtal modulation schemes over combined fading channel by using the model of 1) combined Rician×Rician fading channel and 2) combined Nakagami-*m*×Nakagami-*m* fading channel. The theoretical results and simulation results are compared. The discussions of single and combined fading channels with and without MRC receiver diversity in average BEP are given. The effects of the number of antennas are shown and the upper bound results of average BEP are also shown in this Chapter. Moreover, we show the difference of envelope PDF and the average BEP results from both channel models.

Finally, conclusions are provided in Chapter 5.

CHAPTER 2

STATISTICAL CHARACTERIZATION OF MOBILE SATELLITE COMMUNICATION CHANNELS

Mobile satellite communication systems are commonly accepted for providing the real personal communication services to the user in anywhere, anytime, and any format (namely: voice, data, and multimedia). The mobile satellite communication channels are time varying due to different shadowing and scattering phenomena. Due to the movement of the transmitter and receiver through the environment, the received signals may fluctuate. This fluctuation results from the combining effects of random multipath signal and obstruction of the line-of-sight (LOS) path, which induces various fading phenomena.

In satellite mobile communication system, for instance, signal propagation through the ionosphere and terrestrial region is degraded by the ionospheric scintillation and the terrestrial multipath, respectively, in addition to additive white Gaussian noise (AWGN). The propagation characteristics of the ionospheric scintillation can be studied by the statistical distribution of the received signal envelope or received power from the experience signal fluctuations in mobile satellite communication systems.

In this Chapter, we give a brief overview of the background and characteristics of the ionospheric scintillation in mobile satellite communications. Statistical distribution of the received signal envelope of the ionospheric scintillation is modeled as Rician and Nakagami-*m* distribution. Moreover, we also use Rician and Nakagami-*m* distribution model to derive the statistical distributions of the combined ionospheric scintillation and terrestrial multipath fading in terms of envelope PDF and instantaneous SNR. These PDFs are proposed for all possible cases.

2.1 Background on Ionospheric Scintillation

For mobile satellite communications system from 10 MHz to 6 GHz with propagation through the earth-space path, one of the most deleterious factors along the transionospheric propagation path between transmitter and the receiver is caused by ionospheric scintillation. The effects of ionospheric scintillation are caused by the irregularities of electron density in the F and

E_s layer of the ionosphere which the density of electrons increases with altitude up to highly different from the remaining layers, particularly severe in equatorial and polar region as shown in Figure 2.1. It is situated at a height of about 100 km. Moreover, the magnitude of the ionospheric scintillation varies with time of day month in the year, and year in the 11-yerar solar cycles. The greatest scintillation effects are observed just after local sunset in the equinox periods during the sunspot maximum years and also worst within about ±20° of the geomagnetic equator and over the poles as shown in Figure 2.2. Moreover, equatorial scintillation effects are very high just after local sunset in the equinox periods, i.e., in March-April and October-November, during the sunspot maximum years.

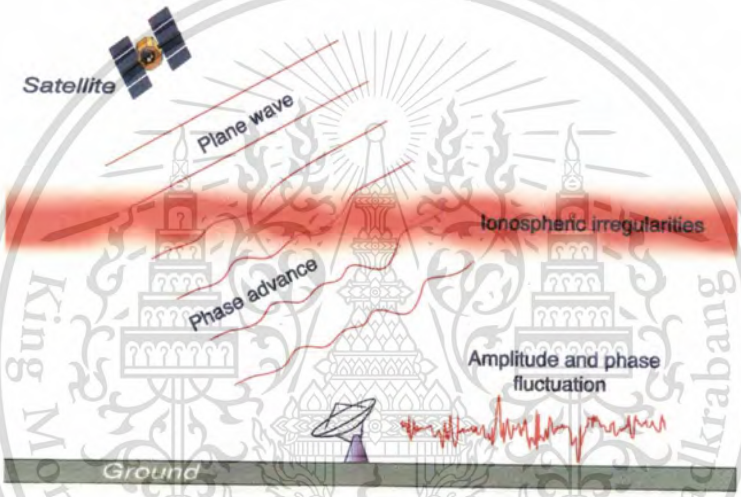

Figure 2.1 The ionospheric scintillation phenomenon [32].

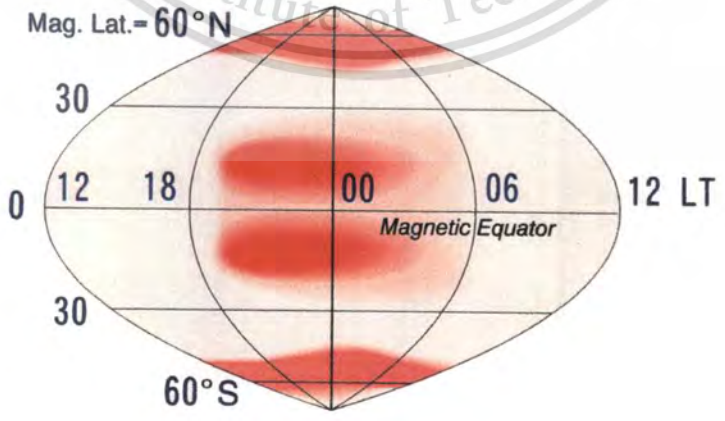

Figure 2.2 The pattern of ionospheric scintillation.

The irregular fluctuations of the electron density in the ionosphere introduce variation of amplitude, phase, and angle of arrival radio waves propagating through the ionosphere.

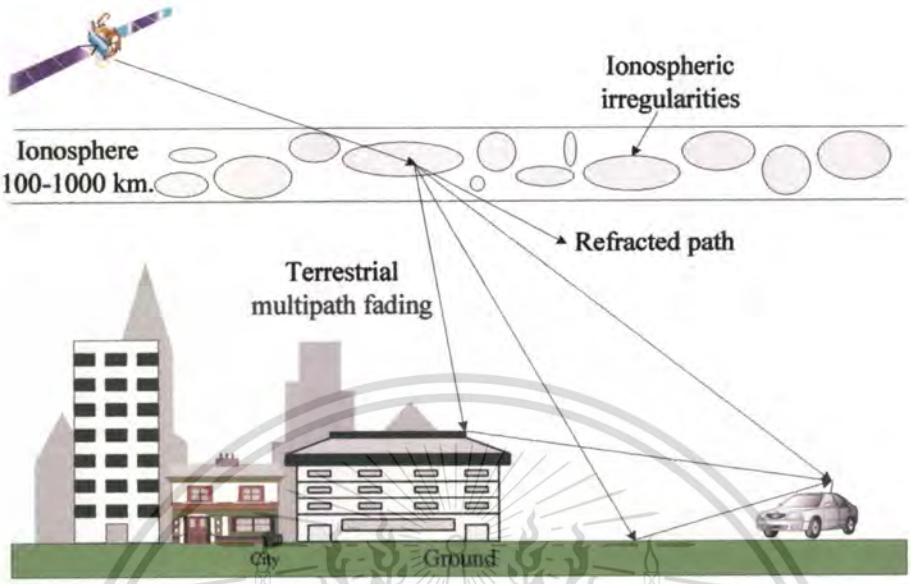

Figure 2.3 Ionospheric scintillation and terrestrial multipath fading in mobile satellite communication system.

In many radio links, it is well known that fading is one of the factors that significantly affect system performance. For mobile satellite communication system, the signals could be degraded by scintillation and terrestrial multipath fading, which may occur singly or as a combination of both effects as shown in Figure 2.3. Both phenomena cause signal fluctuations seen at the receiver. Consider a combined fading in mobile satellite communication system as shown in Figure 1.1, where the environment of mobile satellite communication system includes the satellite link degradations, namely, ionospheric scintillation, terrestrial multipath fading, and perturbation by AWGN.

2.2 The Characterization of Ionospheric Scintillation

In ionospheric scintillation phenomenon, the ions in the ionospheric layers are always in motions by the energy from the sun. This energy causes the ionosphere to grow up during the day and increases the total electron content (TEC). TEC is the total number of electrons that would be in a vertical column of area 1 m^2 from the surface of the earth all the way through the earth's atmosphere which range from ~10^{18} during the day to ~10^{16} during the night. At the local sunset

in the ionosphere, the TEC from the day-time value to the night-time value are rapidly increased, that provides a rise of random irregularities of electron in the ionosphere. Consequently, these irregularities cause to a variation in amplitude and phase of signal, which leads to rapid signal fluctuations. This phenomenon is called *ionospheric scintillations*.

Ionospheric scintillation causes amplitude fluctuation known as amplitude scintillation with its scintillation index related to the *m*-parameter of Nakagami-*m* distribution [4] and Rician factor of Rician distribution[4],[5]. The statistical model of ionospheric scintillation is typically modeled as Rayleigh, Rician[5], or Nakagami-*m* distribution [6]-[8] for small-scale fading. This effect occurs in a narrowband system, such as the mobile user objective system (MUOS) [33] and GPS system. Both Nakagami-*m* distribution and Rician distribution can be used to describe the amplitude distribution of fading signal due to scintillation according to the experimental data [4] and terrestrial multipath fading, thus, causing double or combined fading channels.

The intensity of ionospheric scintillation is often described by using scintillation index S_4, which is defined by [4],[5]

$$S_4 = \frac{\sqrt{\mathrm{var}\left\{\left|\alpha_{sc}\right|^2\right\}}}{E\left\{\left|\alpha_{sc}\right|^2\right\}}, \tag{2.1}$$

where α_{sc} is the scintillation coefficient, var{·} is the variance. In general, the S_4 index has been measured between zero (no scintillation) and approximately 1.5.

Furthermore, the various scintillation indices are defined and approximately correlated by [4],[34]

$$S_1 = \frac{E\left\{\left|\alpha_{sc}\right| - E\left\{\left|\alpha_{sc}\right|\right\}\right\}}{E\left\{\left|\alpha_{sc}\right|\right\}} \approx 0.42 S_4, \tag{2.2}$$

$$S_2 = \frac{\sqrt{E\left\{\left(\left|\alpha_{sc}\right| - E\left|\alpha_{sc}\right|\right)^2\right\}}}{E\left\{\left|\alpha_{sc}\right|\right\}} \approx 0.52 S_4, \tag{2.3}$$

$$S_3 = \frac{E\left\{\left|\alpha_{sc}\right|^2 - E\left\{\left|\alpha_{sc}\right|^2\right\}\right\}}{E\left\{\left|\alpha_{sc}\right|^2\right\}} \approx 0.78 S_4, \tag{2.4}$$

and

$$S_5 = \frac{\left|\alpha_{sc\_\max}\right| - \left|\alpha_{sc\_\min}\right|}{\left|\alpha_{sc\_\max}\right| + \left|\alpha_{sc\_\min}\right|} \approx 0.78 S_4, \tag{2.5}$$

where $\left|\alpha_{sc\_\max}\right|$ and $\left|\alpha_{sc\_\min}\right|$ are the third largest and smallest coefficient.

2.3 PDF of Ionospheric Scintillation

The attenuation of scintillation fading α_k can be modeled as

$$\alpha_{sc} = a_{sc} e^{j\phi_{sc}} + b_{sc}(t), \tag{2.6}$$

where a_{sc}^2 is the received signal power of the LOS path, ϕ_{sc} is random phase shift in $[-\pi, \pi)$, and $b_{sc}(t)$ is a complex Gaussian random process from scattered signal over non line-of-sight (NLOS) paths with power $2\sigma_{sc}^2$ associated with scintillation.

The envelope PDF of scintillation coefficient $r_{sc} = \left|\alpha_{sc}\right|$ has a Nakagami-Rician distribution which referred by ionospheric physicists, while communication engineers call it simply the Rician distribution when $0<S_4<1$ [5],[35]. The distribution of ionospheric scintillation fading envelope r_{sc} can be described by Rician distribution with the PDF

$$p_{R_{sc}}(r_{sc}) = \frac{2r_{sc}(\kappa_{sc}+1)}{\Omega_{sc}} \exp\left(-\frac{r_{sc}^2(\kappa_{sc}+1)}{\Omega_{sc}} - \kappa_{sc}\right) I_0\left\{2r_{sc}\sqrt{\frac{\kappa_{sc}(\kappa_{sc}+1)}{\Omega_{sc}}}\right\}, \tag{2.7}$$

where $\Omega_{sc} = a_{sc}^2 + 2\sigma_{sc}^2$ is average envelope power, and $I_0\{\cdot\}$ is the zeroth-order modified Bessel function of the first kind. The relationship between scintillation index S_4 and Rician factor κ_{sc} is [4],[5]

$$\kappa_{sc} = \frac{\sqrt{1-S_4^2}}{\left(1-\sqrt{1-S_4^2}\right)}, \tag{2.8}$$

and

$$S_4 = \sqrt{1 - \left(\frac{\kappa_{sc}}{\kappa_{sc} + 1} \right)^2}. \tag{2.9}$$

Notice that at as $S_4 = 1$ (very strong scintillation), $\kappa_{sc} = 0$ and as S_4 approaches 0 (no scintillation), κ_{sc} approaches infinity. In general, S_4 is between 0 and 1. When $S_4 = 0$, it translates to an ideal non-fading channel, with $0 \le S_4 \le 1$, it is Rician fading channel, and with $S_4 = 1$, it is Rayleigh fading channel. This relationship is graphically shown in Figure 2.4

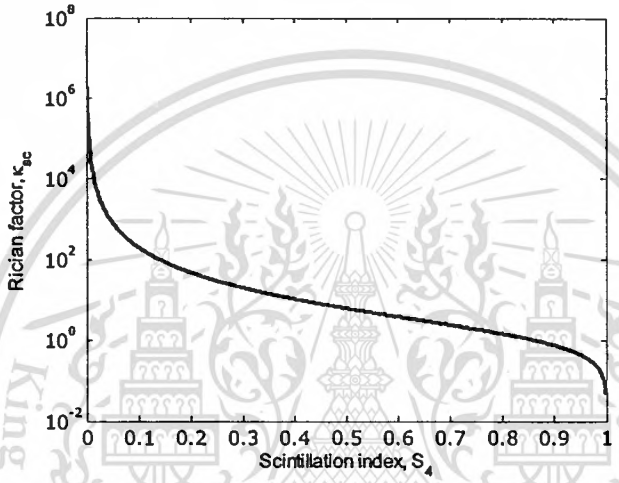

Figure 2.4 The relationship between Rician factor κ_{sc} and the scintillation index S_4.

The Rician PDF of the ionospheric scintillation can thus be expressed in terms of S_4 as

$$p_{R_{sc}}(r_{sc}) = \frac{2r_{sc}}{\Omega_{sc}\left(1-\sqrt{1-S_4^2}\right)} \exp\left(-\frac{1}{1-\sqrt{1-S_4^2}} \left[\frac{r_{sc}^2}{\Omega_{sc}} + \sqrt{1-S_4^2} \right] \right) \cdot I_0 \left\{ \frac{2r_{sc}}{1-\sqrt{1-S_4^2}} \sqrt{\frac{\sqrt{1-S_4^2}}{\Omega_{sc}}} \right\}, \tag{2.10}$$

In the limit when the scintillation index approaches 1, the envelope density function reduces to the Rayleigh distribution with the PDF

$$p_{sc}(r_{sc}) = \frac{2r_{sc}}{\Omega_{sc}} \exp\left(-\frac{r_{sc}^2}{\Omega_{sc}} \right), \tag{2.11}$$

where $\Omega_{sc} = 2\sigma_{sc}^2$ is the power of scattered path.

However, the Nakagami-*m* distribution can often be used to fit the experimental data. The literature contains results of many propagation studies where experimenters have found close agreement between the Nakagami-*m* distribution and scintillation data [6]-[8] with the PDF

$$p_{R_{sc}}(r_{sc}) = \frac{2r_{sc}^{2m_{sc}-1}}{\Gamma(m_{sc})}\left(\frac{m_{sc}}{\Omega_{sc}}\right)^{m_{sc}} \exp\left(-\frac{m_{sc}r_{sc}^2}{\Omega_{sc}}\right), \tag{2.12}$$

where

$$m_{sc} = \frac{\left(E\left\{|\alpha_{sc}|^2\right\}\right)^2}{\mathrm{var}\left\{|\alpha_{sc}|^2\right\}} \geq \frac{1}{2} \tag{2.13}$$

is the Nakagami shape factor, and $\Gamma(\cdot)$ is the gamma fuction. As a special case, the PDF in (2.12) becomes the one-sided Gaussian distribution when m_{sc} = 0.5 but the model of ionospheric scintillation distribution is specified for only $0 \leq S_4 \leq 1$. Consequently, the distribution of ionospheric scintillation when $m_{sc} < 1$ (or $S_4 > 1$) can not defined. Moreover, the PDF in (2.12) becomes the Rayleigh distribution when m_{sc}= 1, and non-fading when m_{sc} goes to infinity. The relationship between scintillation index S_4 and Nakagami shape factor m_{sc} can be written as [4]

$$m_{sc} = \frac{1}{S_4^2}. \tag{2.14}$$

This relationship is graphically shown in Figure 2.5.

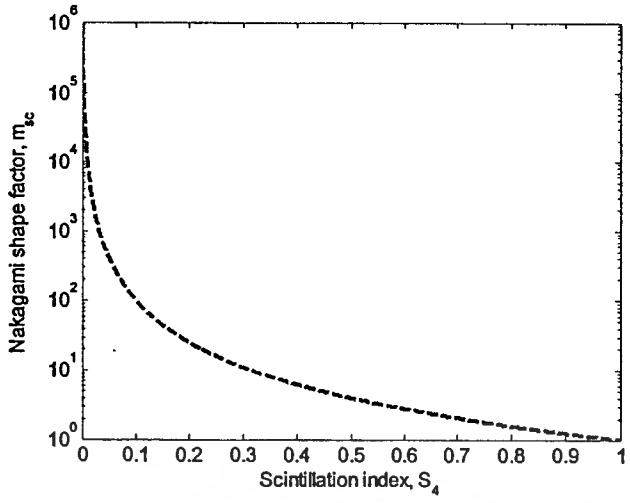

Figure 2.5 The relationship between the Nakagami shape factor m_{sc} and the scintillation index S_4.

The Nakagami-*m* PDF of the ionospheric scintillation can thus be expressed in terms of S_4 as

$$p_{R_{sc}}(r_{sc}) = \frac{2r_{sc}^{2S_4^{-2}-1}}{\Gamma\left(\frac{1}{S_4^2}\right)}\left(\frac{1}{\Omega_{sc}S_4^2}\right)^{S_4^{-2}} \exp\left(-\frac{r_{sc}^2}{\Omega_{sc}S_4^2}\right), \tag{2.15}$$

In the limit when the scintillation index approaches 1, this PDF also reduces to the Rayleigh distribution.

2.4 PDF of Combined Fading Channels

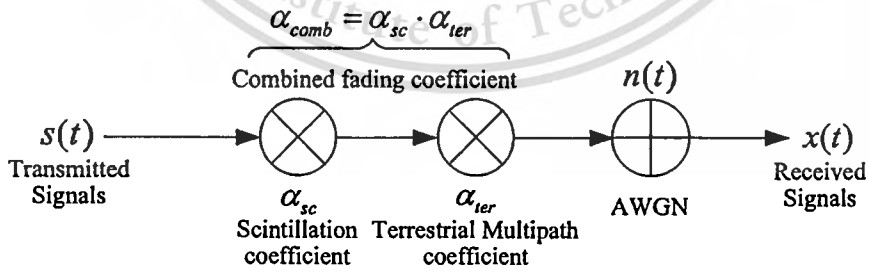

Figure 2.6 The attenuation due to combined fading channel in mobile satellite communication system.

The attenuation due to combined flat scintillation and flat terrestrial multipath fading, α_{comb}, as shown in Figure 2.6 can be modeled as

$$\alpha_{comb} = \alpha_{sc} \cdot \alpha_{ter} = \left[a_{sc} e^{j\phi_{sc}} + n_{sc}(t) \right] \cdot \left[a_{ter} e^{j\phi_{ter}} + n_{ter}(t) \right], \tag{2.16}$$

where α_{ter} are the coefficients of terrestrial multipath fadings, a_{ter}^2 is the received signal power of the LOS path, ϕ_{sc_k} is assumed to be uniformly distributed over in $[-\pi, \pi)$, and $n_{ter}(t)$ is a complex Gaussian random process from scattered signal over NLOS paths with power $2\sigma_{ter}^2$ associated with terrestrial multipath fading. Given the envelope $r_{sc} = |\alpha_{sc}|$ of scintillation coefficient and $r_{ter} = |\alpha_{ter}|$ of terrestrial multipath fading coefficient are independent, the envelope distribution of combined channels is

$$r_{comb} = r_{sc} \times r_{ter} = |\alpha_{sc}| \cdot |\alpha_{ter}|. \tag{2.17}$$

The joint statistics of two random variables r_{sc} and r_{ter} can be found from

$$p_{R_{comb}}(r_{comb}) = \iint_{D_{comb}} p_{R_{sc},R_{ter}}(r_{sc}, r_{ter}) dr_{sc} dr_{ter}, \tag{2.18}$$

where D_{comb} is the region of the $r_{sc} r_{ter}$ plane. Given that both envelope of scintillation r_{sc} and multipath fading r_{ter} are independent random variables, then [36]

$$p_{R_{sc},R_{ter}}(r_{sc}, r_{ter}) = p_{R_{sc}}(r_{sc}) \cdot p_{R_{ter}}(r_{ter}). \tag{2.19}$$

Substituting $r_{ter} = r_{comb}/r_{sc}$ and $dr_{ter} = dr_{comb}/r_{sc}$, the joint PDF can be found as follows [36].

$$\begin{aligned} p_{R_{comb}}(r_{comb}) dr_{comb} &= \iint_{D} p_{R_{sc}}(r_{sc}) p_{R_{ter}}(r_{ter}) dr_{sc} dr_{ter} \\ &= \int_0^{\infty} p_{R_{sc}}(r_{sc}) p_{R_{ter}}\left(\frac{r_{comb}}{r_{sc}} \right) dr_{sc} \frac{dr_{comb}}{r_{sc}}. \end{aligned} \tag{2.20}$$

Thus,

$$p_{R_{comb}}(r_{comb}) = \int_0^{\infty} \frac{1}{r_{sc}} p_{R_{sc}}(r_{sc}) p_{R_{ter}}\left(\frac{r_{comb}}{r_{sc}} \right) dr_{sc}. \tag{2.21}$$

From Section 2.3, the distribution of ionospheric scintillation can be model as two type of distribution, i.e., Rician PDF and Nagakami-*m* PDF. In this Section, the PDFs of combined fading channels in the form of Rician and Nakagami-*m* are derived. We now present 5 different cases of combined fadings; 1) combined Rician×Rician, 2) combined Rician×Rayleigh, 3) combined Rayleigh×Rayleigh, 4) combined Nakagami-*m*×Rayleigh, and 5) Nakagami-*m*×Nakagami-*m*. These corresponding the envelope PDFs, PDFs in term of instantaneous signal-to-noise ratio (SNR). These special case properties are summarized in the diagram as shown in Figure 2.7.

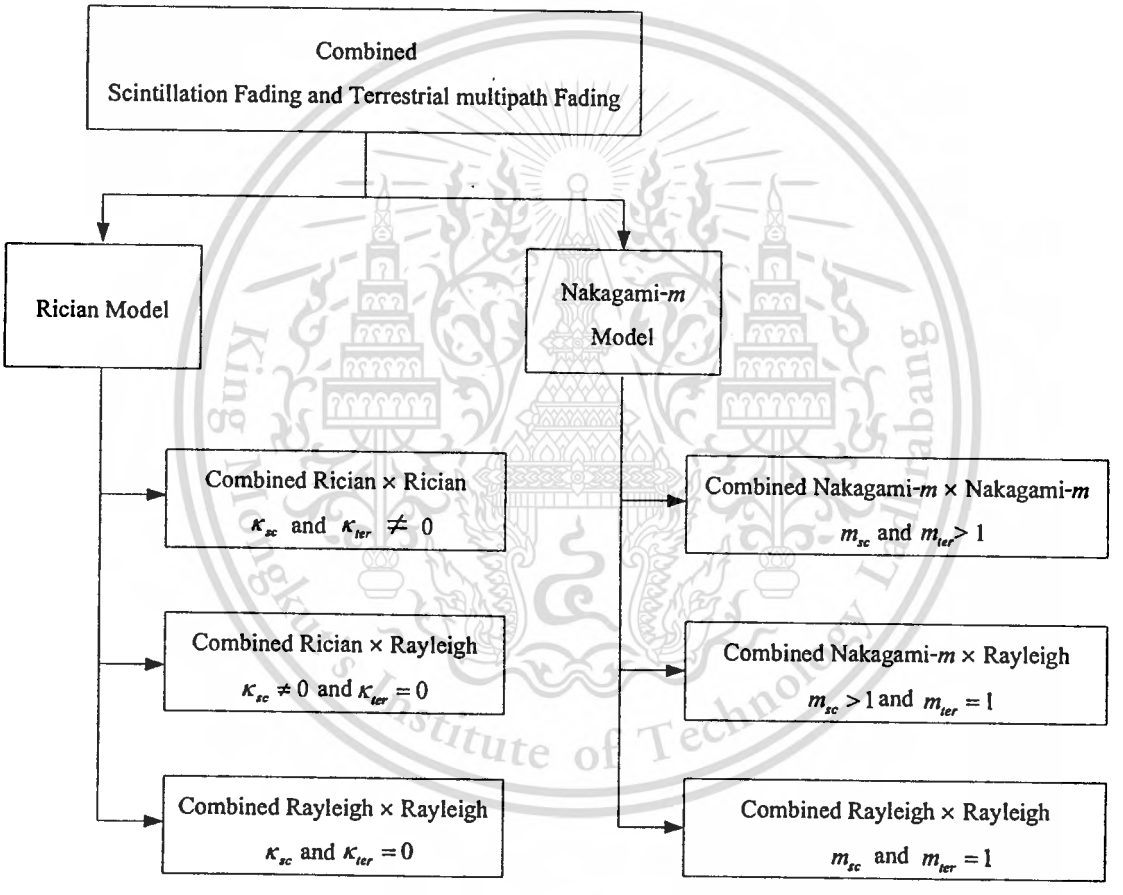

Figure 2.7 Special cases of combined fading channel.

2.4.1 Probability Distribution Function of Combined Rician×Rician Fading Channels

Let the fading envelope r_{sc} and r_{ter} be independent Rician random variables, each with the PDF

$$p_{R_{sc}}(r_{sc}) = \frac{2r_{sc}(\kappa_{sc}+1)}{\Omega_{sc}} \exp\left(-\frac{r_{sc}^2(\kappa_{sc}+1)}{\Omega_{sc}} - \kappa_{sc}\right) I_0\left\{2r_{sc}\sqrt{\frac{\kappa_{sc}(\kappa_{sc}+1)}{\Omega_{sc}}}\right\}, \tag{2.22}$$

$$p_{R_{ter}}(r_{ter}) = \frac{2r_{ter}(\kappa_{ter}+1)}{\Omega_{ter}} \exp\left(-\frac{r_{ter}^2(\kappa_{ter}+1)}{\Omega_{ter}} - \kappa_{ter}\right) I_0\left\{2r_{ter}\sqrt{\frac{\kappa_{ter}(\kappa_{ter}+1)}{\Omega_{ter}}}\right\}, \tag{2.23}$$

where κ_{ter} is the Rician factor of terrestrial multipath fading defined by $\kappa_{ter} = \alpha_{ter}^2/2\sigma_{ter}^2$ and $\Omega_{ter} = a_{ter}^2 + 2\sigma_{ter}^2$ is the average envelope power of terrestrial multipath fading coefficients.

Substituting (2.22) and (2.23) into (2.20), and replacing the modified Bessel function I_0 by series representation as

$$I_v\{z\} = \sum_{a=0}^{\infty} \frac{1}{a!\Gamma(v+a+1)}\left(\frac{z}{2}\right)^{v+2a}, \qquad z \geq 0. \tag{2.24}$$

The PDF $p_{R_{comb}}(r_{comb})$ can be expressed as

$$\begin{aligned} p_{R_{comb}}(r_{comb}) = {} & \frac{4r_{comb}(\kappa_{sc}+1)(\kappa_{ter}+1)}{\Omega_{comb}} \exp(-\kappa_{sc}-\kappa_{ter}) \\ & \cdot \sum_{i=0}^{\infty}\sum_{j=0}^{\infty} \frac{1}{(i!)^2(j!)^2}\left(\frac{r_{comb}^{2j}\kappa_{sc}^{i}(\kappa_{sc}+1)^{i}}{\Omega_{sc}^{i}}\right)\left(\frac{\kappa_{ter}^{j}(\kappa_{ter}+1)^{j}}{\Omega_{ter}^{j}}\right) \\ & \cdot \int_0^{\infty} r_{sc}^{2i-2j-1} \exp\left(-\frac{r_{sc}^2(\kappa_{sc}+1)}{\Omega_{sc}} - \frac{r_{comb}^2(\kappa_{ter}+1)}{r_{sc}^2\Omega_{ter}}\right) dr_{sc}. \end{aligned} \tag{2.25}$$

In the case of combined Rician scintillation and Rician terrestrial fading channels and with the use of [37]

$$\int_0^{\infty} x^{v-1}\exp\left(-\beta x^p - \gamma x^{-p}\right)dx = \frac{2}{p}\left(\frac{\gamma}{\beta}\right)^{\frac{v}{2p}} K_{\frac{v}{p}}\left\{2\sqrt{\beta\gamma}\right\}, \tag{2.26}$$

the PDF of the envelope of the received signal can be written as

$$p_{R_{comb}}(r_{comb}) = \frac{4r_{comb}(\kappa_{sc}+1)(\kappa_{ter}+1)}{\Omega_{comb}} \exp(-\kappa_{sc}-\kappa_{ter}) \cdot \sum_{i=0}^{\infty}\sum_{j=0}^{\infty} \frac{\kappa_{sc}^{i}\kappa_{ter}^{j}}{(i!)^2(j!)^2} \left(\sqrt{\frac{r_{comb}^2(\kappa_{sc}+1)(\kappa_{ter}+1)}{\Omega_{comb}}} \right)^{(i+j)} \cdot K_{i-j}\left\{ 2\sqrt{\frac{r_{comb}^2(\kappa_{sc}+1)(\kappa_{ter}+1)}{\Omega_{comb}}} \right\}, \tag{2.27}$$

where $K_{\alpha}\{\cdot\}$ is α -th order modified Bessel function of the second kind and Ω_{comb} is the average envelope power of combined fading channels which can be obtained from

$$\Omega_{comb} = \Omega_{sc}\Omega_{ter} = \left(a_{sc}^2 + 2\sigma_{sc}^2\right)\cdot\left(a_{ter}^2 + 2\sigma_{ter}^2\right) = a_{sc}^2 a_{ter}^2 + a_{sc}^2 2\sigma_{ter}^2 + a_{ter}^2 2\sigma_{sc}^2 + 4\sigma_{sc}^2\sigma_{ter}^2. \tag{2.28}$$

If both Rician factors $\kappa_{sc}, \kappa_{ter} >> 1$ (both powers of LOS path $a_{sc_k}^2, a_{ter_k}^2 >> 1$), the Rician factor can be approximated by [5]

$$\kappa_T \approx \frac{a_{sc}^2 a_{ter}^2}{a_{ter}^2 2\sigma_{sc}^2 + a_{sc}^2 2\sigma_{ter}^2} \approx \frac{\kappa_{sc}\kappa_{ter}}{\kappa_{sc}+\kappa_{ter}}. \tag{2.29}$$

Accordingly, the envelope distribution can be defined by a single Rician distribution with Rician factor = κ_T. Moreover, it is interesting to note when $\kappa_{sc} >> \kappa_{ter}$, then $\kappa_T \approx \kappa_{ter}$ and vice versa.

In the case of combined Rician scintillation and Rayleigh terrestrial fading channels, we have $\kappa_{ter} = 0$. Thus, the envelope PDF in (2.27) becomes

$$p_{R_{comb}}(r_{comb}) = \frac{4r_{comb}(\kappa_{sc}+1)}{\Omega_{comb}} \exp(-\kappa_{sc}) \cdot \sum_{i=0}^{\infty} \frac{\kappa_{sc}^{i}}{(i!)^2} \sqrt{\frac{r_{comb}^2(\kappa_{sc}+1)}{\Omega_{comb}}}^{i} K_i\left\{ 2\sqrt{\frac{r_{comb}^2(\kappa_{sc}+1)}{\Omega_{comb}}} \right\}, \tag{2.30}$$

where Ω_{comb} can be obtained from

$$\Omega_{comb} = \left(a_{sc}^2 + 2\sigma_{sc}^2\right)\cdot\left(2\sigma_{ter}^2\right) = a_{sc}^2 2\sigma_{ter}^2 + 4\sigma_{sc}^2\sigma_{ter}^2. \tag{2.31}$$

Note that when $\kappa_{sc} >> 1$, then $\kappa_T \approx 0$, thus, the combined envelope has Rayleigh distribution.

When both Rician factors $\kappa_{sc}, \kappa_{ter}$ = 0, i.e., the channel has a combination of severe scintillation (Rayleigh scintillation) and Rayleigh terrestrial multipath fading. The envelope PDF of this case is

$$p_{R_{comb}}(r_{comb}) = \frac{4r_{comb}}{\Omega_{comb}} K_0\left\{2\sqrt{\frac{r_{comb}^2}{\Omega_{comb}}}\right\}, \tag{2.32}$$

where Ω_{comb} is given by

$$\Omega_{comb} = 4\sigma_{sc}^2\sigma_{ter}^2. \tag{2.33}$$

The combination of combined Rayleigh×Rayleigh distribution is considered to be the most severe case among all cases.

Alternatively, the derived results in (2.27), (2.30), and (2.32) can be expressed in a product of RVs as shown in [38] where the parameter κ_{sc}, κ_{ter}, and Ω_{comb} in (2.27), (2.30), and (2.32) are equal to $a_1^2/2\sigma_1^2$, $a_2^2/2\sigma_2^2$, and $4\sigma_1^2\sigma_2^2$, respectively, in (6.51), (6.63) and (6.66) of [38]. In addition, n_1 and n_2 in [38] are equal to 2.

Equivalently, the received instantaneous signal power is modulated by r_{comb}^2 when we define the instantaneous SNR per bit of the combined envelope by

$$\gamma_{comb} = \frac{E_b}{N_0} r_{comb}^2 = \frac{E_b}{N_0}|\alpha_{sc}|^2 \cdot |\alpha_{ter}|^2, \tag{2.34}$$

where E_b is average bit energy and N_0 is noise variance.

To obtain the PDF of instantaneous SNR, $p_{\Gamma_{comb}}(\gamma_{comb})$, the PDF of combined envelope with the change-of-variables are used to obtain [36]

$$\begin{aligned} p_{\Gamma_{comb}}(\gamma_{comb}) &= \frac{1}{\frac{d}{dr_{comb}}\left\{r_{comb}\sqrt{\frac{E_b}{N_0}}\right\}}\left[p_{R_{comb}}\left(\sqrt{r_{comb}^2}\right) + p_{R_{comb}}\left(-\sqrt{r_{comb}^2}\right)\right] \\ &= \frac{1}{2\sqrt{\frac{E_b}{N_0}}\sqrt{\gamma_{comb}\frac{N_0}{E_b}}}\left[p_{R_{comb}}\left(\sqrt{\gamma_{comb}\frac{N_0}{E_b}}\right) + p_{R_{comb}}\left(-\sqrt{\gamma_{comb}\frac{N_0}{E_b}}\right)\right], \end{aligned} \tag{2.35}$$

However, $p_{R_{comb}}$ have only positive term, hence,

$$p_{\Gamma_{comb}}(\gamma_{comb}) = \frac{p_{R_{comb}}\left(\sqrt{\gamma_{comb}\frac{N_0}{E_b}}\right)}{2\frac{E_b}{N_0}\sqrt{\gamma_{comb}\frac{N_0}{E_b}}} \tag{2.36}$$

Substituting the PDF $p_{R_{comb}}(r_{comb})$ of combined Rician fading channels in (2.30) into (2.36), the PDF of instantaneous SNR $p_{\Gamma_{comb}}(\gamma_{comb})$ of combined Rician fading channels can be expressed as

$$\begin{aligned} p_{\Gamma_{comb}}(\gamma_{comb}) &= \frac{2(\kappa_{sc}+1)(\kappa_{ter}+1)}{\bar{\gamma}_{comb}}\exp(-\kappa_{sc}-\kappa_{ter}) \\ &\cdot\sum_{l=0}^{\infty}\sum_{j=0}^{\infty}\frac{\kappa_{sc}^{l}\kappa_{ter}^{j}}{(i!)^2(j!)^2}\left(\sqrt{\frac{\gamma_{comb}(\kappa_{sc}+1)(\kappa_{ter}+1)}{\bar{\gamma}_{comb}}}\right)^{(l+j)} \\ &\cdot K_{l-j}\left\{2\sqrt{\frac{\gamma_{comb}(\kappa_{sc}+1)(\kappa_{ter}+1)}{\bar{\gamma}_{comb}}}\right\}, \end{aligned} \tag{2.37}$$

where the average SNR per bit $\bar{\gamma}_{comb}$ is defined by

$$\bar{\gamma}_{comb} = \frac{E_b}{N_0}\Omega_{comb}. \tag{2.38}$$

In the case of combined Rician scintillation and Rayleigh terrestrial fading channels, the PDF in terms of instantaneous SNR becomes

$$\begin{aligned} p_{\Gamma_{comb}}(\gamma_{comb}) &= \frac{2(\kappa_{sc}+1)}{\bar{\gamma}_{comb}}\exp(-\kappa_{sc}) \\ &\cdot\sum_{l=0}^{\infty}\frac{\kappa_{sc}^{l}}{(i!)^2}\left(\sqrt{\frac{\gamma_{comb}(\kappa_{sc}+1)}{\bar{\gamma}_{comb}}}\right)^{l}K_l\left\{2\sqrt{\frac{\gamma_{comb}(\kappa_{sc}+1)}{\bar{\gamma}_{comb}}}\right\}. \end{aligned} \tag{2.39}$$

For the channel with a combination of severe scintillation (Rayleigh scintillation) and Rayleigh terrestrial multipath fading, the PDF of the instantaneous SNR becomes

$$p_{\Gamma_{comb}}(\gamma_{comb}) = \frac{2}{\bar{\gamma}_{comb}}K_0\left\{2\sqrt{\frac{\gamma_{comb}}{\bar{\gamma}_{comb}}}\right\}. \tag{2.40}$$

2.4.2 PDF of Combined Nakagami-*m*×Nakagami-*m* Fading Channels

For doubly independent Nakagami-*m* random variables, i.e., the fading envelope r_{sc} and r_{ter} are independent Nakagami-*m* random variables, with the PDF

$$p_{R_{sc}}(r_{sc}) = \frac{2r_{sc}^{2m_{sc}-1}}{\Gamma(m_{sc})}\left(\frac{m_{sc}}{\Omega_{sc}}\right)^{m_{sc}} \exp\left(-\frac{m_{sc}r_{sc}^2}{\Omega_{sc}}\right), \tag{2.41}$$

and

$$p_{R_{ter}}(r_{ter}) = \frac{2r_{ter}^{2m_{ter}-1}}{\Gamma(m_{ter})}\left(\frac{m_{ter}}{\Omega_{ter}}\right)^{m_{ter}} \exp\left(-\frac{m_{ter}r_{ter}^2}{\Omega_{ter}}\right), \tag{2.42}$$

where m_{ter} is the Nakagami shape factor of terrestrial multipath fading. Substituting (2.41) and (2.42) into (2.20), the combined Nakagami-*m* PDF can be expressed as

$$\begin{aligned} p_{R_{comb}}(r_{comb}) = {} & \frac{4r^{2m_{ter}-1}}{\Gamma(m_{sc})\Gamma(m_{ter})}\left(\frac{m_{sc}}{\Omega_{sc}}\right)^{m_{sc}}\left(\frac{m_{ter}}{\Omega_{ter}}\right)^{m_{ter}} \\ & \cdot \int_0^{\infty} r_{sc}^{2m_{sc}-2m_{ter}-1} \exp\left(-\frac{m_{sc}r_{sc}^2}{\Omega_{sc}} - \frac{m_{ter}r_{comb}^2}{r_{sc}^2\Omega_{ter}}\right) dr_{sc}. \end{aligned} \tag{2.43}$$

Using the relation in (2.26), hence, the combined PDF in (2.43) becomes

$$p_{R_{comb}}(r_{comb}) = \frac{4r_{comb}^{m_{sc}+m_{ter}-1}}{\Gamma(m_{sc})\Gamma(m_{ter})}\left(\sqrt{\frac{m_{sc}m_{ter}}{\Omega_{comb}}}\right)^{m_{sc}+m_{ter}} K_{m_{sc}-m_{ter}}\left\{2\sqrt{\frac{r_{comb}^2 m_{sc}m_{ter}}{\Omega_{comb}}}\right\}, \tag{2.44}$$

In the case of combined Nakagami-*m* scintillation and Rayleigh terrestrial multipath fading channels, we have $m_{ter} = 1$. Thus, the envelope PDF in (2.44) becomes

$$p_{R_{comb}}(r_{comb}) = \frac{4r_{comb}^{m_{sc}}}{\Gamma(m_{sc})}\left(\sqrt{\frac{m_{sc}}{\Omega_{comb}}}\right)^{m_{sc}+1} K_{m_{sc}-1}\left\{2\sqrt{\frac{r_{comb}^2 m_{sc}}{\Omega_{comb}}}\right\}. \tag{2.45}$$

In this case, both Nakagami shape factors m_{sc} and m_{ter} = 1, i.e., the PDF of combined Nakagami-*m* scintillation and Nakagami-*m* terrestrial multipath fading channels in (2.44) reduces to a combination of Rayleigh scintillation and Rayleigh terrestrial multipath fading as shown in (2.32).

The PDF of instantaneous SNR $p_{\Gamma_{comb}}(\gamma_{comb})$ can be computed by substituting the combined Nakagami-m PDF in (2.44) into (2.36), hence,

$$p_{\Gamma_{comb}}(\gamma_{comb}) = \frac{2}{\Gamma(m_{sc})\Gamma(m_{ter})\gamma_{comb}} \left(\sqrt{\frac{m_{sc} m_{ter} \gamma_{comb}}{\overline{\gamma}_{comb}}} \right)^{m_{sc}+m_{ter}} \cdot K_{m_{sc}-m_{ter}} \left\{ 2\sqrt{\frac{m_{sc} m_{ter} \gamma_{comb}}{\overline{\gamma}_{comb}}} \right\}. \tag{2.46}$$

In the case of combined Nakagami-m scintillation and Rayleigh terrestrial multipath fading channels, the PDF of the instantaneous SNR in (2.46) becomes

$$p_{\Gamma_{comb}}(\gamma_{comb}) = \frac{2}{\Gamma(m_{sc})\gamma_{comb}} \left(\sqrt{\frac{m_{sc}\gamma_{comb}}{\overline{\gamma}_{comb}}} \right)^{m_{sc}+1} K_{m_{sc}-1} \left\{ 2\sqrt{\frac{m_{sc}\gamma_{comb}}{\overline{\gamma}_{comb}}} \right\}. \tag{2.47}$$

The PDF in (2.47) can be deduced to the PDF of combined Rayleigh scintillation and Rayleigh terrestrial multipath fading as shown in (2.40).

The envelope PDFs of the single ionospheric scintillation fading channel and combined ionospheric scintillation and terrestrial multipath fading channel are summarized in Table 2.1-Table 2.2. The PDFs of the instantaneous SNR of combined ionospheric scintillation and terrestrial multipath fading channel are summarized in Table 2.3.

2.5 Conclusions

Ionospheric scintillation causes signal fluctuations with the intensity of ionospheric scintillation is often described by the scintillation index S_4. Statistical distribution of the received signal envelope of the ionospheric scintillation can be typically modeled as Rician or Nakagami-m distribution. From the relationship between Rician factor κ, Nakagami-m shape factor m, and scintillation index S_4, the envelope PDF of the ionospheric scintillation with Rician and Nakagami-m distribution can thus be expressed in terms of S_4 index. Moreover, the signal in mobile satellite communication is also degraded by terrestrial multipath fading. As a result, this system has a double or combined fading channel. In this Chapter, the PDFs of combined fading channel are derived by using Rician and Nakagami-m distribution model in terms of envelope PDF and instantaneous SNR. The special case of combined fading in Rician model can be

expressed as 1) Rician×Rician, 2) Rician×Rayleigh, and 3) Rayleigh×Rayleigh. While the special case of combined fading in Nakagami-*m* model can be expressed as 1) Nakagami-*m*× Nakagami-*m*, 2) Nakagami-*m*×Rayleigh, and 3) Rayleigh×Rayleigh. These PDFs are summarized for all possible cases.

Table 2.1 The envelope PDFs of the ionospheric scintillation fading channel.

Fading Types	PDF $p_{R_{sc}}(r_{sc})$
Single Rayleigh ionospheric scintillation	$p_{sc}(r_{sc}) = \frac{2r_{sc}}{\Omega_{sc}} \exp\left(-\frac{r_{sc}^2}{\Omega_{sc}}\right)$,
Single Rician ionospheric scintillation	In terms of Rician factor κ_{sc} $p_{R_{sc}}(r_{sc}) = \frac{2r_{sc}(\kappa_{sc}+1)}{\Omega_{sc}} \exp\left(-\frac{r_{sc}^2(\kappa_{sc}+1)}{\Omega_{sc}} - \kappa_{sc}\right) I_0\left\{2r_{sc}\sqrt{\frac{\kappa_{sc}(\kappa_{sc}+1)}{\Omega_{sc}}}\right\}$ In terms of scintillation index S_4 $p_{R_{sc}}(r_{sc}) = \frac{2r_{sc}}{\Omega_{sc}\left(1-\sqrt{1-S_4^2}\right)} \exp\left(-\frac{1}{1-\sqrt{1-S_4^2}}\left[\frac{r_{sc}^2}{\Omega_{sc}} + \sqrt{1-S_4^2}\right]\right) I_0\left\{\frac{2r_{sc}}{1-\sqrt{1-S_4^2}}\sqrt{\frac{\sqrt{1-S_4^2}}{\Omega_{sc}}}\right\}$
Single Nakagami-*m* ionospheric scintillation	In terms of Nakagami shape factor $p_{R_{sc}}(r_{sc}) = \frac{2r_{sc}^{2m_{sc}-1}}{\Gamma(m_{sc})}\left(\frac{m_{sc}}{\Omega_{sc}}\right)^{m_{sc}} \exp\left(-\frac{m_{sc}r_{sc}^2}{\Omega_{sc}}\right)$ In terms of scintillation index S_4 $p_{R_{sc}}(r_{sc}) = \frac{2r_{sc}^{2S_4^{-2}-1}}{\Gamma\left(\frac{1}{S_4^2}\right)}\left(\frac{1}{\Omega_{sc}S_4^2}\right)^{S_4^{-2}} \exp\left(-\frac{r_{sc}^2}{\Omega_{sc}S_4^2}\right)$

Table 2.2 The envelope PDFs of combined ionospheric scintillation and terrestrial multipath fading channel.

Fading Types	PDF $p_{R_{comb}}(r_{comb})$
Combined Rician × Rician fading channel	$p_{R_{comb}}(r_{comb}) = \frac{4r_{comb}(\kappa_{sc}+1)(\kappa_{ter}+1)}{\Omega_{comb}} \exp(-\kappa_{sc}-\kappa_{ter}) \sum_{i=0}^{\infty}\sum_{j=0}^{\infty} \frac{\kappa_{sc}^{i}\kappa_{ter}^{j}}{(i!)^2(j!)^2} \left(\sqrt{\frac{r_{comb}^2(\kappa_{sc}+1)(\kappa_{ter}+1)}{\Omega_{comb}}}\right)^{(i+j)} \cdot K_{i-j}\left\{2\sqrt{\frac{r_{comb}^2(\kappa_{sc}+1)(\kappa_{ter}+1)}{\Omega_{comb}}}\right\}$
Combined Rician × Rayleigh fading channel	$p_{R_{comb}}(r_{comb}) = \frac{4r_{comb}(\kappa_{sc}+1)}{\Omega_{comb}} \exp(-\kappa_{sc}) \sum_{i=0}^{\infty} \frac{\kappa_{sc}^{i}}{(i!)^2} \sqrt{\frac{r_{comb}^2(\kappa_{sc}+1)}{\Omega_{comb}}}^{i} K_i\left\{2\sqrt{\frac{r_{comb}^2(\kappa_{sc}+1)}{\Omega_{comb}}}\right\}$
Combined Rayleigh × Rayleigh fading channel	$p_{R_{comb}}(r_{comb}) = \frac{4r_{comb}}{\Omega_{comb}} K_0\left\{2\sqrt{\frac{r_{comb}^2}{\Omega_{comb}}}\right\}$
Combined Nakagami-*m* × Nakagami-*m* fading channel	$p_{R_{comb}}(r_{comb}) = \frac{4r_{comb}^{m_{sc}+m_{ter}-1}}{\Gamma(m_{sc})\Gamma(m_{ter})} \left(\sqrt{\frac{m_{sc}m_{ter}}{\Omega_{comb}}}\right)^{m_{sc}+m_{ter}} K_{m_{sc}-m_{ter}}\left\{2\sqrt{\frac{r_{comb}^2 m_{sc}m_{ter}}{\Omega_{comb}}}\right\}$
Combined Nakagami-*m* × Rayleigh fading channel	$p_{R_{comb}}(r_{comb}) = \frac{4r_{comb}^{m_{sc}}}{\Gamma(m_{sc})} \left(\sqrt{\frac{m_{sc}}{\Omega_{comb}}}\right)^{m_{sc}+1} K_{m_{sc}-1}\left\{2\sqrt{\frac{r_{comb}^2 m_{sc}}{\Omega_{comb}}}\right\}$

Table 2.3 The PDFs in terms of instantaneous SNR of combined ionospheric scintillation and terrestrial multipath fading channel.

Fading Types	PDF $p_{\Gamma_{comb}}(\gamma_{comb})$
Combined Rician × Rician fading channel	$p_{\Gamma_{comb}}(\gamma_{comb}) = \frac{2(\kappa_{sc}+1)(\kappa_{ter}+1)}{\overline{\gamma}_{comb}} \exp(-\kappa_{sc}-\kappa_{ter}) \sum_{i=0}^{\infty}\sum_{j=0}^{\infty} \frac{\kappa_{sc}^{i}\kappa_{ter}^{j}}{(i!)^2 (j!)^2} \left(\sqrt{\frac{\gamma_{comb}(\kappa_{sc}+1)(\kappa_{ter}+1)}{\overline{\gamma}_{comb}}} \right)^{(i+j)} \cdot K_{i-j}\left\{ 2\sqrt{\frac{\gamma_{comb}(\kappa_{sc}+1)(\kappa_{ter}+1)}{\overline{\gamma}_{comb}}} \right\},$
Combined Rician × Rayleigh fading channel	$p_{\Gamma_{comb}}(\gamma_{comb}) = \frac{2(\kappa_{sc}+1)}{\overline{\gamma}_{comb}} \exp(-\kappa_{sc}) \sum_{i=0}^{\infty} \frac{\kappa_{sc}^{i}}{(i!)^2} \left(\sqrt{\frac{\gamma_{comb}(\kappa_{sc}+1)}{\overline{\gamma}_{comb}}} \right)^{i} K_{i}\left\{ 2\sqrt{\frac{\gamma_{comb}(\kappa_{sc}+1)}{\overline{\gamma}_{comb}}} \right\}.$
Combined Rayleigh × Rayleigh fading channel	$p_{\Gamma_{comb}}(\gamma_{comb}) = \frac{2}{\overline{\gamma}_{comb}} K_0\left\{ 2\sqrt{\frac{\gamma_{comb}}{\overline{\gamma}_{comb}}} \right\}.$
Combined Nakagami-*m* × Nakagami-*m* fading channel	$p_{\Gamma_{comb}}(\gamma_{comb}) = \frac{2}{\Gamma(m_{sc})\Gamma(m_{ter})\gamma_{comb}} \left(\sqrt{\frac{m_{sc}m_{ter}\gamma_{comb}}{\overline{\gamma}_{comb}}} \right)^{m_{sc}+m_{ter}} K_{m_{sc}-m_{ter}}\left\{ 2\sqrt{\frac{m_{sc}m_{ter}\gamma_{comb}}{\overline{\gamma}_{comb}}} \right\}.$
Combined Nakagami-*m* × Rayleigh fading channel	$p_{\Gamma_{comb}}(\gamma_{comb}) = \frac{2}{\Gamma(m_{sc})\gamma_{comb}} \left(\sqrt{\frac{m_{sc}\gamma_{comb}}{\overline{\gamma}_{comb}}} \right)^{m_{sc}+1} K_{m_{sc}-1}\left\{ 2\sqrt{\frac{m_{sc}\gamma_{comb}}{\overline{\gamma}_{comb}}} \right\}.$

CHAPTER 3

PERFORMANCE ANANYSIS OVER COMBINED FADING CHANNELS

In this chapter, we derive and simplify the average BEP for some common modulation schemes and derive the outage probability of combined fading channels with and without MRC diversity by using the MGF based approach. This requires the use of the PDF in terms of the instantaneous SNR per bit as derived in Chapter 3. First, the MGFs of the instantaneous SNR per bit are computed. The derived MGF results are expressed using 2 types of fading channel models, i.e., 1) combined Rician×Rician fading channel and 2) combined Nakagami-m×Nakagami-m fading channel. The average BEP of digital modulation schemes over combined fading channel can be computed by using these MGF results.

3.1 MGF of Instantaneous SNR of Combined Fading Channels

In this Section, we derive the MGF of the instantaneous SNR per bit necessary for the computation of the average BEP and the outage probability in the next Section. The MGF $\Phi_{\gamma_{comb}}(-s)$ can be defined as

$$\Phi_{\gamma_{comb}}(-s) = \int_0^\infty \exp(-s\gamma_{comb}) p_{\Gamma_{comb}}(\gamma_{comb}) d\gamma_{comb}, \tag{3.1}$$

where s is a complex and $p_{\Gamma_{comb}}(\gamma_{comb})$ is the envelope PDF of combined fading channels. Replacing $p_{\Gamma_{comb}}(\gamma_{comb})$ in (3.1) with the PDF in terms of the instantaneous SNR of combined fading channel as shown in Chapter 3, we obtain the MGF of the instantaneous SNR per bit of combined fading channels which can be derived into 2 types of fading channel model.

3.1.1 MGF of the Instantaneous SNR of Combined Rician×Rician Fading Channels

The MGF of the instantaneous SNR of combined Rician fading channel can be derived by replacing $p_{\Gamma_{comb}}(\gamma_{comb})$ in (3.1) with (2.37), to obtain

$$\Phi_{\gamma_{comb}}(-s)=\int_0^{\infty}\exp(-s\gamma_{comb})\frac{2(\kappa_{sc}+1)(\kappa_{ter}+1)}{\overline{\gamma}_{comb}}\exp(-\kappa_{sc}-\kappa_{ter})$$
$$\cdot\sum_{i=0}^{\infty}\sum_{j=0}^{\infty}\frac{\kappa_{sc}^{i}\kappa_{ter}^{j}}{(i!)^2(j!)^2}\left(\sqrt{\frac{\gamma_{comb}(\kappa_{sc}+1)(\kappa_{ter}+1)}{\overline{\gamma}_{comb}}}\right)^{(i+j)} \tag{3.2}$$
$$\cdot K_{i-j}\left\{2\sqrt{\frac{\gamma_{comb}(\kappa_{sc}+1)(\kappa_{ter}+1)}{\overline{\gamma}_{comb}}}\right\}d\gamma_{comb}.$$

The goal is to simplify the expression of MGF in (3.2). Using the relation [37, Eq. (6.643.3)]

$$\int_0^{\infty}x^{\mu-\frac{1}{2}}\exp(-\alpha x)K_{2\nu}\left\{2\beta\sqrt{x}\right\}dx=\frac{\Gamma(\mu+\nu+\frac{1}{2})\Gamma(\mu-\nu+\frac{1}{2})}{2\beta}\exp\left(\frac{\beta^2}{2\alpha}\right)\alpha^{-\mu}W_{-\mu,\nu}\left(\frac{\beta^2}{\alpha}\right), \tag{3.3}$$

where $[\mathrm{Re}(\mu+\nu+\frac{1}{2})>0]$ and $W_{\mu,\nu}(z)$ is the Whittaker-W function, we can be expressed (3.3) as

$$\Phi_{\gamma_{comb}}(-s)=\exp(-\kappa_{sc}-\kappa_{ter})\sum_{i=0}^{\infty}\sum_{j=0}^{\infty}\frac{\kappa_{sc}^{i}\kappa_{ter}^{j}}{i!\,j!}\left(\sqrt{\frac{(\kappa_{sc}+1)(\kappa_{ter}+1)}{\overline{\gamma}_{comb}s}}\right)^{(i+j+1)}$$
$$\cdot\exp\left[\frac{(\kappa_{sc}+1)(\kappa_{ter}+1)}{2\overline{\gamma}_{comb}s}\right]W_{\frac{i+j+1}{2},\frac{i-j}{2}}\left(\frac{(\kappa_{sc}+1)(\kappa_{ter}+1)}{\overline{\gamma}_{comb}s}\right). \tag{3.4}$$

The Whittaker-W function is related to the confluent hypergeometric function of the second kind $\Psi(a,b;z)$, defined by the formula [39, Eq. (13.3.33)]

$$W_{\mu,\nu}(z)=z^{\nu+0.5}\exp\{-0.5z\}\Psi(0.5-\mu+\nu,2\nu+1;z), \tag{3.5}$$

where $|\arg z|<\pi$ and the confluent hypergeometric function of the second kind is defined by the integral [37]

$$\Psi(a,b;z)=\frac{1}{\Gamma(a)}\int_0^{\infty}t^{a-1}(1+t)^{b-a-1}\exp(-zt)dt;\quad a>0. \tag{3.6}$$

As a result, the MGF in (3.4) becomes

$$\Phi_{\gamma_{comb}}(-s)=\exp(-\kappa_{sc}-\kappa_{ter})\sum_{i=0}^{\infty}\sum_{j=0}^{\infty}\frac{\kappa_{sc}^{i}\kappa_{ter}^{j}}{i!j!}\left(\frac{(\kappa_{sc}+1)(\kappa_{ter}+1)}{\overline{\gamma}_{comb}s}\right)^{(i+1)} \cdot\Psi\left(i+1,i-j+1;\frac{(\kappa_{sc}+1)(\kappa_{ter}+1)}{\overline{\gamma}_{comb}s}\right). \tag{3.7}$$

Moreover, the confluent hypergeometric function of the second kind can be further expressed as [39]

$$\Psi(a,b;z)=z^{-a}\,{}_2F_0\left(a,1+a-b;\ ;-1/z\right), \tag{3.8}$$

where ${}_2F_0(a,b;;z)$ is the generalized hypergeometric function expressed by the series expansions as[40]

$${}_2F_0(a,b;\ ;z)=\sum_{n=0}^{\infty}\frac{(a)_n(b)_n}{n!}z^n, \tag{3.9}$$

where the symbol $(\lambda)_n=\lambda(\lambda+1)...(\lambda+n-1)$ with $(\lambda)_0=1$ denotes the Pochhammer symbol. Note that the generalized hypergeometric function ${}_2F_0(a,b;;z)$ can be easily computed using commercial softwares such as MATLAB and MATHEMATICA. It follows from (3.8) that

$$\Phi_{\gamma_{comb}}(-s)=\exp(-\kappa_{sc}-\kappa_{ter})\sum_{i=0}^{\infty}\sum_{j=0}^{\infty}\frac{\kappa_{sc}^{i}\kappa_{ter}^{j}}{i!j!}\,{}_2F_0\left(i+1,j+1;\ ;-\frac{\overline{\gamma}_{comb}s}{(\kappa_{sc}+1)(\kappa_{ter}+1)}\right). \tag{3.10}$$

For practical purposes, the evaluation of (3.10) obviously requires a truncation of the infinite series. As a consequence, it would be interesting to calculate how many terms are needed to obtain an approximation with high accuracy. For analytical evaluation of the truncation error, we plot (3.10) versus the summation index i and j, for different values of the parameters κ_{sc} and κ_{ter} given fixed $\overline{\gamma}_{comb}s=1$. The double summation in (3.10) is computed with the indices i and j running from 0 to 50, which are sufficient for the convergence of the summation. The obtained MGF results for various Rician factor κ_{sc} and κ_{ter} are illustrated in Figure 3.1-Figure 3.4.

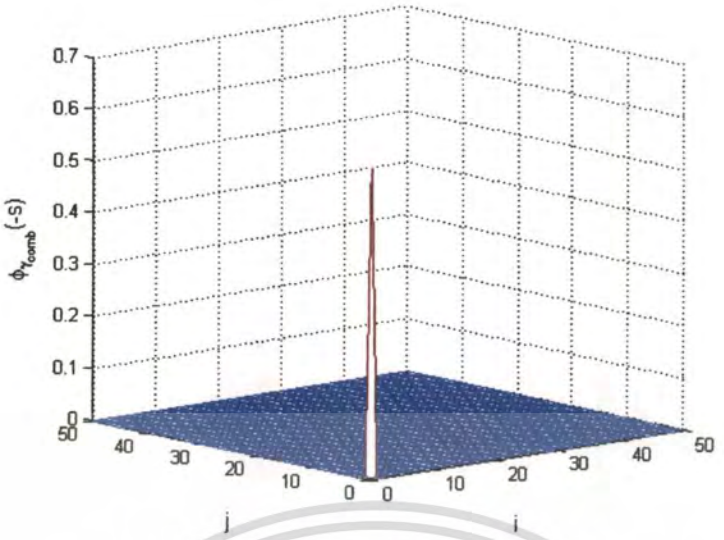

(a) 3-Dimensional (i-j-$\Phi_{\gamma_{comb}}(-s)$ plane).

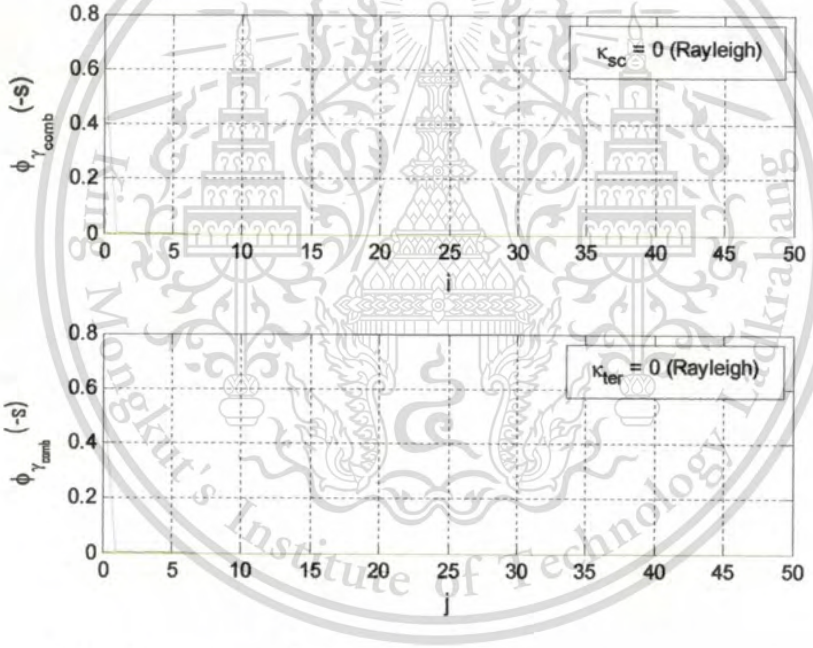

(b) 2-Dimensional (i-$\Phi_{\gamma_{comb}}(-s)$ plane and j-$\Phi_{\gamma_{comb}}(-s)$ plane).

Figure 3.1 The results from (3.10) with Rician factor parameters κ_{sc} and κ_{ter} = 0 (Rayleigh).

In Figure 3.1 (a), we show the contour plot of (3.10) when both channels are Rayleigh fading (κ_{sc} and κ_{ter} = 0) and the 2-dimensional plot of the results are shown in Figure 3.1 (b). As seen in Figure 3.1 (b), a maximum value of $\Phi_{\gamma_{comb}}(-s)$ from (3.10) in i-$\Phi_{\gamma_{comb}}(-s)$ plane and j-$\Phi_{\gamma_{comb}}(-s)$ plane of 2-dimensional occurs at i and j = 0. As a result in this case, we can computed $\Phi_{\gamma_{comb}}(-s)$ from (3.10) by using only i and j = 0.

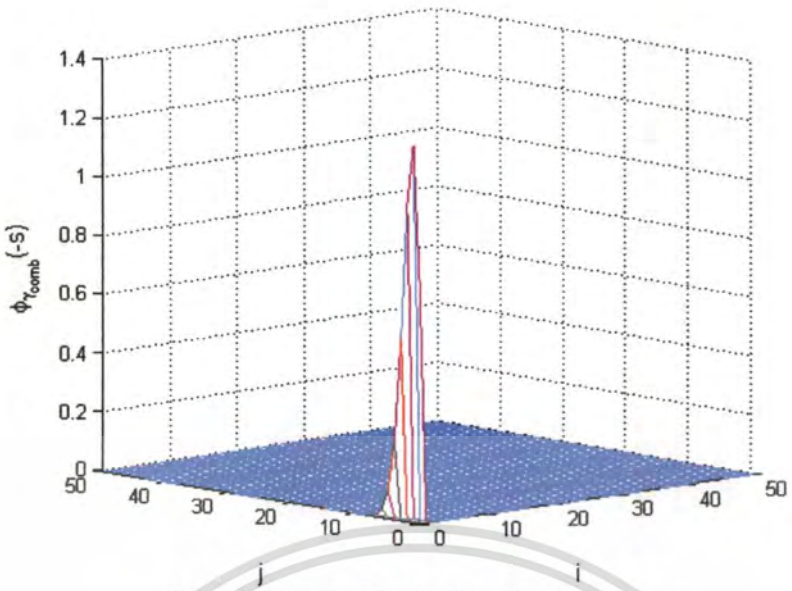

(a) 3-Dimensional (i-j-$\Phi_{\gamma_{comb}}(-s)$ plane).

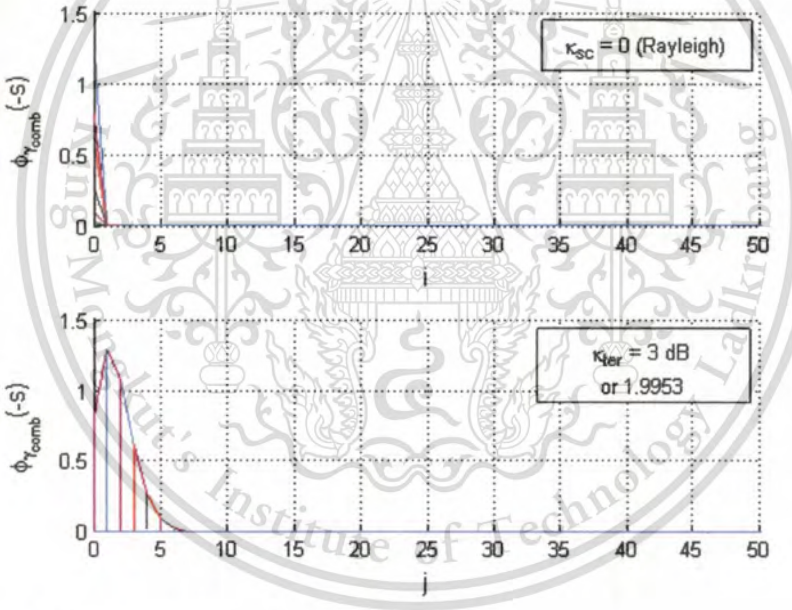

(b) 2-Dimensional (i-$\Phi_{\gamma_{comb}}(-s)$ plane and j-$\Phi_{\gamma_{comb}}(-s)$ plane).

Figure 3.2 The results from (3.10) in Rician factor parameters κ_{sc} = 0(Rayleigh) and κ_{ter} = 3 dB.

In Figure 3.2, we show the results from (3.10) when the Rician factor parameters κ_{sc} = 0 (Rayleigh) and κ_{ter} = 3 dB. The results as shown in this figure have increasing continuously to the maximum and decreasing thereafter. A maximum value of $\Phi_{\gamma_{comb}}(-s)$ occurs at i = 0 and j = 1 while the result becomes 0 when i and j are increasing. The majority of $\Phi_{\gamma_{comb}}(-s)$ occurs at i = 0 while j = 0 to 6.

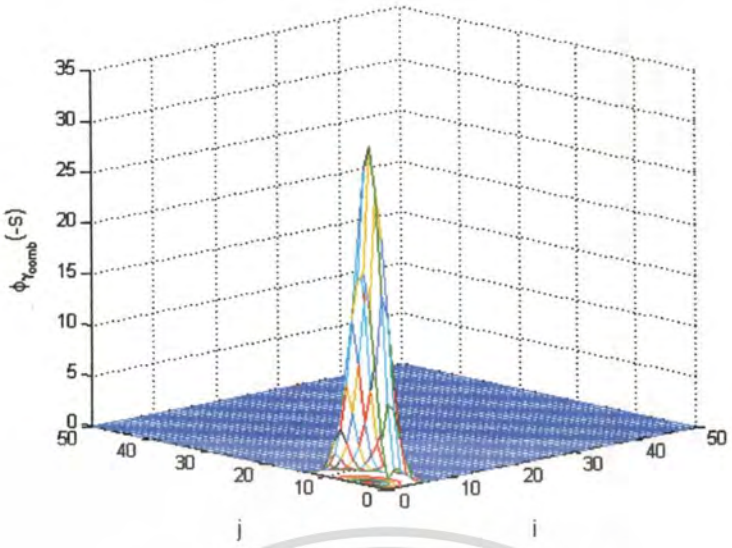

(a) 3-Dimensional (i-j-$\Phi_{\gamma_{comb}}(-s)$ plane).

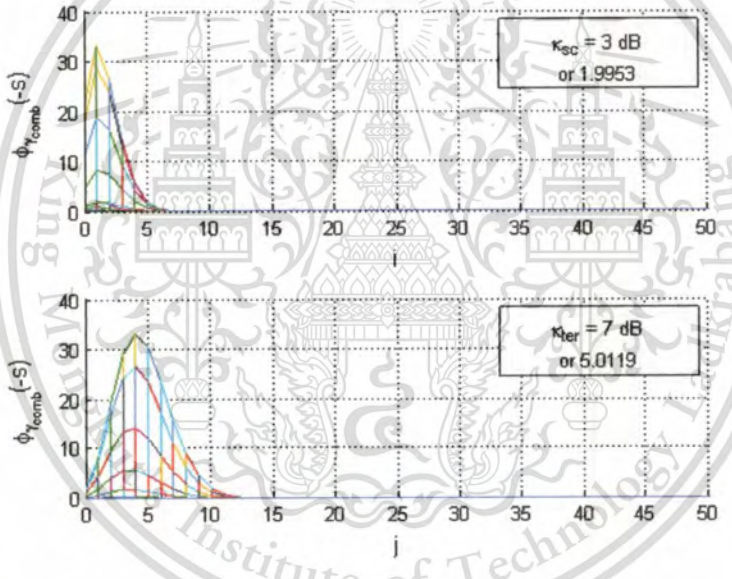

(b) 2-Dimensional (i-$\Phi_{\gamma_{comb}}(-s)$ plane and j-$\Phi_{\gamma_{comb}}(-s)$ plane).

Figure 3.3 The results from (3.10) in Rician factor parameters κ_{sc} = 3 dB and κ_{ter} = 7 dB.

The results from (3.10) when the Rician factor parameters κ_{sc} = 3 dB and κ_{ter} = 7 dB are shown in Figure 3.3. As seen from Figure in 2-dimensional, we can see the similarity result in j-$\Phi_{\gamma_{comb}}(-s)$ plane of Figure 3.2 (a) and result in i-$\Phi_{\gamma_{comb}}(-s)$ of Figure 3.3 (b) when κ_{ter} in Figure 3.2 and κ_{sc} in Figure 3.3 equal to 3 dB. A maximum value $\Phi_{\gamma_{comb}}(-s)$ as shown in this Figure occurs at i = 1 and j = 5. Previously, the results decrease and become to 0. Moreover, the majority of $\Phi_{\gamma_{comb}}(-s)$ occurs at i = 0 to 6 and j = 0 to 12.

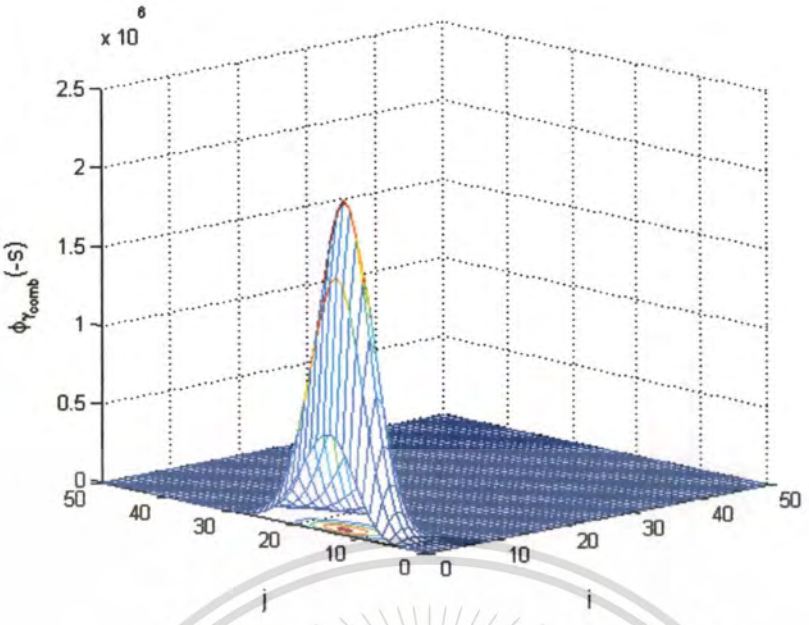

(a) 3-Dimensional (i-j-$\Phi_{\gamma_{comb}}(-s)$ plane).

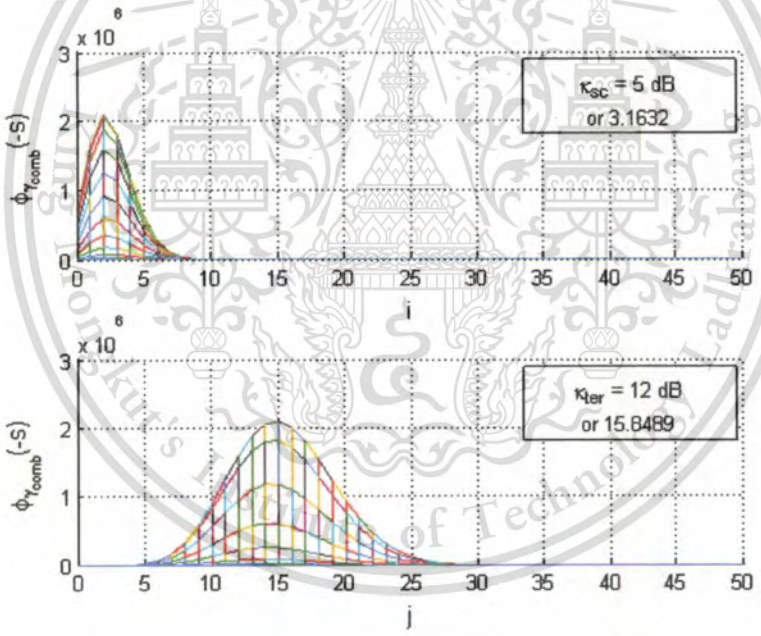

(b) 2-Dimensional (i-$\Phi_{\gamma_{comb}}(-s)$ plane and j-$\Phi_{\gamma_{comb}}(-s)$ plane).

Figure 3.4 The results from (3.10) in Rician factor parameters κ_{sc} = 5 dB and κ_{ter} = 12 dB.

The results from (3.10) when Rician factor parameters κ_{sc} = 5 dB and κ_{ter} = 12 dB are shown in Figure 3.4. As seen from Figure, a maximum value occurs at i = 3 and j = 15. After that, the results also decrease and become to 0. In this case, the majority of $\Phi_{\gamma_{comb}}(-s)$ occurs at about i = 0 to 8 and j = 5 to 29.

As seen in Figure 3.1-Figure 3.4, the behaviour of (3.10) that depend on the some values of Rician factor κ_{sc} and κ_{ter} in 3-dimensional (X-Y-Z plane or i-j-$\Phi_{\gamma_{comb}}(-s)$), and 2-dimensional (X-Z plane or i-$\Phi_{\gamma_{comb}}(-s)$ and Y-Z plane or j-$\Phi_{\gamma_{comb}}(-s)$) are illustrated. Interestingly, from these Figures, the relevant terms of the series in (3.10) are continuous and the dispersion characteristic becomes large when κ_{sc} and κ_{ter} increase. The maximum value of the results occurs at $i=\lfloor \kappa_{sc} \rfloor$ and $j=\lfloor \kappa_{ter} \rfloor$, where $\lfloor x \rfloor$ is the flooring operation. While the results occur near $i=\lfloor \kappa_{sc} \rfloor$ and $j=\lfloor \kappa_{ter} \rfloor$ gradually decrease to the point where they become 0.

The series of (3.10) can be rewritten as

$$\begin{aligned}\Phi_{\gamma_{comb}}(-s) &= \exp(-\kappa_{sc}-\kappa_{ter})\cdot[\alpha] \\ &= \exp(-\kappa_{sc}-\kappa_{ter})\cdot[\tilde{\alpha}+\varepsilon],\end{aligned} \tag{3.11}$$

where

$$\alpha = \sum_{i=0}^{\infty}\sum_{j=0}^{\infty}\frac{\kappa_{sc}^{i}\kappa_{ter}^{j}}{i!\,j!}\,{}_2F_0\left(i+1,j+1;\ ;-\frac{\bar{\gamma}_{comb}s}{(\kappa_{sc}+1)(\kappa_{ter}+1)}\right), \tag{3.12}$$

$$\tilde{\alpha} = \sum_{i=i_{\min}}^{i_{\max}}\sum_{j=j_{\min}}^{j_{\max}}\frac{\kappa_{sc}^{i}\kappa_{ter}^{j}}{i!\,j!}\,{}_2F_0\left(i+1,j+1;\ ;-\frac{\bar{\gamma}_{comb}s}{(\kappa_{sc}+1)(\kappa_{ter}+1)}\right), \tag{3.13}$$

$$\varepsilon = \sum_{\substack{i=0 \\ i\notin[i_{\min},i_{\max}]}}^{\infty}\sum_{\substack{j=0 \\ j\notin[j_{\min},j_{\max}]}}^{\infty}\frac{\kappa_{sc}^{i}\kappa_{ter}^{j}}{i!\,j!}\,{}_2F_0\left(i+1,j+1;\ ;-\frac{\bar{\gamma}_{comb}s}{(\kappa_{sc}+1)(\kappa_{ter}+1)}\right), \tag{3.14}$$

Note that the term $\tilde{\alpha}$ in (3.13) is an approximation of the term α in (3.12). Appromixation error can be reduced by adjusting the error term ε. We would like to choose the range of double summation $[i_{\min}, i_{\max}]$ and $[j_{\min}, j_{\max}]$ so that the sharper estimate can be obtained, i.e., $\varepsilon \to 0$

Based on the observation from Figure 3.1 - Figure 3.4, the desirable choices of the interval $[i_{\min}, i_{\max}]$ and $[j_{\min}, j_{\max}]$ to approximate $\Phi_{\gamma_{comb}}(-s)$ are

$$i_{\min} = \max\{0, \lfloor \kappa_{sc} - \varphi_{sc} \rfloor\} \quad \text{and} \quad i_{\max} = \lceil \kappa_{sc} + \varphi_{sc} \rceil, \tag{3.15}$$

and

$$j_{\min} = \max\left\{0, \lfloor \kappa_{ter} - \varphi_{ter} \rfloor\right\} \text{ and } j_{\max} = \lceil \kappa_{ter} + \varphi_{ter} \rceil, \tag{3.16}$$

where $\lceil x \rceil$ is the ceiling operation and the variables φ_{sc} and φ_{ter} are the inverse values of the standard deviation of Rician distribution κ_{sc} and κ_{ter}, respectively, as expressed by

$$\varphi_{sc} = \frac{\eta}{\sigma_{sc}} = \eta\sqrt{2(\kappa_{sc}+1)}, \tag{3.17}$$

$$\varphi_{ter} = \frac{\eta}{\sigma_{ter}} = \eta\sqrt{2(\kappa_{ter}+1)}. \tag{3.18}$$

Suitable values of η can be determined from the approximation error from using $\tilde{\alpha}$ instead of α. In Table 3.1, we compare the percentage error of the estimate $\tilde{\alpha}$ from α for various κ_{sc} and κ_{ter}.

The values of α are considered with the range of summation from 0 to 50 for both i and j indices as they are within acceptable accuracy below 1×10^{-8}%. It is evident that in general for larger κ_{sc} and κ_{ter}, larger values of η should be selected. For the approximation error lower than 0.05%, suitable values of η for Case 1-4 are 1, 2, and 3, respectively. In Figure 3.5, we plot the relationship between percentage of error and the parameter η in a semi-log scale. For the range of κ_{sc} and κ_{ter} under consideration, there is a linear relationship with the upper bound with the slope of 10^{-2} as indicated by the dotted line, i.e.,

$$\text{Percentage of error} = C10^{-2}\eta, \tag{3.19}$$

where C is a constant value. Hence, the percentage of error $\to 0$ as η becomes higher.

Therefore, a good approximation of the exact result in (3.11) can be obtained as

$$\Phi_{\gamma_{comb}}(-s) \approx \exp(-\kappa_{sc}-\kappa_{ter}) \sum_{i=i_{\min}}^{i_{\max}} \sum_{j=j_{\min}}^{j_{\max}} \frac{\kappa_{sc}^{i}\kappa_{ter}^{j}}{i!\,j!}\, {}_2F_0\left(i+1, j+1; ; -\frac{\bar{\gamma}_{comb}s}{(\kappa_{sc}+1)(\kappa_{ter}+1)}\right), \tag{3.20}$$

by neglecting ε. By using (3.20) instead of (3.10), we are able to reduce the computational complexity of the MGF evaluation.

Table 3.1 The approximation in (3.13) with a relative error.

i,j / Rician factor	$\alpha = \sum_{i=0}^{50}\sum_{j=0}^{50}\cdots$	$\tilde{\alpha}(\eta=1)$	$\tilde{\alpha}(\eta=2)$	$\tilde{\alpha}(\eta=3)$
Case 1	0.60839	0.60839	0.60839	0.60839
κ_{sc} **= 0 (Rayleigh)** κ_{ter} **= 0 (Rayleigh)**		Error 1.3e-05 %	Error 2.67e-08 %	Error 7.3e-014 %
Case 2	4.18579	4.1480	4.1837	4.1858
κ_{sc} **= 0 (Rayleigh)** κ_{ter} **= 3 dB (1.9953)**		Error 0.903 %	Error 0.0499 %	Error 3.0e-04 %
Case 3	5.49119e+002	5.28904e+002	5.48405e+002	5.49114e+002
κ_{sc} **= 3 dB (1.9953)** κ_{ter} **= 7 dB (5.0119)**		Error 3.6814 %	Error 0.13 %	Error 9.31e-04 %
Case 4	8.20002e+007	7.3196e+007	8.18580e+007	8.19989e+007
κ_{sc} **= 5 dB (3.1632)** κ_{ter} **= 12 dB (15.8489)**		Error 10.74 %	Error 0.1733 %	Error 0.0015 %

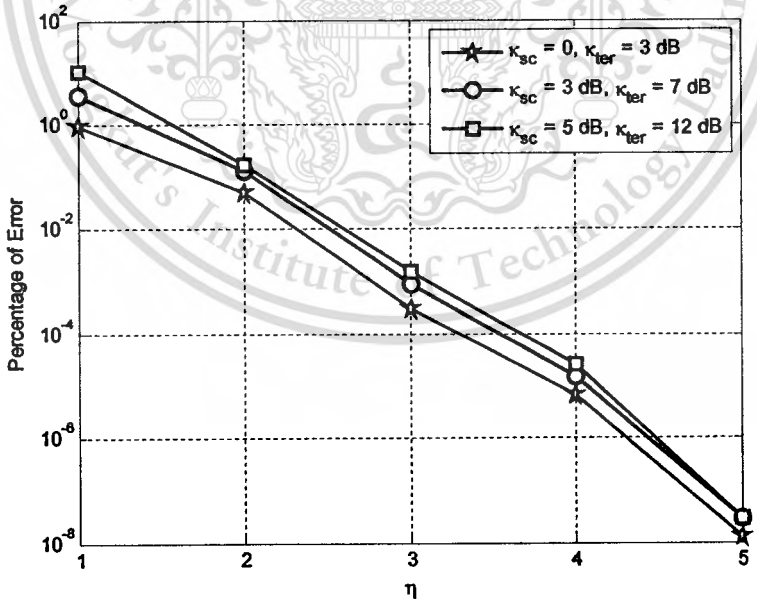

Figure 3.5 Percentage of error compares with η for some κ_{sc} and κ_{ter}.

The result as shown in Table 3.1 indicate that we can approximate the series expansion using (3.13) with a relative error that is well below 1% at least when $\eta = 2$.

In addition, the MGF result of combined Rician fading channel in (3.10) can be analyzed depending on the Rician factor (κ_{sc} and κ_{ter}). They are summarized as shown in Figure 3.6 and listed as special cases below.

Special cases

- **Case 1: $\kappa_{sc} \neq 0$ and $\kappa_{ter} \to 0$.** This means that one of channels is Rayleigh fading when either Rician factor goes to zero, the MGF in (3.10) reduced to a single summation as

$$\Phi_{\gamma_{comb}}(-s) = \exp(-\kappa_{sc}) \sum_{i=0}^{\infty} \frac{\kappa_{sc}^{i}}{i!} {}_2F_0\left(i+1, 1; \; ; -\frac{\overline{\gamma}_{comb} s}{(\kappa_{sc}+1)} \right). \tag{3.21}$$

This result is the MGF for *combined Rician×Rayleigh fading channel.* Similar result can also be obtained when $\kappa_{ter} \neq 0$ and $\kappa_{sc} \to 0$.

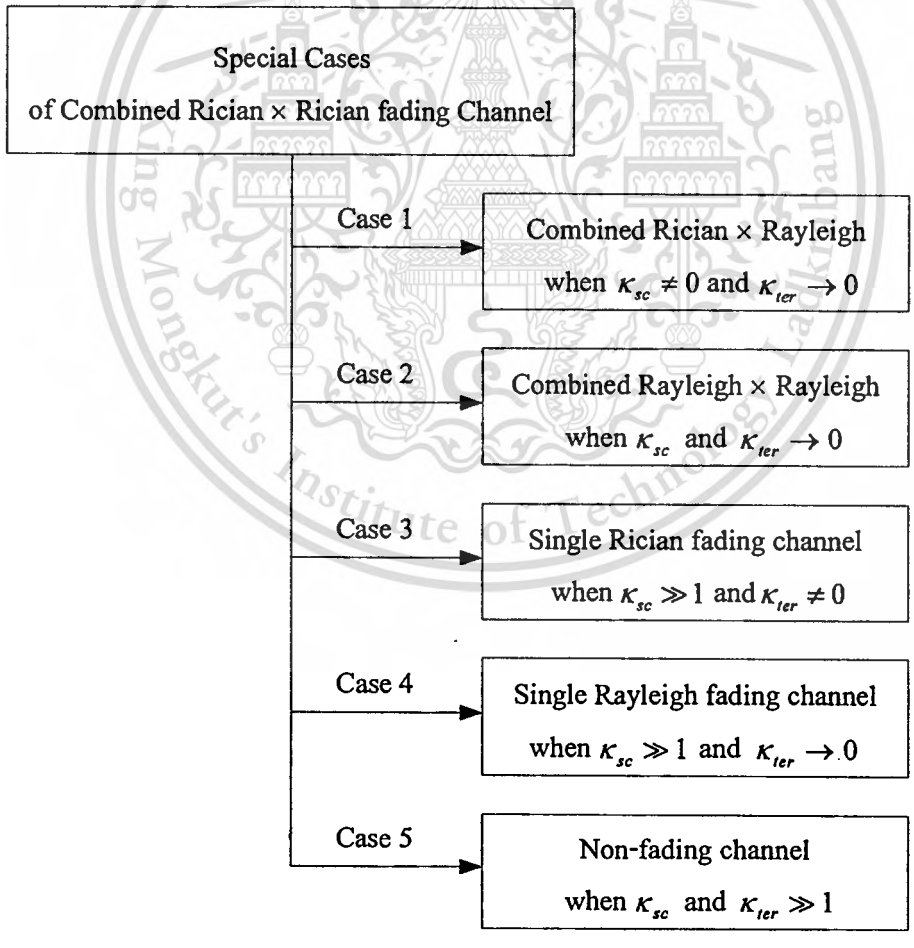

Figure 3.6 Special cases of combined Rician×Rician fading channel.

- **Case 2: κ_{sc} and $\kappa_{ter} \to 0$.** This case means both channels are Rayleigh fading channel, the MGF in (3.10) can be reduced to

$$\Phi_{\gamma_{comb}}(-s) = {}_2F_0\left(1,1;\ ;-\overline{\gamma}_{comb}s\right). \tag{3.22}$$

This result is the MGF for *combined Rayleigh×Rayleigh fading channel.*

- **Case 3: $\kappa_{sc} >> 1$ and $\kappa_{ter} \neq 0$.** In this case, the double summation in (3.10) can be approximated by

$$\begin{aligned}\sum_{i=0}^{\infty}\sum_{j=0}^{\infty}\frac{\kappa_{sc}^{i}\kappa_{ter}^{j}}{i!\,j!}\,{}_2F_0\left(i+1,j+1;;-\frac{\overline{\gamma}_{comb}s}{(\kappa_{sc}+1)(\kappa_{ter}+1)}\right)\\ \approx \exp(\kappa_{sc})\sum_{j=0}^{\infty}\frac{\kappa_{ter}^{j}}{j!}\,{}_2F_0\left(\kappa_{sc}+1,j+1;;-\frac{\overline{\gamma}_{comb}s}{(\kappa_{sc}+1)(\kappa_{ter}+1)}\right).\end{aligned} \tag{3.23}$$

To show (3.23), we use the numerical observation that, for $\kappa_{sc} >> 1$ and fixed j, the ${}_2F_0\left(i+1,j+1;;-\frac{\overline{\gamma}_{comb}s}{(\kappa_{sc}+1)(\kappa_{ter}+1)}\right)$ term is an approximately constant function of i, so we write it as ${}_2F_0\left(\kappa_{sc}+1,j+1;;-\frac{\overline{\gamma}_{comb}s}{(\kappa_{sc}+1)(\kappa_{ter}+1)}\right)$. By using the relation

$$\exp(\kappa_{sc}) = \sum_{i=0}^{\infty}\frac{\kappa_{sc}^{i}}{i!}, \tag{3.24}$$

and using the following reduction formula [41]

$$\lim_{a\to\infty}\ {}_pF_q\left(a,a_2,\ldots,a_p;b_1,\ldots,b_q;\frac{z}{a}\right) = {}_{p-1}F_q\left(a_2,\ldots,a_p;b_1,\ldots,b_q;z\right), \tag{3.25}$$

to write ${}_2F_0(a,b;;z)$ as ${}_1F_0\left(a;;z\right)$, (3.23) becomes

$$\begin{aligned}\sum_{i=0}^{\infty}\sum_{j=0}^{\infty}\frac{\kappa_{sc}^{i}\kappa_{ter}^{j}}{i!\,j!}\,{}_2F_0\left(i+1,j+1;;-\frac{\overline{\gamma}_{comb}s}{(\kappa_{sc}+1)(\kappa_{ter}+1)}\right)\\ \approx \exp(\kappa_{sc})\sum_{j=0}^{\infty}\frac{\kappa_{ter}^{j}}{j!}\,{}_1F_0\left(j+1;;-\frac{\overline{\gamma}_{comb}s}{(\kappa_{ter}+1)}\right).\end{aligned} \tag{3.26}$$

where the expression of ${}_1F_0\left(a;;z\right)$ in the series form is [42]

$$ {}_1F_0(a;;z)=\sum_{k=0}^{\infty}\frac{(a)_k}{k!}z^k=(1-z)^{-a}; \qquad |z|<1. \tag{3.27} $$

As a result, (3.23) can be expressed without the infinite summation as

$$ \begin{aligned} \sum_{i=0}^{\infty}\sum_{j=0}^{\infty}\frac{\kappa_{sc}^{i}\kappa_{ter}^{j}}{i!\,j!}\,{}_2F_0\left(i+1,j+1;;-\frac{\overline{\gamma}_{comb}s}{(\kappa_{sc}+1)(\kappa_{ter}+1)}\right) \\ \approx\sum_{j=0}^{\infty}\frac{\kappa_{ter}^{j}}{j!}\left[\exp(\kappa_{sc})\left(1+\frac{\overline{\gamma}_{comb}s}{(\kappa_{ter}+1)}\right)^{-j-1}\right] \\ \approx\exp(\kappa_{sc})\exp\left(\frac{\kappa_{ter}}{1+\frac{\overline{\gamma}_{comb}s}{(\kappa_{ter}+1)}}\right)\left(\frac{1}{1+\frac{\overline{\gamma}_{comb}s}{(\kappa_{ter}+1)}}\right). \end{aligned} \tag{3.28} $$

Substituting (3.28) into (3.10), we obtain the MGF for the case of $\kappa_{sc} >> 1$ and $\kappa_{ter} \neq 0$ as

$$ \begin{aligned} \Phi_{\gamma_{comb}}(-s)&\approx\exp(-\kappa_{ter})\exp\left(\frac{\kappa_{ter}}{1+\frac{\overline{\gamma}_{comb}s}{(\kappa_{ter}+1)}}\right)\left(\frac{1}{1+\frac{\overline{\gamma}_{comb}s}{(\kappa_{ter}+1)}}\right) \\ &\approx\exp\left(-\frac{\kappa_{ter}\overline{\gamma}_{comb}s}{(\kappa_{ter}+1)+\overline{\gamma}_{comb}s}\right)\left(\frac{(\kappa_{ter}+1)}{(\kappa_{ter}+1)+\overline{\gamma}_{comb}s}\right). \end{aligned} \tag{3.29} $$

As expected, when $\kappa_{sc} >> 1$, the MGF in (3.29) approaches that a *single Rician fading channel* with Rician factor κ_{ter} [43]. Similar result can also be obtained when $\kappa_{ter} >> 1$ and $\kappa_{sc} \neq 0$.

- **Case 4: $\kappa_{sc} >> 1$ and $\kappa_{ter} \to 0$.** By using the method as used in case 3 and using the relation (3.24), (3.25), and (3.27), the summation term in (3.10) when $\kappa_{sc} >> 1$ can be approximated as

$$ \begin{aligned} \sum_{i=0}^{\infty}\sum_{j=0}^{\infty}\frac{\kappa_{sc}^{i}\kappa_{ter}^{j}}{i!\,j!}\,{}_2F_0\left(i+1,j+1;;-\frac{\overline{\gamma}_{comb}s}{(\kappa_{sc}+1)(\kappa_{ter}+1)}\right) \\ \approx\sum_{i=0}^{\infty}\frac{\kappa_{sc}^{i}}{i!}\,{}_2F_0\left(i+1,1;;-\frac{\overline{\gamma}_{comb}s}{(\kappa_{sc}+1)}\right) \\ \approx\sum_{i=0}^{\infty}\frac{\kappa_{sc}^{i}}{i!}\,{}_2F_0\left(\kappa_{sc}+1,1;;-\frac{\overline{\gamma}_{comb}s}{(\kappa_{sc}+1)}\right) \\ \approx\sum_{i=0}^{\infty}\frac{\kappa_{sc}^{i}}{i!}\,{}_1F_0\left(1;;-\overline{\gamma}_{comb}s\right) \\ \approx\exp(\kappa_{sc})\frac{1}{(1+\overline{\gamma}_{comb}s)}. \end{aligned} \tag{3.30} $$

Substituting (3.30) into (3.10), the MGF in this case becomes

$$\Phi_{\gamma_{comb}}(-s) \approx (1+\bar{\gamma}_{comb}s)^{-1}. \tag{3.31}$$

As a result, the MGF in this case is the MGF of *single Rayleigh fading channel*[43].

- **Case 5: κ_{sc} and κ_{ter} >> 1.** The method which used in case 3 can be used to obtain approximation when both Rician factor κ_{sc} and κ_{ter} >> 1, in which case the double summation in (3.10) can be approximated as

$$\begin{aligned}\sum_{i=0}^{\infty}\sum_{j=0}^{\infty}\frac{\kappa_{sc}^{i}\kappa_{ter}^{j}}{i!\,j!}\,{}_2F_0\left(i+1,j+1;;-\frac{\bar{\gamma}_{comb}s}{(\kappa_{sc}+1)(\kappa_{ter}+1)}\right)&\\ \approx \exp(\kappa_{sc}+\kappa_{ter})\,{}_2F_0\left(\kappa_{sc}+1,\kappa_{ter}+1;;-\frac{\bar{\gamma}_{comb}s}{(\kappa_{sc}+1)(\kappa_{ter}+1)}\right)&\\ \approx \exp(\kappa_{sc}+\kappa_{ter})\,{}_0F_0(\,;;-\bar{\gamma}_{comb}s).&\end{aligned} \tag{3.32}$$

where the function ${}_0F_0(\,;;z)$ can be defined by [40],[42]

$${}_0F_0(\,;;z)=\sum_{k=0}^{\infty}\frac{z^k}{k!}=\exp(z). \tag{3.33}$$

Consequently, the approximation in (3.32) can be rewritten as

$$\sum_{i=0}^{\infty}\sum_{j=0}^{\infty}\frac{\kappa_{sc}^{i}\kappa_{ter}^{j}}{i!\,j!}\,{}_2F_0\left(i+1,j+1;;-\frac{\bar{\gamma}_{comb}s}{(\kappa_{sc}+1)(\kappa_{ter}+1)}\right)\approx\exp(\kappa_{sc}+\kappa_{ter})\exp(-\bar{\gamma}_{comb}s). \tag{3.34}$$

By using this approximation, the MGF in (3.10) becomes

$$\Phi_{\gamma_{comb}}(-s)\approx\exp(-\bar{\gamma}_{comb}s). \tag{3.35}$$

The MGF in this case approaches the MGF of non-fading or *AWGN channel* with $\bar{\gamma}_{comb}=\gamma_{comb}$.

3.1.2 MGF of Instantaneous SNR of Combined Nakagami-*m*×Nakagami-*m* Fading Channels

In this Subsection, we derive the MGF of instantaneous SNR per bit of combined Nakagami-*m* fading channels by replacing $p_{\Gamma_{comb}}(\gamma_{comb})$ in term of Nakagami-*m* distribution in (3.1) with (2.47), we obtain

$$\Phi_{\gamma_{comb}}(-s)=\frac{2}{\Gamma(m_{sc})\Gamma(m_{ter})}\left(\sqrt{\frac{m_{sc}m_{ter}}{\overline{\gamma}_{comb}}}\right)^{m_{sc}+m_{ter}} \cdot\int_0^{\infty}\gamma_{comb}^{\frac{m_{sc}+m_{ter}}{2}-1}\exp(-s\gamma_{comb})\cdot K_{m_{sc}-m_{ter}}\left\{2\sqrt{\frac{m_{sc}m_{ter}\gamma_{comb}}{\overline{\gamma}_{comb}}}\right\}d\gamma_{comb}. \tag{3.36}$$

Using the relation [37, Eq. (6.643.3)], The integral term on the right side of (3.36) can be expressed in terms of the Whittaker-*W* function, and with the function $\Gamma(\cdot)$ cancelled out, (3.36) becomes

$$\Phi_{\gamma_{comb}}(-s)=\left(\sqrt{\frac{m_{sc}m_{ter}}{\overline{\gamma}_{comb}s}}\right)^{m_{sc}+m_{ter}-1}\exp\left[\frac{m_{sc}m_{ter}}{2\overline{\gamma}_{comb}s}\right]\cdot W_{-\frac{1}{2}(m_{sc}+m_{ter}-1),\frac{1}{2}(m_{sc}-m_{ter})}\left(\frac{m_{sc}m_{ter}}{\overline{\gamma}_{comb}s}\right). \tag{3.37}$$

Now, we simplify the expression (3.37). Applying the relations of the Whittaker-*W* function with the confluent hypergeometric function of the second kind $\Psi(a,b;z)$ in (3.5) [39, Eq. (13.3.33)], and the generalized hypergeometric function ${}_2F_0(a,b;;z)$ in (3.8) [39, Eq. (13.1.10)]. We have a final result of the MGF in (3.37), after cancelling some terms, in terms of a generalized hypergeometric function ${}_2F_0(a,b;;z)$ as

$$\Phi_{\gamma_{comb}}(-s)={}_2F_0\left(m_{sc},m_{ter};\ ;-\frac{\overline{\gamma}_{comb}s}{m_{sc}m_{ter}}\right). \tag{3.38}$$

Alternatively, in [44], this final result can be expressed in terms of the Meijer's *G*-function [37, Eq. (9.34.8)].

The resulting MGF of combined Nakagami-*m* fading channels in (3.38) will be investigated next for five special cases depending on the Nakagami-*m* shape factor (m_{sc} and m_{ter}). They are summarized as shown in Figure 3.7 and listed as special cases below.

Special cases

- **Case 1:** m_{sc} **or** $m_{ter} = 1$. If $m_{ter} = 1$, then the MGF in (3.38) becomes

$$\Phi_{\gamma_{comb}}(-s) = {}_2F_0\left(m_{sc}, 1; \; ; -\frac{\overline{\gamma}_{comb} s}{m_{ter}}\right). \tag{3.39}$$

Similar result can also be obtained when $m_{sc} = 1$. This result is the MGF for *combined Nakagami-m×Rayleigh fading channel.*

- **Case 2:** m_{sc} *and* $m_{ter} = 1$. In this case, both fading channels have Rayleigh distribution. The MGF in (3.38) becomes

$$\Phi_{\gamma_{comb}}(-s) = {}_2F_0\left(1,1; \; ; -\overline{\gamma}_{comb} s\right). \tag{3.40}$$

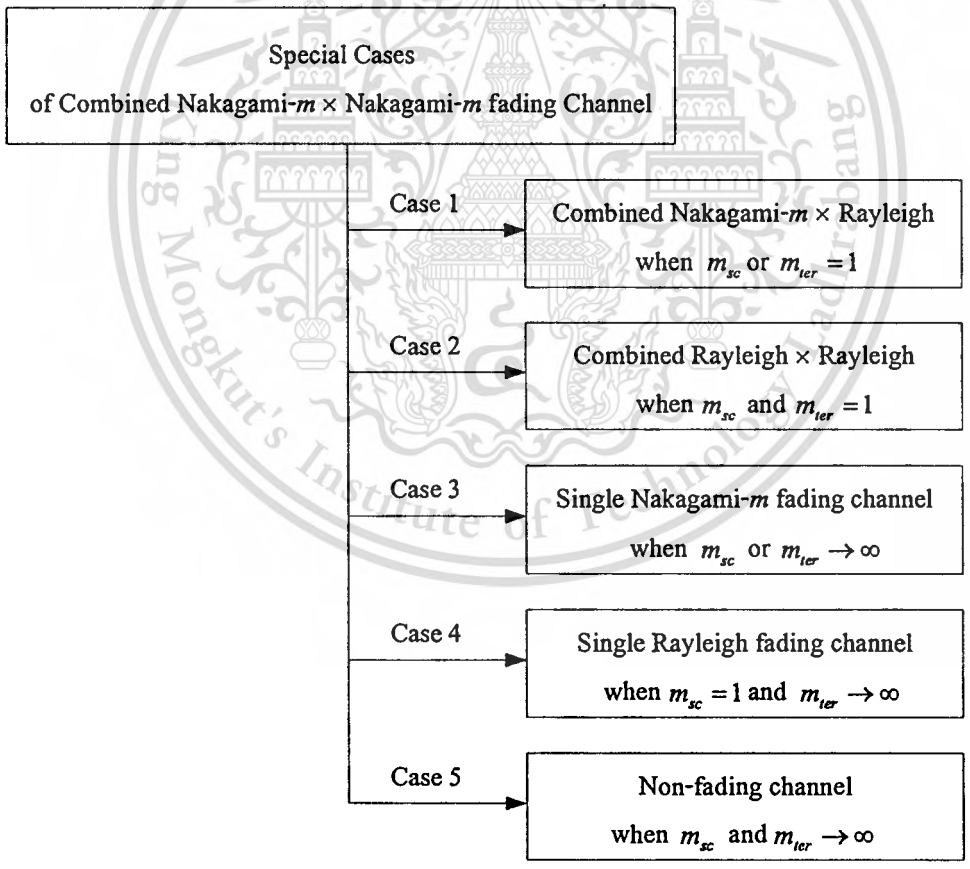

Figure 3.7 Special cases of combined Nakagami-*m*×Nakagami-*m* fading channel.

This result is the MGF for *combined Rayleigh×Rayleigh fading channel.* This result is similar to case 2 of combined Rician×Rician when κ_{sc} and $\kappa_{ter} \to 0$.

- **Case 3: either m_{sc} or $m_{ter} \to \infty$.** This means that one of channels is Nakagami-*m* fading channel, while the other is non-fading channel. By using the reduction formula in (3.25) with $m_{ter} \to \infty$, the MGF in (3.38) reduces to

$$\Phi_{\gamma_{comb}}(-s) = {}_1F_0\left(m_{sc}; ; -\frac{\overline{\gamma}_{comb}s}{m_{sc}}\right). \tag{3.41}$$

Alternatively, by expressing ${}_1F_0(a;;z)$ as the series as shown in (3.27), (3.41) can be rewritten as

$$\Phi_{\gamma_{comb}}(-s) = \left(1+\frac{\overline{\gamma}_{comb}s}{m_{sc}}\right)^{-m_{sc}}. \tag{3.42}$$

As a result, the MGF for this case is the MGF of a *single Nakagami-m fading channel* [43].

- **Case 4: $m_{sc} = 1$ and $m_{ter} \to \infty$.** This means that one of channels is Rayleigh fading channel, while the other is non-fading channel. By using the reduction formula in (3.25), (3.38) becomes

$$\Phi_{\gamma_{comb}}(-s) = (1+\overline{\gamma}_{comb}s)^{-1}, \tag{3.43}$$

which is the MGF of a *single Rayleigh fading channel* [43]. We can see the similarity between this result and the result from case 4 of combined Rician×Rician when $\kappa_{sc} >> 1$ and $\kappa_{ter} \to 0$.

- **Case 5: m_{sc} and $m_{ter} \to \infty$.** This means both channels are non-fading channels, thus, (3.38) becomes

$$\Phi_{\gamma_{comb}}(-s) = {}_0F_0(\,;\,;-\overline{\gamma}_{comb}s). \tag{3.44}$$

Using the series expression of function ${}_0F_0(\,;;z)$ [40],[42] as shown in (3.33), the MGF in (3.44) then becomes

$$\Phi_{\gamma_{comb}}(-s) = \exp(-\overline{\gamma}_{comb}s), \tag{3.45}$$

which is the MGF of non-fading channel or *AWGN channel* with $\overline{\gamma}_{comb} = \gamma_{comb}$ and similar to the result from case 5 of combined Rician×Rician when κ_{sc} and $\kappa_{ter} >> 1$.

The MGF results of combined Rician×Rician and combined Nakagami-*m*×Nakagami-*m* fading channel are tabulated for each special case in Table 3.2-Table 3.3.

Table 3.2 The MGFs of Instantaneous SNR of Combined Rician Fading Channels.

Case of κ_{sc} and κ_{ter}	The MGF of Instantaneous SNR $\Phi_{\gamma_{comb}}(-s)$
κ_{sc} and $\kappa_{ter} \neq 0$ (Rician × Rician)	$\Phi_{\gamma_{comb}}(-s) = \exp(-\kappa_{sc} - \kappa_{ter}) \sum_{i=0}^{\infty} \sum_{j=0}^{\infty} \frac{\kappa_{sc}^{i} \kappa_{ter}^{j}}{i!\, j!} \cdot {}_2F_0\left(i+1, j+1; \; ; -\frac{\overline{\gamma}_{comb} s}{(\kappa_{sc}+1)(\kappa_{ter}+1)} \right)$
$\kappa_{sc} \neq 0$ and $\kappa_{ter} \to 0$ (Rician × Rayleigh)	$\Phi_{\gamma_{comb}}(-s) = \exp(-\kappa_{sc}) \sum_{i=0}^{\infty} \frac{\kappa_{sc}^{i}}{i!} {}_2F_0\left(i+1, 1; \; ; -\frac{\overline{\gamma}_{comb} s}{(\kappa_{sc}+1)} \right)$
κ_{sc} and $\kappa_{ter} \to 0$ (Rayleigh × Rayleigh)	$\Phi_{\gamma_{comb}}(-s) = {}_2F_0(1, 1; \; ; -\overline{\gamma}_{comb} s)$
$\kappa_{sc} >> 1$ and $\kappa_{ter} \neq 0$ ≈ Single Rician fading (Gaussian × Rician)	$\Phi_{\gamma_{comb}}(-s) \approx \exp\left(-\frac{\kappa_{ter} \overline{\gamma}_{comb} s}{(\kappa_{ter}+1) + \overline{\gamma}_{comb} s} \right) \left(\frac{(\kappa_{ter}+1)}{(\kappa_{ter}+1) + \overline{\gamma}_{comb} s} \right)$
$\kappa_{sc} >> 1$ and $\kappa_{ter} \to 0$ ≈ Single Rayleigh fading (Gaussian × Rayleigh)	$\Phi_{\gamma_{comb}}(-s) \approx (1 + \overline{\gamma}_{comb} s)^{-1}$
κ_{sc} and $\kappa_{ter} >> 1$ (AWGN channel)	$\Phi_{\gamma_{comb}}(-s) \approx \exp(-\overline{\gamma}_{comb} s)$

Table 3.3 The MGFs of Instantaneous SNR of Combined Nakagami-*m* Fading Channels.

Case of m_{sc} and m_{ter}	The MGF of Instantaneous SNR $\Phi_{\gamma_{comb}}(-s)$
m_{sc} and $m_{ter} \neq 0$ (Nakagami-*m* × Nakagami-*m*)	$\Phi_{\gamma_{comb}}(-s) = {}_2F_0\left(m_{sc}, m_{ter}; \; ; -\frac{\overline{\gamma}_{comb} s}{m_{sc} m_{ter}} \right)$
m_{sc} or $m_{ter} = 1$ (Nakagami-*m* × Rayleigh)	$\Phi_{\gamma_{comb}}(-s) = {}_2F_0\left(m_{sc}, 1; \; ; -\frac{\overline{\gamma}_{comb} s}{m_{ter}} \right)$

Table 3.4(cont.) The MGFs of Instantaneous SNR of Combined Nakagami-*m* Fading Channels.

Case of m_{sc} and m_{ter}	The MGF of Instantaneous SNR $\Phi_{\gamma_{comb}}(-s)$
m_{sc} and $m_{ter}=1$ (Rayleigh × Rayleigh)	$\Phi_{\gamma_{comb}}(-s)={}_2F_0(1,1;\ ;-\overline{\gamma}_{comb}s)$
Either m_{sc} or $m_{ter}\to\infty$ Single Nakagami-*m* fading (Gaussian × Nakagami-*m*)	$\Phi_{\gamma_{comb}}(-s)=\left(1+\frac{\overline{\gamma}_{comb}s}{m_{sc}}\right)^{-m_{sc}}$
m_{sc}=1 and $m_{ter}\to\infty$ Single Rayleigh fading (Gaussian × Rayleigh)	$\Phi_{\gamma_{comb}}(-s)=(1+\overline{\gamma}_{comb}s)^{-1}$
m_{sc} and $m_{ter}\to\infty$ (AWGN channel)	$\Phi_{\gamma_{comb}}(-s)\approx\exp(-\overline{\gamma}_{comb}s)$

3.2 Maximal-Ratio Combining (MRC)

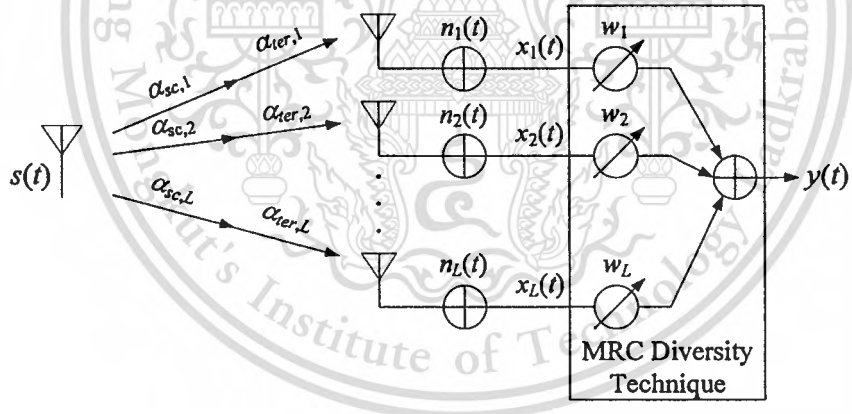

Figure 3.8 System model of *L*-branch MRC receiver diversity over double fading channel.

A communication system with *L*-order MRC receiver diversity combining is shown in Figure 3.8. The transmitted signal $s(t)$ is modulated with some common modulation schemes. The received signal $x_l(t)$ in each diversity branch *assuming slow fading with constant fading loss over each symbol interval*, can be expressed as

$$x_l(t)=\alpha_{comb,l}s(t)+n_l(t). \tag{3.46}$$

The fading coefficient $\alpha_{comb,l}$ in each diversity branch can be expressed as

$$\alpha_{comb,l} = \alpha_{sc,l} \cdot \alpha_{ter,l}, \tag{3.47}$$

where $\alpha_{comb,l}$ is the attenuation due to scintillation and terrestrial multipath fading in each diversity branch and $n_l(t)$ denotes the complex AWGN with zero mean and variance $N_0/2$ per dimension in each branch. The diversity system, in general, refers to a system in which one may have L such copies and it will have fluctuating local statistics in which each $x_l(t)$ is weighted by a weighting coefficient w_l. It will be convenient to consider the weighted sum of the $x_l(t)$ as follows

$$y(t) = w_1 x_1(t) + w_2 x_1(t) + \ldots + w_L x_L(t) = \sum_{l=1}^{L} w_l x_l(t), \tag{3.48}$$

where the weighting coefficient w_k in MRC diversity system is defined by $w_l = \alpha^*_{comb,l}$.

Consequently, the output signal $y(t)$ is the weighted sum of the received signal $x_l(t)$ in each l-th diversity branch, i.e.,[45]

$$\begin{aligned} y(t) &= y_1(t) + y_2(t) + \ldots + y_L(t) = \sum_{l=1}^{L} y_l(t) \\ &= \sum_{l=1}^{L} w_l x_l(t) = \sum_{l=1}^{L} w_l \left(\alpha_{comb,l} s(t) + n_l(t) \right), \end{aligned} \tag{3.49}$$

where each $y_l(t)$, $l = 1, 2, \ldots, L$ represents the corrupted signal in the l-th channel containing the originally transmitted signal $s(t)$. Now in (3.49), let us write

$$a(t) = \sum_{l=1}^{L} w_l \alpha_{comb,l} s(t), \quad \text{and} \quad n(t) = \sum_{l=1}^{L} w_l n_l(t). \tag{3.50}$$

So that $y(t) = a(t) + n(t)$, and $\gamma_T = \overline{a^2} / \overline{n^2}$ is the local power ratio of y or the total instantaneous SNR per bit, where

$$\begin{aligned}\overline{a^2} &= E\left\{\left[\sum_{l=1}^{L} w_l \alpha_{comb,l} s(t)\right]^2\right\} \\ &= E\left\{s^2(t)\left[\sum_{l=1}^{L} w_l \alpha_{comb,l}\right]^2\right\} \\ &= E\left\{s^2(t)\right\}\left[\sum_{l=1}^{L} w_l \alpha_{comb,l}\right]^2,\end{aligned} \tag{3.51}$$

and since $\left[\sum_{l=1}^{L} w_l \alpha_{comb,l}\right]^2$ is locally constant and can be taken outside the average and since $E\left\{s^2(t)\right\} = E_b$, so

$$\overline{a^2} = E_b\left[\sum_{l=1}^{L} w_l \alpha_{comb,l}\right]^2. \tag{3.52}$$

Furthermore,

$$\begin{aligned}\overline{n^2} &= E\left\{\left[\sum_{l=1}^{L} w_l n_l(t)\right]^2\right\} \\ &= \sum_{l=1}^{L} \overline{w_l^2 n_l^2(t)} \\ &= \sum_{l=1}^{L} w_l^2 \overline{n_l^2(t)} \\ &= N_0 \sum_{l=1}^{L} w_l^2.\end{aligned} \tag{3.53}$$

By using a mathematical device known as the Schwarz inequality, [45]

$$\left[\sum_{l=1}^{L} w_l \alpha_{comb,l}\right]^2 \le \left[\sum_{l=1}^{L} w_l^2\right]\left[\sum_{l=1}^{L} \alpha_{comb,l}^2\right]. \tag{3.54}$$

Hence,[45]

$$\gamma_T = \frac{E_b\left[\sum_{l=1}^{L} w_l \alpha_{comb,l}\right]^2}{N_0 \sum_{l=1}^{L} w_l^2} \le \frac{E_b}{N_0} \frac{\left[\sum_{l=1}^{L} w_l^2\right]\left[\sum_{l=1}^{L} \alpha_{comb,l}^2\right]}{\left[\sum_{l=1}^{L} w_l^2\right]}. \tag{3.55}$$

With MRC receiver diversity, the total instantaneous SNR per bit γ_T at the output of the MRC receiver is

$$\begin{aligned}\gamma_T &= \frac{E_b}{N_0}\left[\sum_{l=1}^{L}\alpha_{comb,l}^2\right] \\ &= \frac{E_b}{N_0}\left[\sum_{l=1}^{L}\left|\alpha_{sc,l}\right|^2\cdot\left|\alpha_{ter,l}\right|^2\right] \\ &= \sum_{l=1}^{L}\gamma_{comb,l}.\end{aligned} \tag{3.56}$$

Thus, the instantaneous received SNR per bit in each diversity branch $\gamma_{comb,l}$ is defined as

$$\gamma_{comb,l} = \frac{E_b}{N_0}\left|\alpha_{sc,l}\right|^2\cdot\left|\alpha_{ter,l}\right|^2, \tag{3.57}$$

and the average SNR $\overline{\gamma}_{comb,l}$ is

$$\overline{\gamma}_{comb,l} = \frac{E_b}{N_0}\Omega_{comb,l} = \frac{E_b}{N_0}\Omega_{sc,l}\cdot\Omega_{ter,l}. \tag{3.58}$$

Given that the random variables $\{\gamma_k\}_{k=1}^{L}$ are statistically independent, the joint PDF of instantaneous SNR can be expressed as

$$p_{\Gamma_T}(\gamma_T) = p_{\Gamma_{comb,1},\Gamma_{comb,2},\ldots,\Gamma_{comb,L}}(\gamma_{comb,1},\gamma_{comb,2},\ldots,\gamma_{comb,L}) = \prod_{l=1}^{L} p_{\Gamma_{comb,l}}\left(\gamma_{comb,l}\right). \tag{3.59}$$

3.3 Average BEP over Combined Fading Channels

The average BEP $P_b(E)$ for various digital modulation schemes with Gray code mapping can be obtained by averaging the conditional BEP over the PDF's of total instantaneous SNR per bit, γ_T, i.e.,

$$P_b(E) = \frac{1}{\log_2 M}\int_0^{\infty} P(E\,|\,\gamma_T)\,p_{\Gamma_T}(\gamma_T)\,d\gamma_T, \tag{3.60}$$

where $P_b(E|\gamma_T)$ is the conditional BEP of linear modulation in AWGN channel. Throughout the thesis, we define the conditional BEP for some common modulation schemes and coherent rectangular quadrature amplitude modulation (QAM)

3.3.1 Average BEP for some common modulation schemes

In this Subsection, we defined the conditional BEP for some common modulation sechmes depending on the parameter a and g as

$$P_b(E|\gamma_T) = aQ\left(\sqrt{2g\gamma_T \log_2 M}\right), \tag{3.61}$$

where $Q(\cdot)$ is the Gaussian Q-function which is defined by

$$Q(x) = \frac{1}{\sqrt{2\pi}} \int_x^\infty \exp\left(-\frac{t^2}{2}\right) dt, \tag{3.62}$$

and $M = 2^b$ where b is the number of bits/symbol. The values of a and g for some common modulation schemes are tabulated in Table 3.5 [43], [46],[47].

Moreover, the Gaussian Q-function can be alternatively defined in the definite integral form as [11]

$$Q(x) = \frac{1}{\pi} \int_0^{\pi/2} \exp\left(-\frac{x^2}{2\sin^2\theta}\right) d\theta. \tag{3.63}$$

Using (3.56) and (3.63), the conditional BEP in (3.61) can thus be rewritten in a product form as

$$\begin{aligned} P_b(E|\gamma_T) &= \frac{a}{\pi} \int_0^{\pi/2} \exp\left(-\frac{g\gamma_T \log_2 M}{\sin^2\theta}\right) d\theta \\ &= \frac{a}{\pi} \int_0^{\pi/2} \prod_{l=1}^{L} \exp\left(-\frac{g\gamma_{comb,l} \log_2 M}{\sin^2\theta}\right) d\theta. \end{aligned} \tag{3.64}$$

Substituting (3.59) and (3.64) in (3.60), the average BEP becomes

$$P_b(E)=\frac{1}{\log_2 M}\underbrace{\int_0^{\infty}\int_0^{\infty}\cdots\int_0^{\infty}}_{L\text{-flod}}\frac{a}{\pi}$$
$$\cdot\int_0^{\pi/2}\prod_{l=1}^{L}\exp\left(-\frac{g\gamma_{comb,l}\log_2 M}{\sin^2\theta}\right)d\theta\cdot\prod_{l=1}^{L}p_{\Gamma_{comb,l}}(\gamma_{comb,l})d\gamma_{comb,1}d\gamma_{comb,2},\ldots,d\gamma_{comb,L}. \quad (3.65)$$

Table 3.5 The value of a and g for some common modulation schemes.

Modulation schemes	a	g
Coherent Binary Phase-Shift Keying (BPSK)*	1	1
Binary Minimum Shift Keying (BMSK)*	1	0.85
Coherent Binary Frequency-Shift Keying (BFSK) with minimum correlation*	1	0.715
Coherent Binary Frequency-Shift Keying (BFSK)*	1	0.5
Coherent Binary Amplitude-Shift Keying (BASK)*	1	0.25
Coherent M-ary Phase-Shift Keying (M-PSK)	2	$\sin^2\frac{\pi}{M}$
Coherent M-ary Amplitude-Shift Keying (M-ASK)	$\frac{2(M-1)}{M}$	$\frac{3}{(M^2-1)}$
Coherent π/4 Differentially Encoded 4-ary Phase-Shift Keying (π/4 DQPSK)	1	$\sin^2\frac{\pi}{4\sqrt{2}}$
Coherent Differentially Encoded M-ary Phase-Shift Keying (M-DPSK)	2	$\sin^2\frac{\pi}{M\sqrt{2}}$

*For Binary signals, $M=2$.

Interchanging the order of integration and grouping terms of index l, we obtain

$$P_b(E)=\frac{a}{\pi\log_2 M}\int_0^{\pi/2}\left[\prod_{l=1}^{L}\int_0^{\infty}\exp\left(-\frac{g\gamma_{comb,l}\log_2 M}{\sin^2\theta}\right)p_{\Gamma_{comb,l}}(\gamma_{comb,l})d\gamma_{comb,l}\right]d\theta$$
$$=\frac{a}{\pi\log_2 M}\int_0^{\pi/2}\prod_{l=1}^{L}\Phi_{\gamma_{comb,l}}\left(-\frac{g\log_2 M}{\sin^2\theta}\right)d\theta \quad (3.66)$$
$$=\frac{a}{\pi\log_2 M}\int_0^{\pi/2}\Phi_{\gamma_T}\left(-\frac{g\log_2 M}{\sin^2\theta}\right)d\theta.$$

Note that the results in the aforementioned cases for combined Rician×Rician and combined Nakagami-*m*×Nakagami-*m* fading channel as shown in Subsection 3.1.1 and 3.1.2 are the MGF of received SNR in each branch. Under the assumption that the fading in each branch is identically distributed under the same average SNR per bit $\bar{\gamma}$ and the same fading severity for all channels, the MGF of γ_T [43] can be written as

$$\Phi_{\gamma_T}(-s)=\prod_{l=1}^{L}\Phi_{\gamma_{comb,l}}(-s)=\left[\Phi_{\gamma_{comb,l}}(-s)\right]^{L}. \tag{3.67}$$

By using the MGF of γ_T in (3.67) under the assumption of the fading in each branch is identically distributed under the same average SNR per bit $\bar{\gamma}$ and the same fading severity for all channels, the average BEP of digital modulation schemes over combined Rician×Rician and combined Nakagami-*m*×Nakagami-*m* fading channel with MRC diversity can be calculated from:

3.3.1.1 Average BEP Formula over Combined Rician×Rician Fading Channel.

$$P_b(E)=\frac{a}{\pi\log_2 M}\cdot\int_0^{\pi/2}\left[\exp\left(-\kappa_{sc}-\kappa_{ter}\right)\sum_{i=0}^{\infty}\sum_{j=0}^{\infty}\frac{\kappa_{sc}^{i}\kappa_{ter}^{j}}{i!\,j!}\,{}_2F_0\left(i+1,j+1;\ ;-\frac{\bar{\gamma}g\log_2 M}{(\kappa_{sc}+1)(\kappa_{ter}+1)\sin^2\theta}\right)\right]^{L}d\theta, \tag{3.68}$$

where we substituting $s=g\log_2 M/\sin^2\theta$.

From this equation, by a good approximation of the exact result when $i=[i_{\min},i_{\max}]$ and $j=[j_{\min},j_{\max}]$ as shown in (3.20), and it is straightforward to show that over the interval of integration, the minimum of the function $1/\sin^2\theta$ occurs at $\theta=\pi/2$ and $1/\sin^2(\pi/2)=1$ [43]. Using this in the argument of the generalized hypergeometric function ${}_2F_0$ in (3.68), establishes the inequality

$${}_2F_0\left(i+1,j+1;\ ;-\frac{\bar{\gamma}g\log_2 M}{(\kappa_{sc}+1)(\kappa_{ter}+1)\sin^2\theta}\right)\le{}_2F_0\left(i+1,j+1;\ ;-\frac{\bar{\gamma}g\log_2 M}{(\kappa_{sc}+1)(\kappa_{ter}+1)}\right), \tag{3.69}$$

when used this relation in (3.68), leads to the simple (no integration) upper bound

$$P_b(E) \le \frac{a}{\pi \log_2 M} \cdot \left[\exp(-\kappa_{sc} - \kappa_{ter}) \sum_{i=i_{\min}}^{i_{\max}} \sum_{j=j_{\min}}^{j_{\max}} \frac{\kappa_{sc}^i \kappa_{ter}^j}{i!\, j!} {}_2F_0\left(i+1, j+1; ; -\frac{\bar{\gamma} g \log_2 M}{(\kappa_{sc}+1)(\kappa_{ter}+1)} \right) \right]^L . \quad (3.70)$$

3.3.1.2 Average BEP Formula over Combined Nakagami-*m*×Nakagami-*m* Fading Channel.

$$P_b(E) = \frac{a}{\pi \log_2 M} \int_0^{\pi/2} \left[{}_2F_0\left(m_{sc}, m_{ter}; ; -\frac{\bar{\gamma} g \log_2 M}{m_{sc} m_{ter} \sin^2 \theta} \right) \right]^L d\theta. \quad (3.71)$$

Base on the reasoning for (3.70), an upper bound of (3.71) can be obtained by letting $\theta = \pi/2$ [43], yielding

$$P_b(E) \le \frac{a}{\pi \log_2 M} \left[{}_2F_0\left(m_{sc}, m_{ter}; ; -\frac{\bar{\gamma} g \log_2 M}{m_{sc} m_{ter}} \right) \right]^L . \quad (3.72)$$

We can see that the result in (3.71) is expressed in a more compact form than (3.68). In (3.68), the average BEP formula over combined Rician×Rician fading channel is a function of the average SNR $\bar{\gamma}$, Rician factor κ_{sc} and κ_{ter}, M parameter, and L-order diversity in the form of series-i and j. While the average BEP formula over combined Nakagami-m×Nakagami-m in (3.71) is a function of the average SNR $\bar{\gamma}$, Nakagami shape factor m_{sc} and m_{ter}, M parameter, and L-order diversity, respectively, without the form of series i and j.

Although the integrals (3.68) and (3.71) cannot be expressed in closed-forms, they can be easily evaluated numerically. The derived results are simplified in terms of a single finite integral with a compact form using the generalized hypergeometric function ${}_2F_0$ which is easily computed as it is widely used in commercial softwares such as MATLAB and MATHEMATICA.

Finally, note that the average BEP formula of various digital modulation schemes over double fading channel without diversity can be obtained by setting L to be 1.

3.3.2 Average BEP for coherent rectangular *M*-QAM

The conditional BEP for coherent rectangular *M*-QAM modulation with Gray codes mapping in terms of total instantaneous SNR per bit γ_T over AWGN channel at the receiver is given by [12]

$$P_b(E|\gamma_T) = 4qQ\left(\sqrt{2g_{QAM}\gamma_T \log_2 M}\right) - 4q^2Q^2\left(\sqrt{2g_{QAM}\gamma_T \log_2 M}\right), \tag{3.73}$$

where $g_{QAM} = \frac{3}{2(M-1)}$ and $q = 1 - \frac{1}{\sqrt{M}}$. For coherent rectangular *M*-QAM, the constellation size is given by $M = 4^m$ for some integer m. The alternative definite integral form of $Q(t)$ and $Q^2(t)$ can be represented in [11] and [16], respectively, thus the conditional BEP in (3.73) can be rewritten as

$$\begin{aligned} P_b(E|\gamma_T) &= \frac{4q}{\pi}\int_0^{\pi/2} \exp\left(-\frac{g_{QAM}\gamma_T \log_2 M}{\sin^2\theta}\right)d\theta - \frac{4q^2}{\pi}\int_0^{\pi/4} \exp\left(-\frac{g_{QAM}\gamma_T \log_2 M}{\sin^2\theta}\right)d\theta \\ &= \frac{4q}{\pi}\int_0^{\pi/2} \prod_{l=1}^{L} \exp\left(-\frac{g_{QAM}\gamma_{comb,l} \log_2 M}{\sin^2\theta}\right)d\theta - \frac{4q^2}{\pi}\int_0^{\pi/4} \prod_{l=1}^{L} \exp\left(-\frac{g_{QAM}\gamma_{comb,l} \log_2 M}{\sin^2\theta}\right)d\theta. \end{aligned} \tag{3.74}$$

Substituting the conditional BEP of coherent *M*-QAM modulation in (3.74) and the joint PDF of the instantaneous SNR $\gamma_{comb,l}$ in (3.59) into (3.60), afterwards rearranging the order of integration and grouping terms of index *l*, we obtain

$$P_b(E) = \frac{4q}{\pi \log_2 M}\int_0^{\pi/2} \prod_{l=1}^{L} \Phi_{\gamma_{comb,l}}\left(-\frac{g_{QAM}}{\sin^2\theta}\right)d\theta - \frac{4q^2}{\pi \log_2 M}\int_0^{\pi/4} \prod_{l=1}^{L} \Phi_{\gamma_{comb,l}}\left(-\frac{g_{QAM}}{\sin^2\theta}\right)d\theta. \tag{3.75}$$

Following the assumption that the fading in each branch is identically distributed with the same average SNR per bit $\bar{\gamma}$ and the same fading severity for all channels, the average BEP of coherent rectangular *M*-QAM over MRC diversity can be calculated as [43]

$$P_b(E) = \frac{4q}{\pi \log_2 M}\int_0^{\pi/2} \left[\Phi_\gamma\left(-\frac{g_{QAM}}{\sin^2\theta}\right)\right]^L d\theta - \frac{4q^2}{\pi \log_2 M}\int_0^{\pi/4} \left[\Phi_\gamma\left(-\frac{g_{QAM}}{\sin^2\theta}\right)\right]^L d\theta. \tag{3.76}$$

Following the same approach as in the case of some common modulation scheme as shown in Subsection 3.3.1, the average BEP of coherent rectangular M-QAM modulation system over combined Rician×Rician and combined Nakagami-m×Nakagami-m fading channel with MRC diversity can be calculated from:

3.3.2.1 Average BEP formula over combined Rician×Rician Fading Channel.

$$P_b(E) = \frac{4q}{\pi \log_2 M}\int_0^{\pi/2}\left[\exp(-\kappa_{sc}-\kappa_{ter})\sum_{i=0}^{\infty}\sum_{j=0}^{\infty}\frac{\kappa_{sc}^i\kappa_{ter}^j}{i!j!}\,{}_2F_0\left(i+1,j+1;\ ;-\frac{\bar{\gamma}\,g_{QAM}\log_2 M}{(\kappa_{sc}+1)(\kappa_{ter}+1)\sin^2\theta}\right)\right]^L d\theta$$
$$-\frac{4q^2}{\pi \log_2 M}\int_0^{\pi/4}\left[\exp(-\kappa_{sc}-\kappa_{ter})\sum_{i=0}^{\infty}\sum_{j=0}^{\infty}\frac{\kappa_{sc}^i\kappa_{ter}^j}{i!j!}\,{}_2F_0\left(i+1,j+1;\ ;-\frac{\bar{\gamma}\,g_{QAM}\log_2 M}{(\kappa_{sc}+1)(\kappa_{ter}+1)\sin^2\theta}\right)\right]^L d\theta, \tag{3.77}$$

where we substituting $s = g_{QAM}\log_2 M/\sin^2\theta$.

3.3.2.2 Average BEP formula over combined Nakagami-m×Nakagami-m Fading Channel.

$$P_b(E) = \frac{4q}{\pi \log_2 M}\int_0^{\pi/2}\left[{}_2F_0\left(m_{sc},m_{ter};\ ;-\frac{\bar{\gamma}\,g_{QAM}\log_2 M}{m_{sc}m_{ter}\sin^2\theta}\right)\right]^L d\theta$$
$$-\frac{4q^2}{\pi \log_2 M}\int_0^{\pi/4}\left[{}_2F_0\left(m_{sc},m_{ter};\ ;-\frac{\bar{\gamma}\,g_{QAM}\log_2 M}{m_{sc}m_{ter}\sin^2\theta}\right)\right]^L d\theta, \tag{3.78}$$

By letting $L = 1$, the results in (3.77) and (3.78) reduce to the average BEP for the receiver with no diversity.

3.4 Outage Probability over Combined Fading Channels

Outage probability P_{out} is an important performance criterion of communication system over fading channel. It is defined as the probability that the instantaneous receiver output SNR falls below a specified threshold SNR γ_{th}. Alternatively, P_{out} can be defined as the CDF of γ_T evaluated at γ_{th}, i.e.,

$$P_{out} = F[0 \le \gamma_T \le \gamma_{th}] = \int_0^{\gamma_{th}} p_{\Gamma_T}(\gamma_T)\,d\gamma_T. \tag{3.79}$$

The outage probability for L-branch MRC diversity system can be computed by using the numerical inversion method of Laplace transform of probability distribution which is proposed in [48],[49]. It can be computed as

$$P_{\text{out}} = \frac{2^{-Q}\exp(A/2)}{\gamma_{th}} \sum_{q=0}^{Q} \binom{Q}{q} \sum_{n=0}^{N+q} \frac{(-1)^n}{\beta_n} \Re\left\{ \frac{\Phi_{\gamma\Gamma}\left(-\frac{A+j2\pi n}{2\gamma_{th}}\right)}{\frac{A+j2\pi n}{2\gamma_{th}}} \right\} + E(A,N,Q), \tag{3.80}$$

where $\beta_n = 2$ when $n = 0$ and $\beta_n = 1$ for all $n \geq 1$, $\Re\{\cdot\}$ denotes the real parts. A, N and Q are the values which can be set to encounter the desired error bound over all error term $E(A,N,Q)$. It can be approximated by

$$\left|E(A,N,Q)\right| \approx \frac{\exp(-A)}{1-\exp(-A)} + \left| \frac{2^{-Q}\exp\left(\frac{A}{2}\right)}{\gamma_{th}} \sum_{q=0}^{Q} (-1)^{N+1+q} \binom{Q}{q} \Re\left\{ \frac{\Phi_{\gamma\Gamma}\left(-\frac{A+j2\pi(N+q+1)}{2\gamma_{th}}\right)}{\frac{A+j2\pi(N+q+1)}{2\gamma_{th}}} \right\} \right|. \tag{3.81}$$

Substituting the MGF result into (3.80) and (3.81), we obtain the outage probability of MRC system over combined Rician×Rician and combined Nakagami-m×Nakagami-m fading channel.

3.5 Conclusions

In this Chapter, we derive the MGF of instantaneous SNR over combined Rician×Rician and combined Nakagami-m×Nakagami-m fading channel. The derived results of MGF of combined Nakagami-m×Nakagami-m is expressed in a more compact form than the MGF of combined Rician×Rician because the MGF of combined Rician×Rician requires a solution in the form of double summation in the infinite series. Although the summation indices i and j can be computed for a good approximation by a suitable choice of $[i_{\min}, i_{\max}]$ and $[j_{\min}, j_{\max}]$, which are relative with the standard deviation of κ_{sc} and κ_{ter}, respectively.

The MGF results are necessary for the computation of the average BEP and outage probability in some common modulation schemes with and without L-order MRC receiver diversity combining. The derived MGF results are simplified in terms of a generalized hypergeometric function ${}_2F_0$ which is easily computed by commercial software such as MATLAB and MATHEMATICA, to name a few. In addition, the obtained general MGF expression considers combined Rician×Rayleigh, Nakagami-m×Rayleigh, single Rician, single Nakagami-m, single Rayleigh, and non-fading or AWGN channel as special cases.

CHAPTER 4

NUMERICAL RESULTS AND DISCUSSIONS

In this Chapter, we illustrate the results from the derived BEP and outage probability in previous Chapter. The comparisons of the theoretical results and simulation results of the average BEP and the outage probability of various digital modulation schemes over combined scintillation and terrestrial fading channels are shown in this Chapter. We shall present these results in two froms of combined fading channel: 1) combined Rician×Rician and 2) combined Nakagami-*m*×Nakagami-*m* fading channel for over all special cases. These results, together with the average BEP from single fading channel are also compared. The difference in average SNR between the theoretical average BEP and the upper bound are illustrated. Moreover, we also illustrate the difference average BEP results and envelope PDF from the model of combined Rician×Rician and combined Nakagami-*m*×Nakagami-*m* fading channel when Rician factor and Nakagami-*m* shape factor are equal. The some results of this Chapter are applicable to the systems that employ MRC diversity.

4.1 Average BEP

In this Section, we compare the theoretical results and simulation results of the average BEP of various digital modulation schemes over combined scintillation and terrestrial fading channels. For theoretical results, the average BEP is numerically computed using MATLAB. The performance is plotted versus average SNR which is defined by $\bar{\gamma} = \{\Omega_{sc} \cdot \Omega_{ter}\}(E_b/N_0)$ in the range of -10 to 60 dB. This range of average SNR is comparable with those found in the references [26]-[30], which show error performance over combined fading channel in mobile-to-mobile and MIMO systems. We have not found any literature works with bit error rate plot on satellite mobile communications with combined fading channels. However, for single fading in satellite mobile communications, the range of average SNR for single Rayleigh, Rician and/or Nakagami-*m* considered in this thesis is comparable to previous works [50]-[52]. Note that in the case with coding, most works consider the range of average SNR at about 14-20 dB.

For simulation results, the flat scintillation channel is modelled using the structure in [5], while the flat multipath fading is based on Jakes' model. Note that although each fading type can be described by a Rician distribution and Nakagami-*m* distribution, each are generated using a

different model. The simulation parameters are tabulated in Table 4.1.

Table 4.1 Simulation parameters.

Scintillation channel	Scintillation model [5]
Terrestrial multipath fading channel	Jakes' model
Modulation	*M*-PSK, DPSK, $\pi/4$ DQPSK, *M*-QAM
Bit rate	56 K bit/second
Maximum doppler frequency	100 Hz.
# Receiver antenna	1(no diversity), 2, 4, and 8 antenna

4.1.1 Average BEP over Combined Rician×Rician Fading Channels

In this Subsection, some theoretical and simulation results for the average BEP for QPSK modulation over combined flat Rician scintillation and multipath Rician fading channels are presented. For theoretical results, the performance is numerically computed from the corresponding expression derived in Section 3.3 of Chapter 3. The double summation in (3.68) was computed with each of the indices i and j running from i_{min} to i_{max} and j_{min} to j_{max}, respectively, which are sufficient for the convergence of the summation.

Figure 4.1-Figure 4.3 show the average BEP of QPSK modulation over combined Rician×Rician, Rician×Rayleigh, and Rayleigh×Rayleigh channels without diversity ($L = 1$).

In Figure 4.1 and Figure 4.2, the combined Rician×Rician fading channels have fixed κ_{ter} = 10 dB and 15 dB, respectively, with the scintillation level as a parameter. As the index S_4 increases, i.e., a smaller Rician factor, the average BEP degrades due to higher scintillation. Note that, in Figure 4.1, the average BEP is lower bounded by that of QPSK in a single Rician fading channel. When $S_4 \to 0$ ($\kappa_{sc} >> 1$), the average BEP approaches to the performance of single Rician fading as discussed in case 3 of Subsection 3.1.1 of Chapter 3. In Figure 4.2, when both κ_{sc} and $\kappa_{ter} >> 1$, the average BEP becomes the performance of AWGN channel.

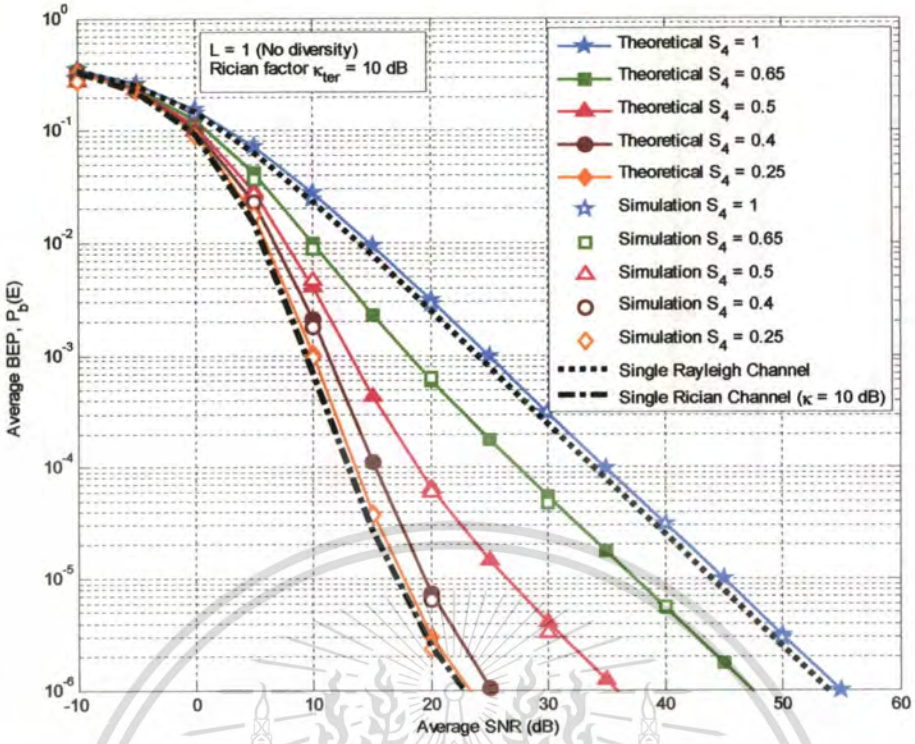

Figure 4.1 Average BEP of QPSK over combined Rician×Rician fading channel with fixed κ_{ter} = 10 dB and various S_4 = 0.25, 0.4, 0.5, 0.65, and 1.

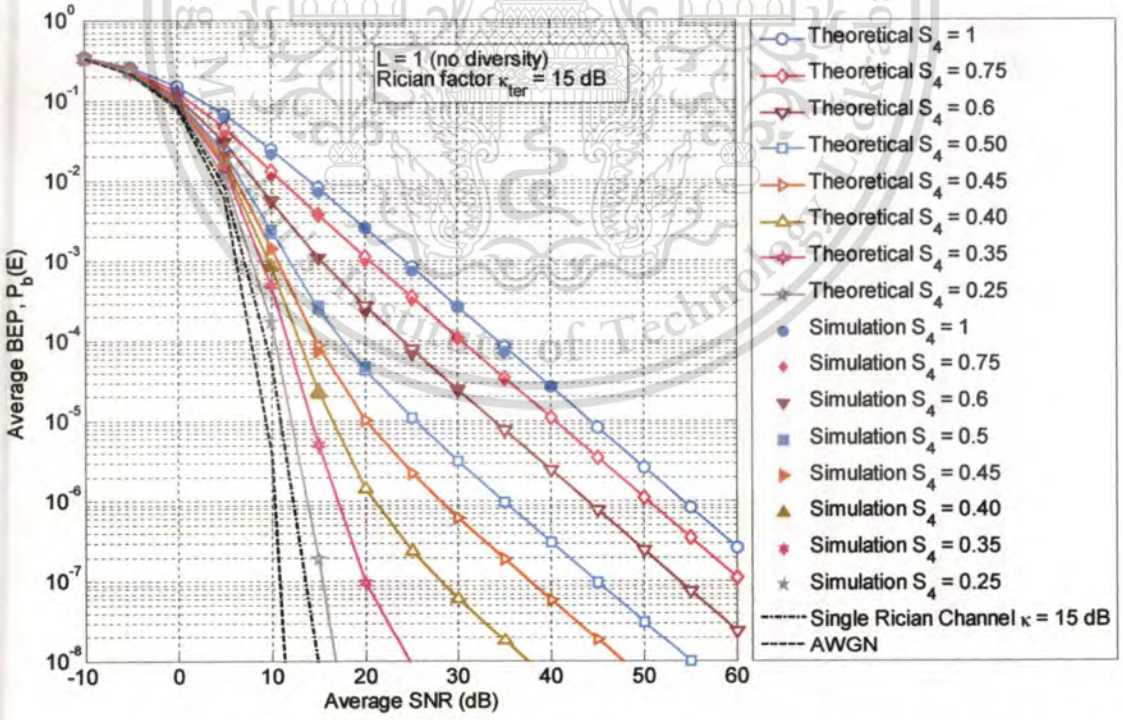

Figure 4.2 Average BEP of QPSK over combined Rician×Rician fading channel with fixed κ_{ter} = 15 dB and various S_4 = 0.25, 0.35, 0.4, 0.45, 0.5, 0.6, 0.75, and 1.

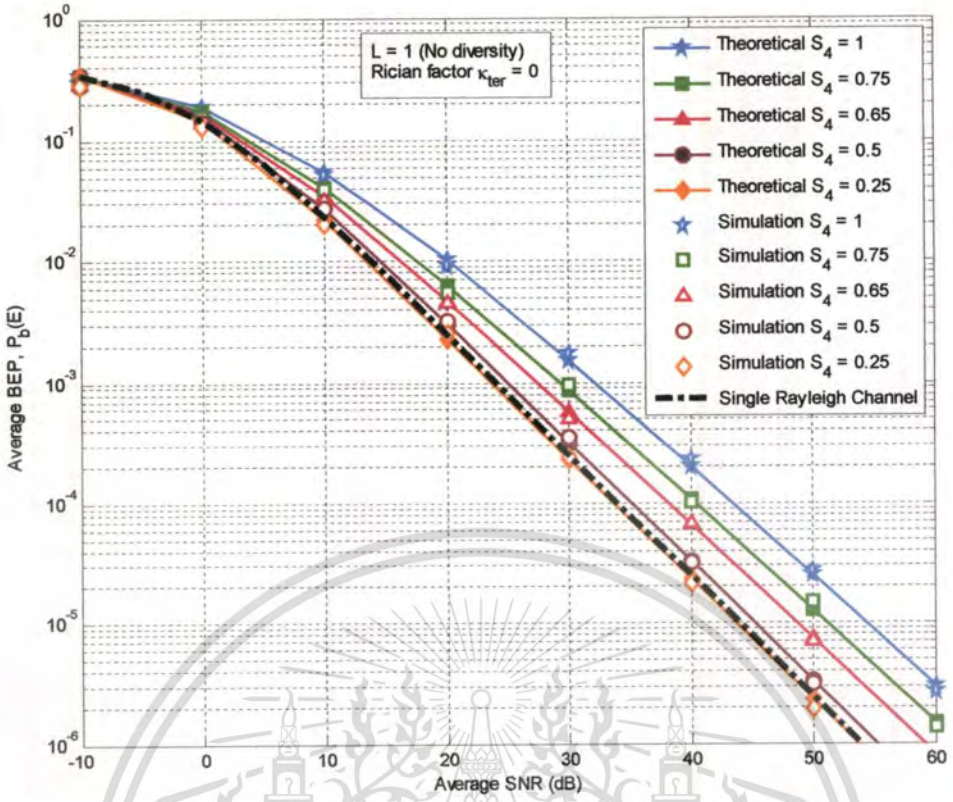

Figure 4.3 Average BEP of QPSK over combined Rician×Rayleigh (S_4 = 0.25, 0.5, 0.65, 0.75) and Rayleigh×Rayleigh (S_4 = 1) fading channels.

In Figure 4.3, we fix the terrestrial Rician factor $\kappa_{ter} = 0$ (Rayleigh fading channel) and vary the scintillation levels, which is equivalent to having a Rician×Rayleigh fading channel. It can be observed that as S_4 approaches 0 ($\kappa_{sc} \to \infty$), the average BEP approaches that of QPSK in a single Rayleigh fading channel as discussed in case 4 of Subsection 3.1.1 of Chapter 3. In a practice, the parameter S_4 ranges between 0 and 1, with $S_4 \geq 0.25$ being considered to have a significant effect on the received signal [1],[2]. We observe that for weak scintillation, $S_4 < 0.5$, the performance over the product channel approaches that of the single Rayleigh fading channel. It is evident from both figures that the theoretical results agree very well with the simulation results. In addition, the most severe performance occurs when the combined channel is Rayleigh×Rayleigh.

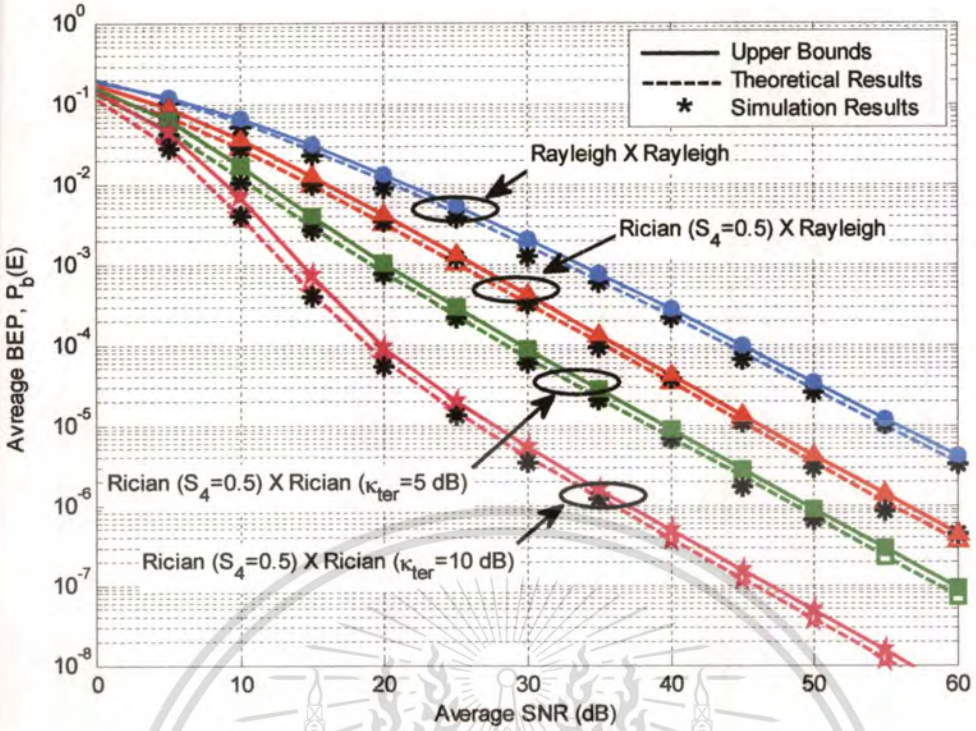

(a) $L = 1$

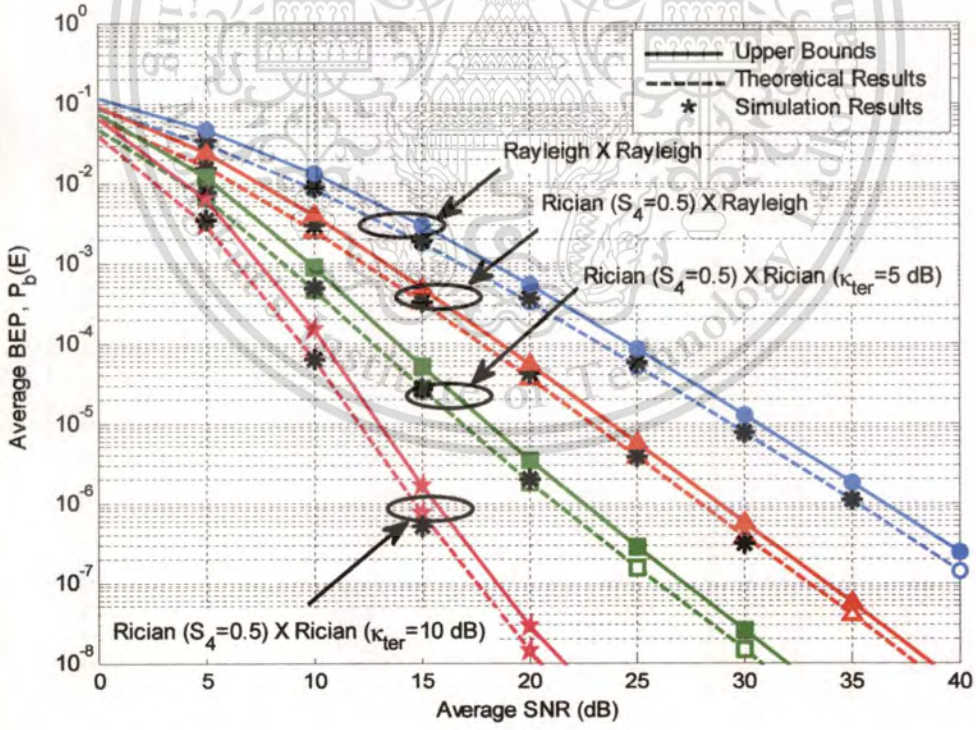

(b) $L = 2$

Figure 4.4 The effects of diversity order L on the average BEP of QPSK over combined Rician×Rician fading channels and comparison of upper bounds, theoretical results, and simulation results.

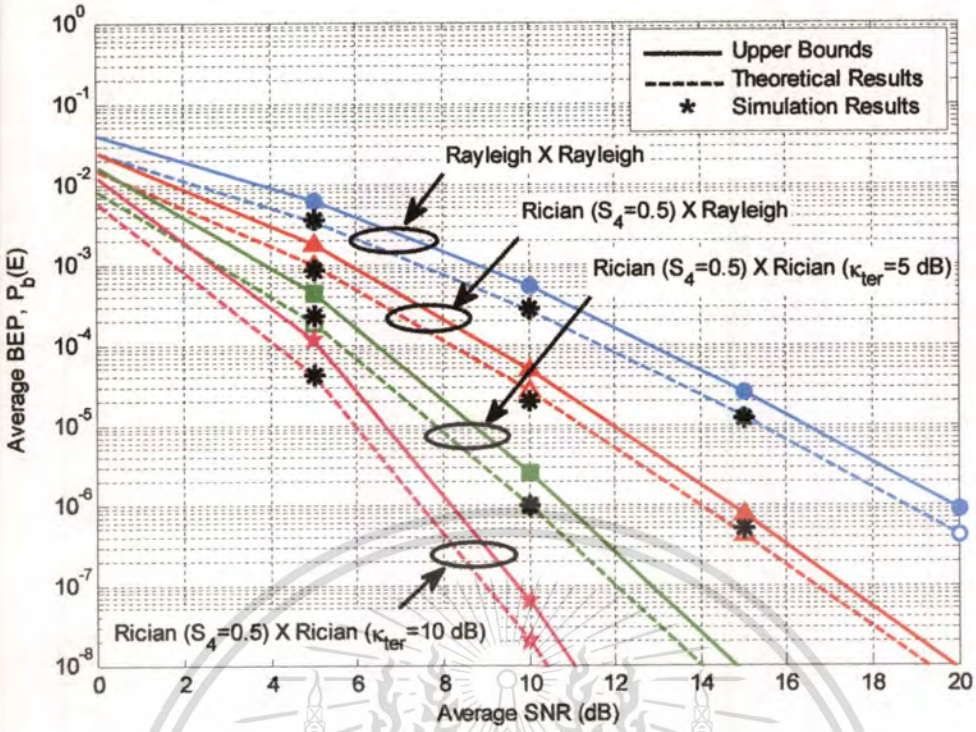

(c) $L = 4$

Figure 4.4(cont.) The effects of diversity order L on the average BEP of QPSK over combined Rician×Rician fading channels and comparison of upper bounds, theoretical results, and simulation results.

In Figure 4.4, the theoretical average BEP in (3.68) and the upper bound for QPSK in (3.70) are compared for various diversity branches and Rician factors κ_{sc} and κ_{ter}. Simulation results are also plotted. Here, each plot, the scintillation index S_4 is fixed at 0.5 except the first curve (Rayleigh×Rayleigh), and the terrestrial Rician factor κ_{ter} is varied for three values (κ_{ter} = 0, 5 dB, and 10 dB). We can see again that the theoretical and simulation results agree well and that the bounds are reasonably tight. Although the upper bound in (3.70) still contains a double summation, it gets rid of the integral found in (3.68). Hence, it is faster to compute and less affected by numerical computation error. The difference in average SNR between (3.68) and the upper bound in (3.70) is less than 1 dB.

The effects of diversity order L for QPSK in combined Rician×Rician fading channel with MRC diversity are shown in Figure 4.4 (a), (b), and (c) where L = 1, 2 and 4, respectively. In these Figure, we can see that as diversity order L increase, the average BEP decreases as expected.

4.1.2 Average BEP over Combined Nakagami-*m*×Nakagami-*m* Fading Channels

Here, we numerically compute the average BEP of QPSK modulation in combined scintillation and multipath fading channel for combined Nakagami-*m*×Nakagami-*m* fading channel with and without MRC receiver diversity.

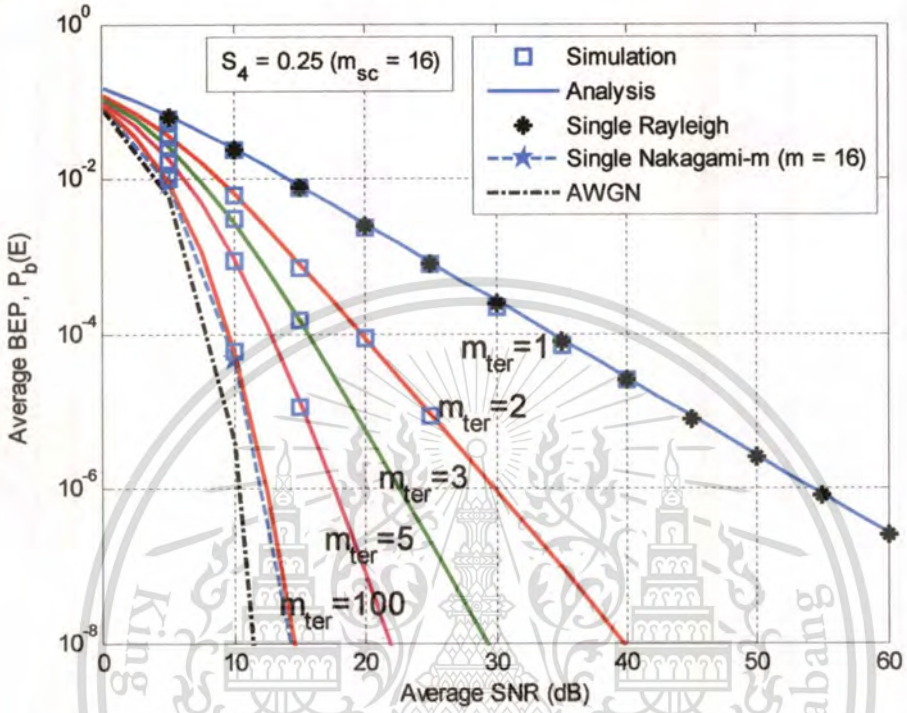

Figure 4.5 The average BEP of QPSK in Satellite Mobile communication over combined Nakagami-*m*×Nakagami-*m* fading channel without MRC diversity (L=1).

In Figure 4.5, the average BEPs of QPSK over combined Nakagami-*m*×Nakagami-*m* fading channel without MRC receiver diversity (L = 1) are illustrated. The scintillation index S_4 = 0.25 (or m_{sc} = 16) and shaping factors of terrestrial multipath fading m_{ter} = 1, 2, 3, 5, and 100 are considered. The performance of single Rayleigh fading, single Nakagami-*m* fading with m = 16, and AWGN channel are also included on the graph. With fixed S_4, the average BEP increases when the m_{ter} decreases. When m_{ter} = 1, the average BEP approaches to the performance of single Rayleigh fading as discussed in case 4 of Subsection 3.1.2 of Chapter 3. When m_{ter} = 100, the average BEP becomes the performance of single Nakagami-*m* with m = 16 as expected in case 3 of Subsection 3.1.2 of Chapter 3. When both m_{ter} and m_{sc} >> 1, we have the average BEP of AWGN channel.

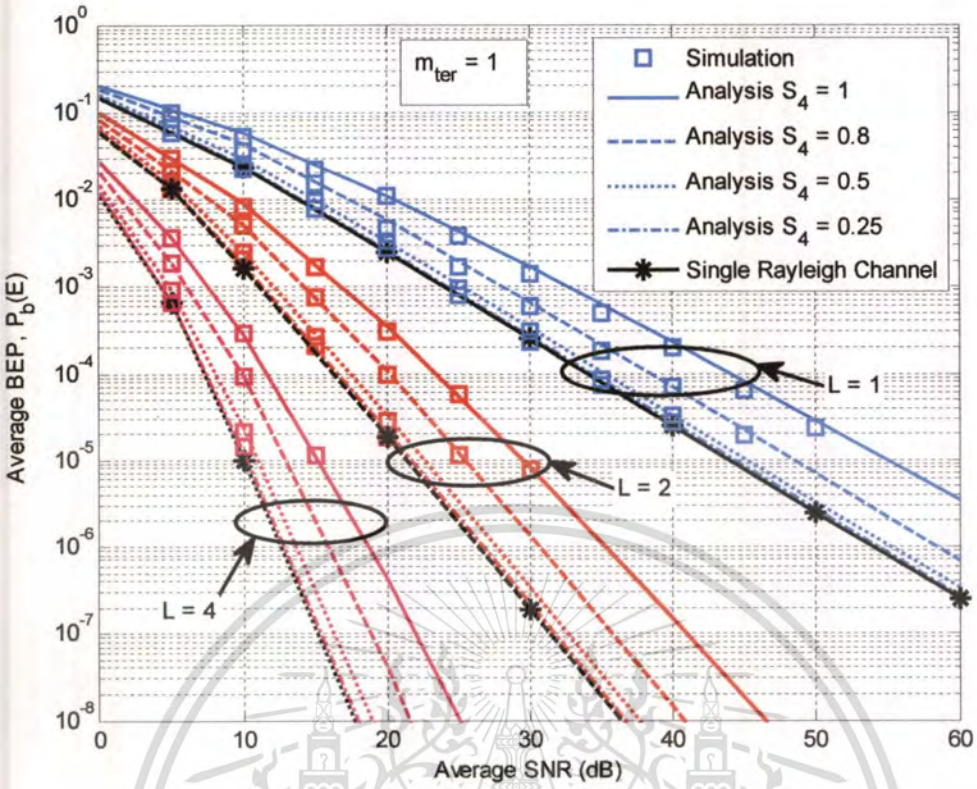

Figure 4.6 The average BEP of QPSK in Satellite Mobile communication over combined Nakagami-*m*×Rayleigh and Rayleigh×Rayleigh fading channel with MRC diversity.

In Figure 4.6, the performance of 1) combined Rayleigh×Nakagami-*m* fading channel and 2) Rayleigh×Rayleigh fading channel with various S_4 values and number of antennas (L=1, 2, and 4) are illustrated. The parameter S_4 = 0.25, 0.5, 0.8, and 1, while m_{ter} = 1(Rayliegh). As seen in the Figure, for increasing S_4, more SNRs is required to maintain the same level of BEP. In addition, the results are compared with the case of single Rayleigh fading channel. The result approaches the performance of a single Rayleigh channel at low S_4 ($\leq$ 0.25). In both Figure 4.5 and Figure 4.6, the numerical results follow the simulation results very well.

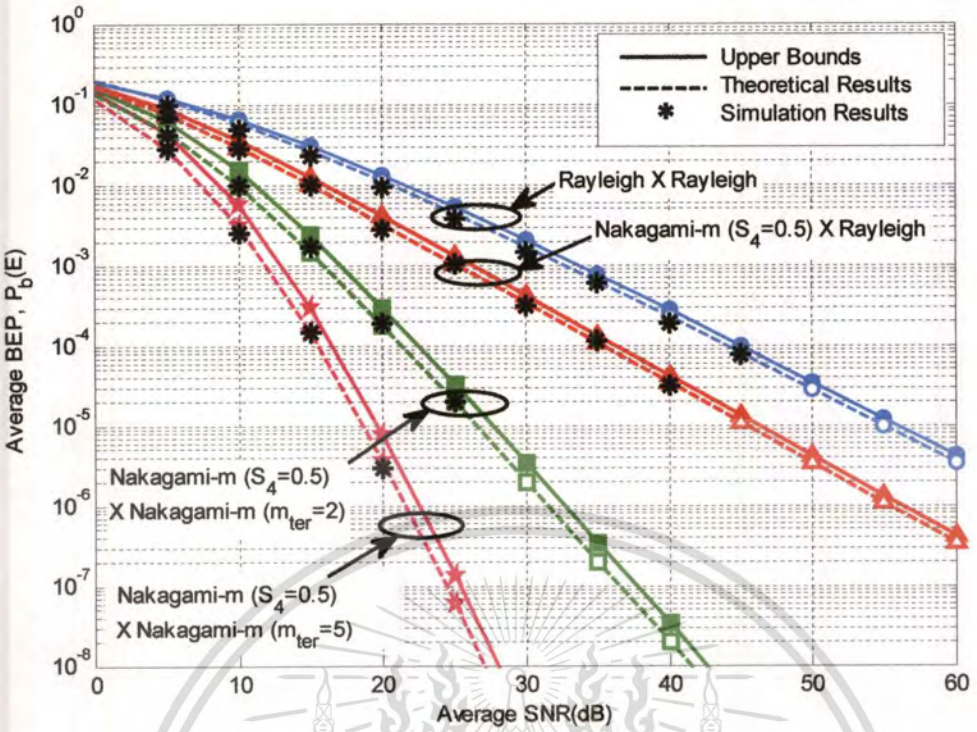

(a) $L = 1$

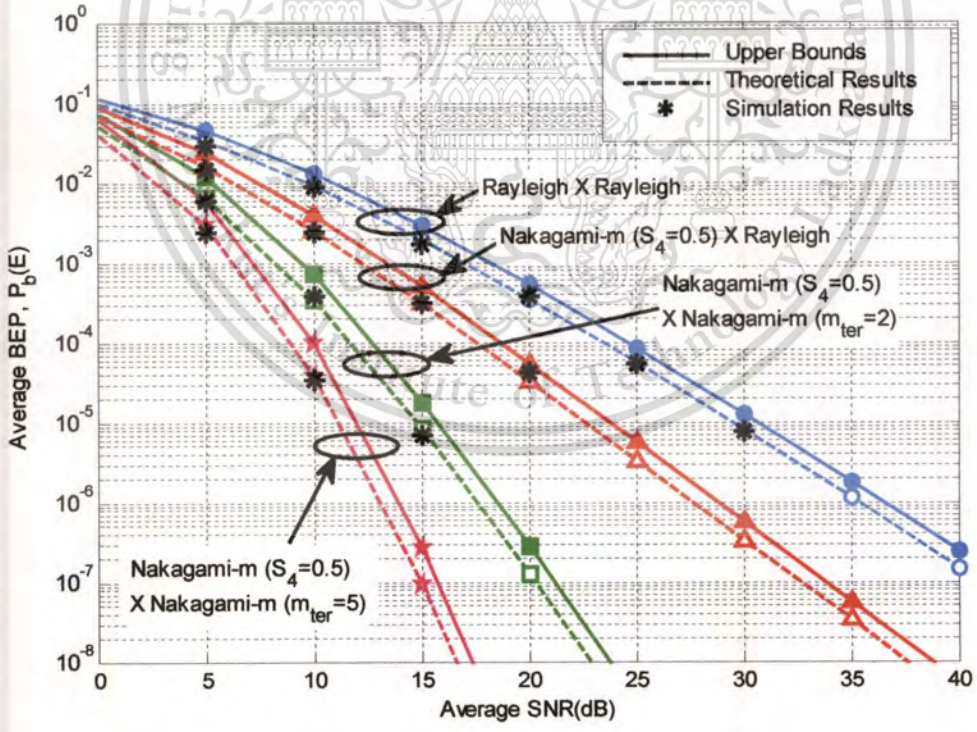

(b) $L = 2$

Figure 4.7 The effects of diversity order L on the average BEP of QPSK over combined Nakagami-m×Nakagami-m fading channels and comparison of upper bounds, theoretical results, and simulation results.

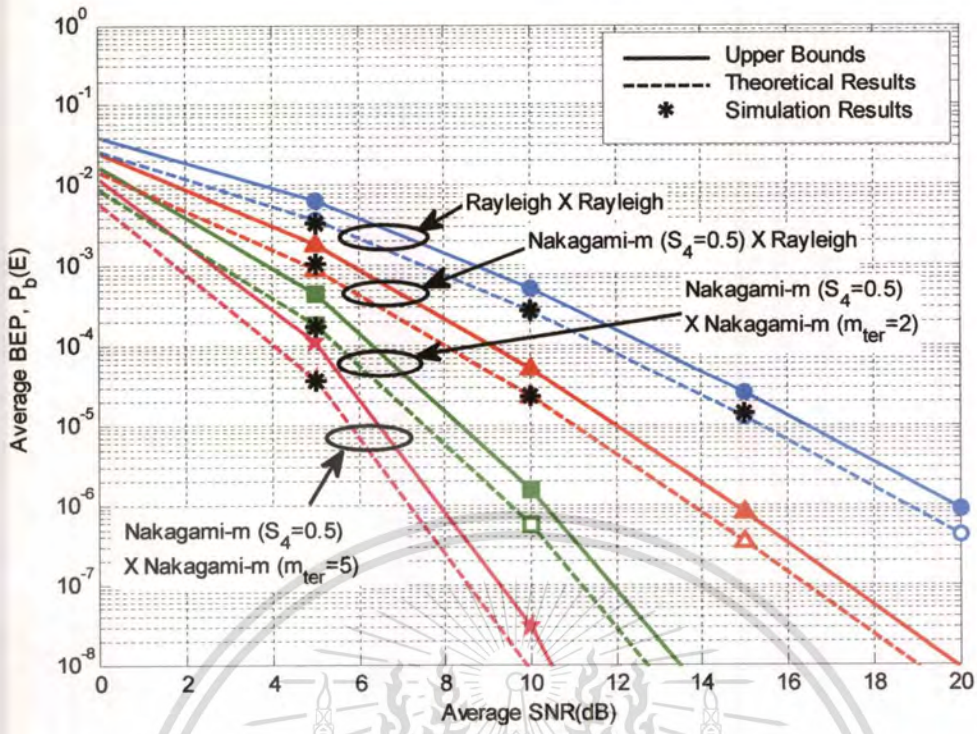

(c) $L = 4$

Figure 4.7(cont.) The effects of diversity order L on the average BEP of QPSK over combined Nakagami-m×Nakagami-m fading channels and comparison of upper bounds, theoretical results, and simulation results.

In Figure 4.7, the theoretical average BEPs in (3.71), the upper bounds for QPSK in (3.72) and simulation results over combined Nakagami-m×Nakagami-m are compared for various diversity branches and Nakagami shape factors. Figure 4.7 (a), (b), and (c) are plots for the performance of antenna diversity $L = 1$, 2, and 4, respectively. The scintillation index S_4 is fixed at 0.5(or $m_{sc} = 4$) and the terrestrial Nakagami-m shape factor $m_{ter} = 1$, 2, and 5 are considered. We can see again that the upper bounds are quite tight over a wide range of values of the average SNR.

Finally, it should be pointed out that when evaluated numerically using MATLAB software, the closed-form upper bounds of combined Rician×Rician in (3.70) and combined Nakagami-m×Nakagami-m in (3.72) offer a significant improvement in speed when compare with the exact single finite-range integrals as given by (3.68) and (3.71), respectively.

4.1.3 Comparison of the Average BEP Between Combined Rician×Rician and Combined Nakagami-*m*×Nakagami-*m* Fading Channel.

In this Subsection, Figure 4.8-Figure 4.10 show the comparison of the average BEP of QPSK over combined Rician×Rician and Nakagami-*m*×Nakagami-*m* fading channels. According to Nakagami[53], the distribution between Rician and Nakagami-*m* are a close fit when the following parameter relationship are [46]

$$\kappa = \frac{\sqrt{m^2 - m}}{m - \sqrt{m^2 - m}}, \qquad \text{for } m \geq 1, \tag{4.1}$$

$$m = \frac{(\kappa + 1)^2}{(2\kappa + 1)}. \tag{4.2}$$

This fit is exact in the extremes when $m = 1$ or $\kappa = 0$ (Rayleigh fading), and $m \to \infty$ or $\kappa \to \infty$ (non fading) but between these values a closed fit applies only over a limited range.

In Figure 4.8, we illustrate the comparison of the average BEP of QPSK over combined Rician×Rician fading channel in Figure 4.8 (a) and Nakagami-*m*×Nakagami-*m* fading channels in Figure 4.8 (b) for κ_{ter}=10 dB (or m_{ter}=5.7619). We can see that the average BEP in Figure 4.8 (a) and (b) are equal when S_4=1 only. When S_4=0.65, 0.5, 0.4, and 0.25, the average BEP over combined Nakagami-*m*×Nakagami-*m* fading channels in Figure 4.8 (b) is lower than that over combined Rician×Rician fading channels in Figure 4.8 (a).

The graph shown in Figure 4.9 illustrates the comparison of the average BEP of QPSK over combined Rician×Rayleigh and Nakagami-*m*×Rayleigh fading channels for $\kappa_{ter} = 0$ (or $m_{ter} = 1$). We observe that this graph follows similar tendency as in Figure 4.8.

The comparison of the average BEP of QPSK over combined Rician×Rician fading channel of (3.68) and Nakagami-*m*×Nakagami-*m* fading channel of (3.71) with various values of antenna diversity L (L = 1, 2, and 4) are illustrated in Figure 4.10 (a)-(d). Each of these four figures uses one of four parameter pairs from (4.1):

$\kappa = 0$,	$m = 1$.	
$\kappa = 3.1623$ (or 5 dB),	$m = 2.3653$.	
$\kappa = 6.4641$,	$m = 4$.	(or S_4=0.5)
$\kappa = 10$ (or 10 dB),	$m = 5.7619$	

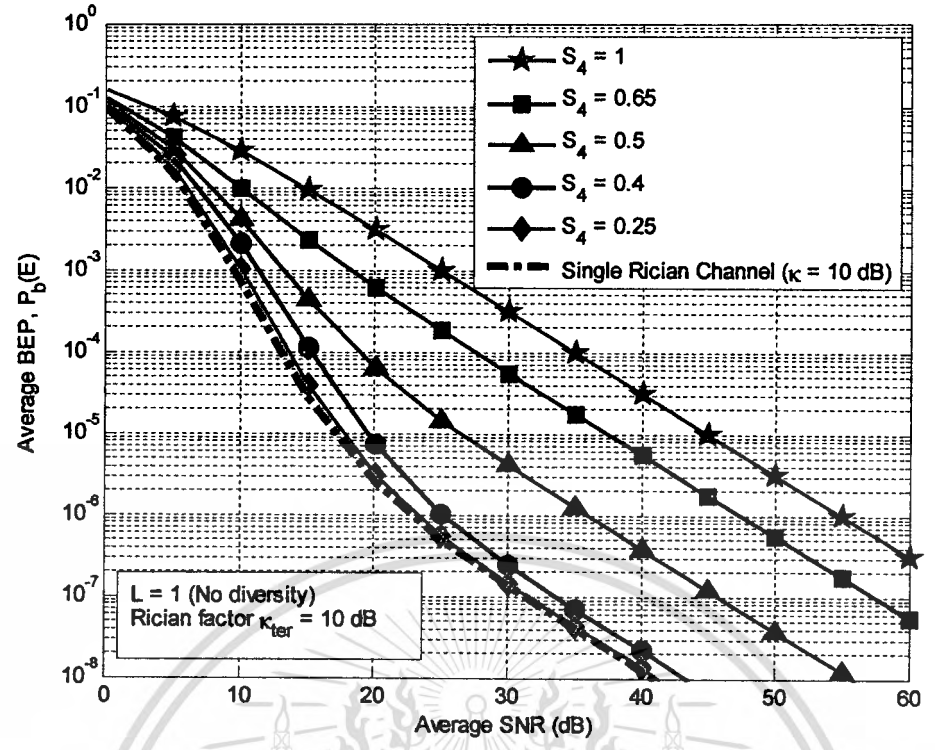

(a) Combined Rician×Rician fading channels.

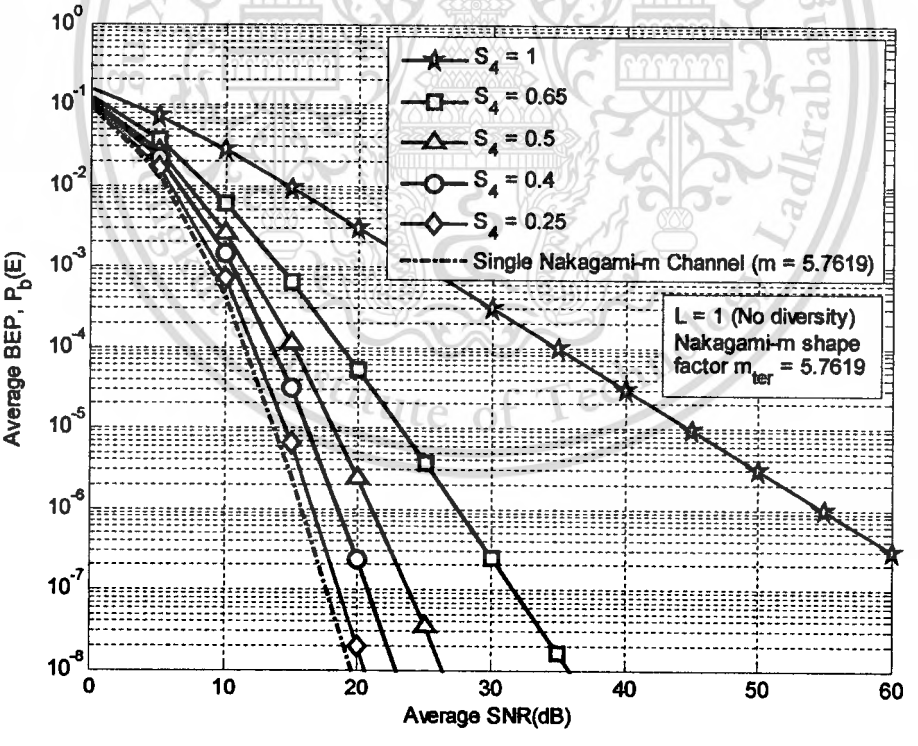

(b) Combined Nakagami-*m*×Nakagami-*m* fading channels.

Figure 4.8 Comparison of the average BEP of QPSK over (a) combined Rician×Rician fading channels and (b) combined Nakagami-*m*×Nakagami-*m* fading channels for κ_{ter} =10 dB (or m_{ter} =5.7619).

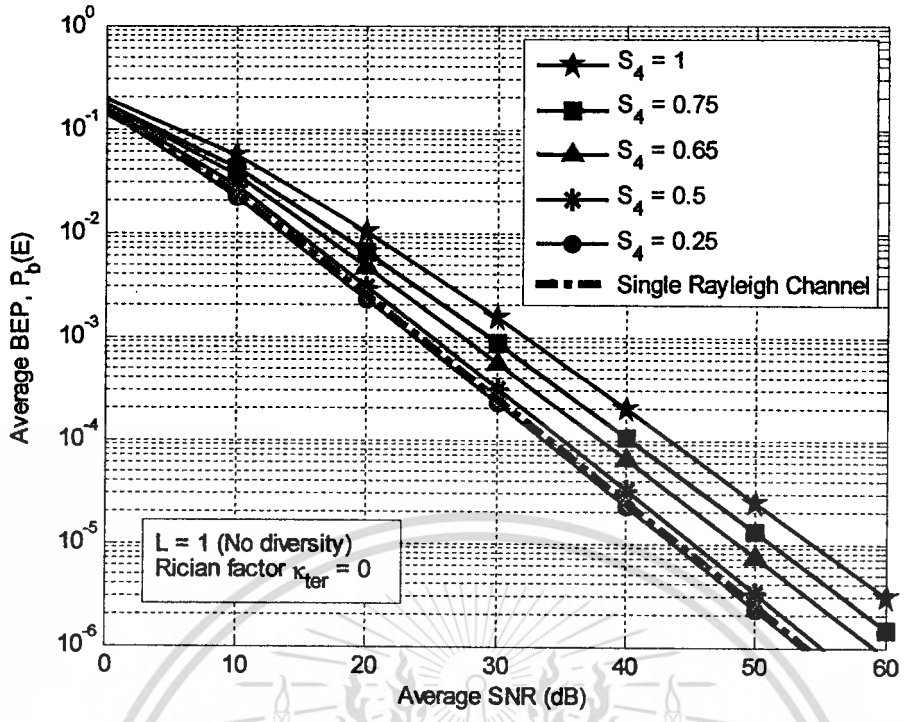

(a) Combined Rician×Rayleigh fading channels.

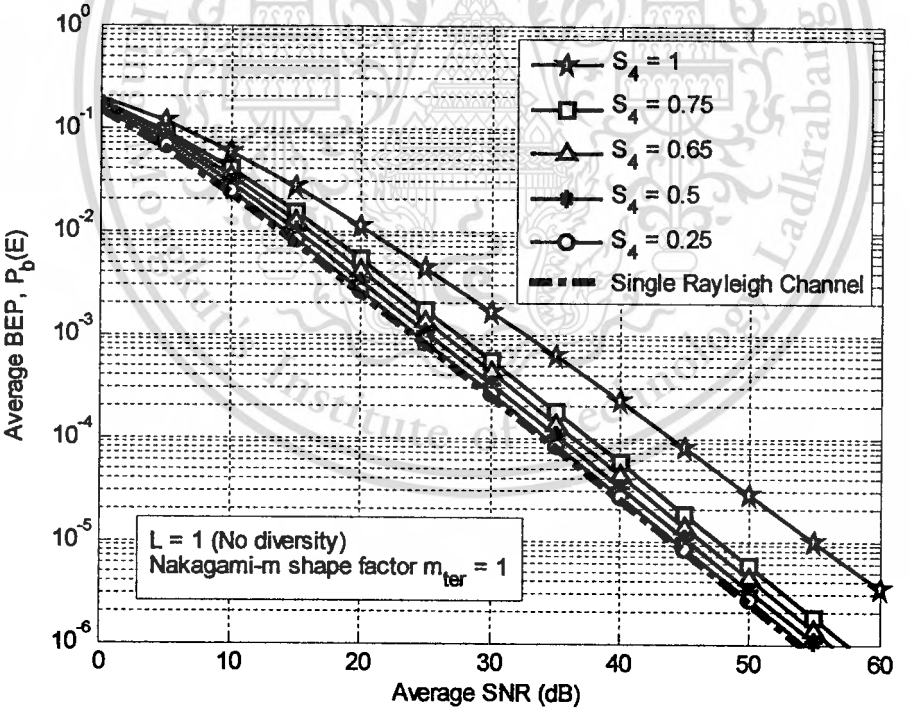

(b) Combined Nakagami-m×Rayleigh fading channels.

Figure 4.9 Comparison of the average BEP of QPSK over (a) combined Rician×Rayleigh fading channels and (b) combined Nakagami-m×Rayleigh fading channels for $\kappa_{ter} = 0$ (or $m_{ter} = 1$).

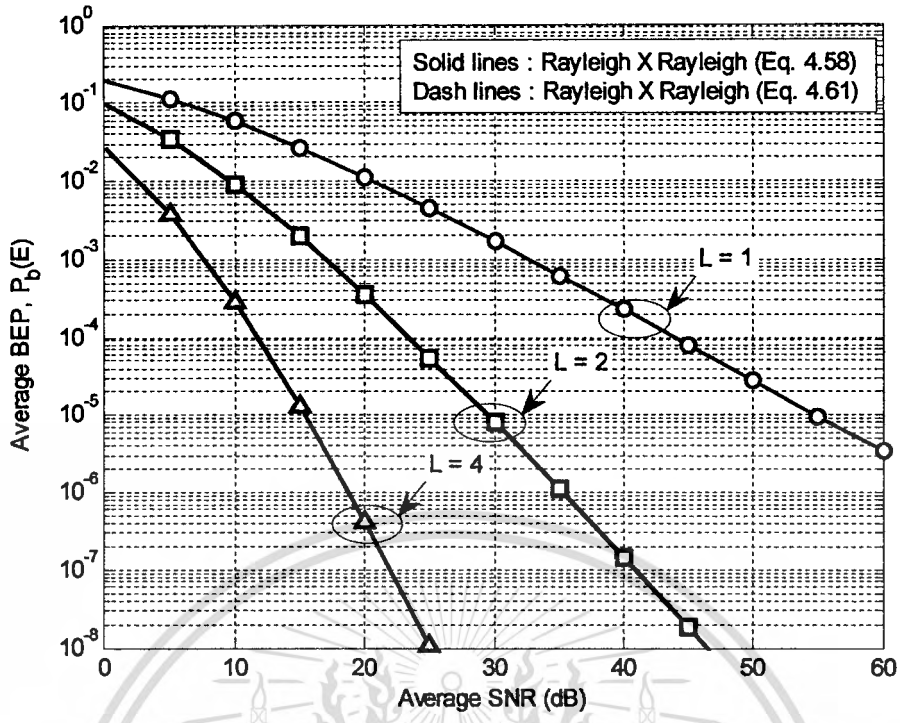

(a) Rayleigh × Rayleigh

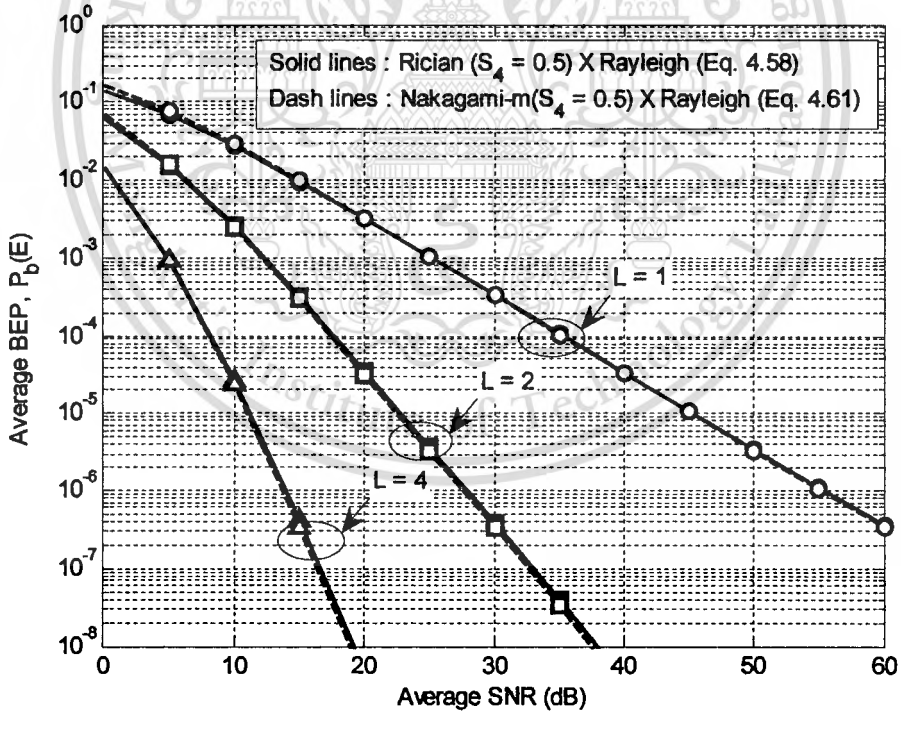

(b) Rician S_4= 0.5 (κ_{sc} = 8.1051 dB or m_{sc} = 4) × Rayleigh

Figure 4.10 Comparison of the average BEP of QPSK over combined Rician×Rician fading channel of (4.58) and Nakagami-*m*×Nakagami-*m* fading channel of (4.61).

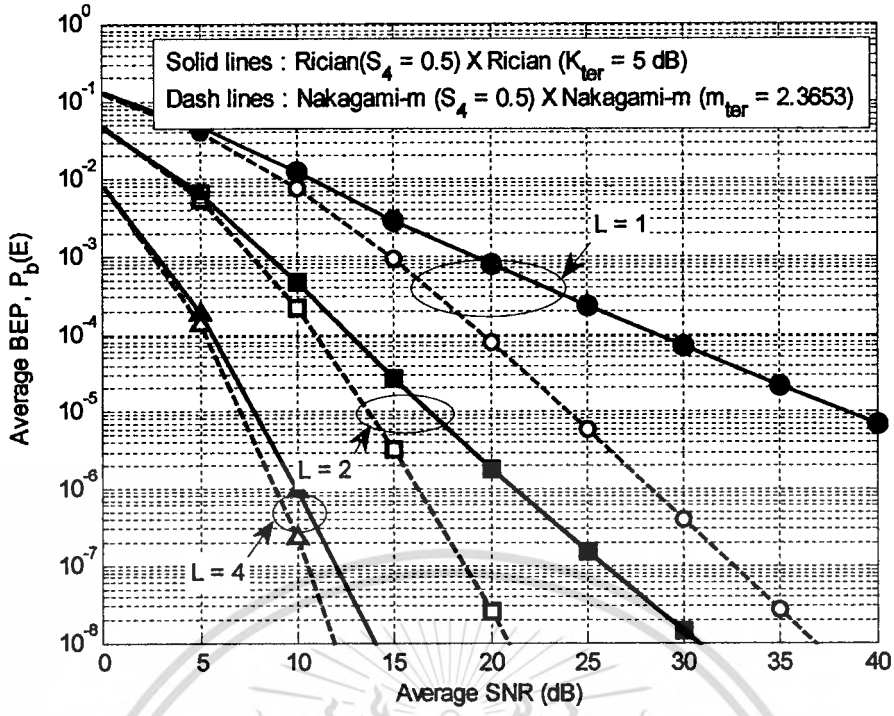

(c) Rician $S_4 = 0.5$ ($\kappa_{sc} = 8.1051$ dB or $m_{sc} = 4$) × Rician $\kappa_{ter} = 5$ dB (or $m_{ter} = 2.3653$)

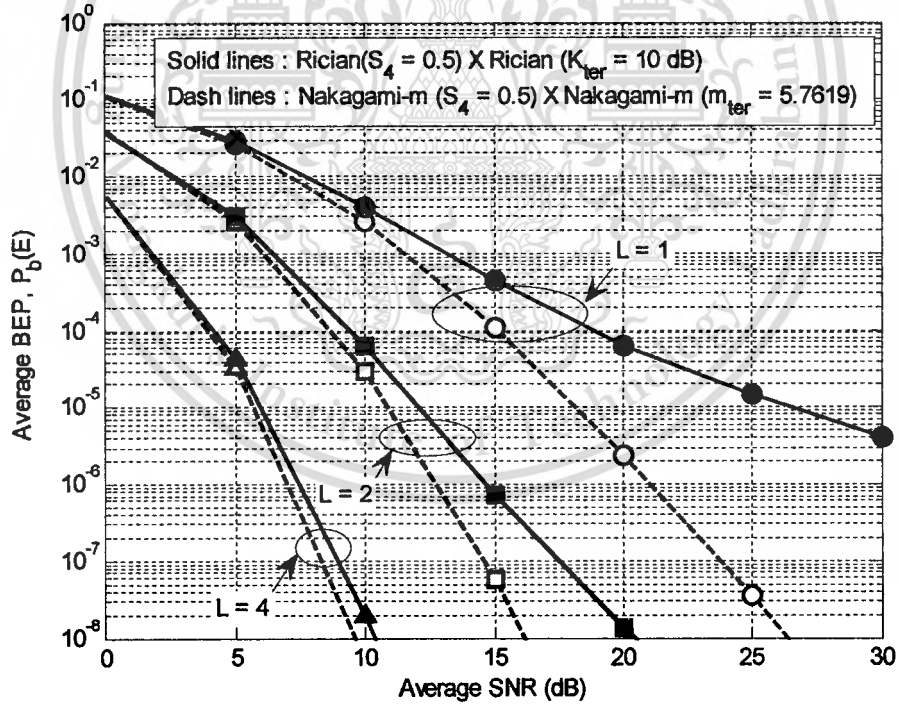

(d) Rician $S_4 = 0.5$ ($\kappa_{sc} = 8.1051$ dB or $m_{sc} = 4$) × Rician $\kappa_{ter} = 10$ dB (or $m_{ter} = 5.7619$)

Figure 4.10(cont.) Comparison of the average BEP of QPSK over combined Rician×Rician fading channel of (4.58) and Nakagami-*m*×Nakagami-*m* fading channel of (4.61).

Based on the results as shown in Figure 4.10 (a)-(d), we compare the average BEP over combined Rician×Rician fading channel from (3.68) with the average BEP over Nakagami-*m*×Nakagami-*m* fading channel from (3.71) when Rician factor and Nakagami-*m* shape factor are equal. In Figure 4.10 (a), we can see that the average BEPs from (3.68) are equal to the results from (3.71). In Figure 4.10 (b), the results from (3.68) and (3.71) have a little difference. From Figure 4.10 (c)-(d), we can see that the average BEP result from (3.68) and (3.71) fit closely for large average BEP (more than 10^{-2}). The combined Rician×Rician fading channel and Nakagami-*m*×Nakagami-*m* fading channel lead to a large difference in required average SNR to achieve a prescribed value of average BEP, when average BEP is small.

When Rician factor and Nakagami-*m* shape factor are equal, some comparisons of the envelope PDF of combined Rician×Rician and Nakagami-*m*×Nakagami-*m* fading channel are shown in Figure 4.11. We can see from these Figures that the envelope distribution of combined Rician×Rician and Nakagami-*m*×Nakagami-*m* fading channel are equal when κ_{sc} and $\kappa_{ter} = 0$ (or m_{sc} and $m_{ter} = 1$) and the case of κ_{sc} and $\kappa_{ter} >> 1$ (or m_{sc} and $m_{ter} >> 1$). Otherwise, the envelope distributions are different.

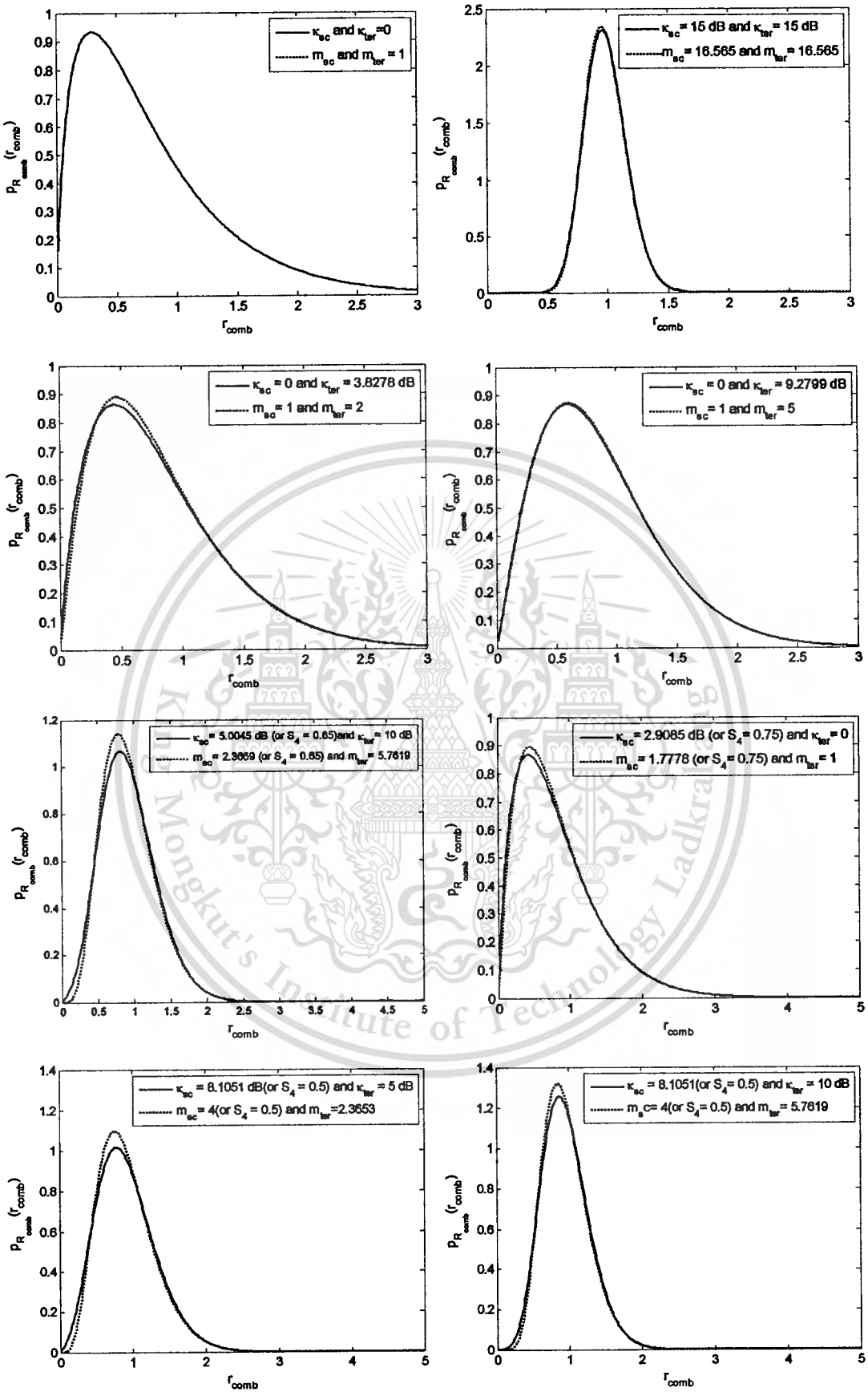

Figure 4.11 Some comparisons of the envelope PDF of combined Rician×Rician and Nakagami-*m*×Nakagami-*m* fading channel.

4.1.4 Average BEP of Some Digital Modulation Schemes

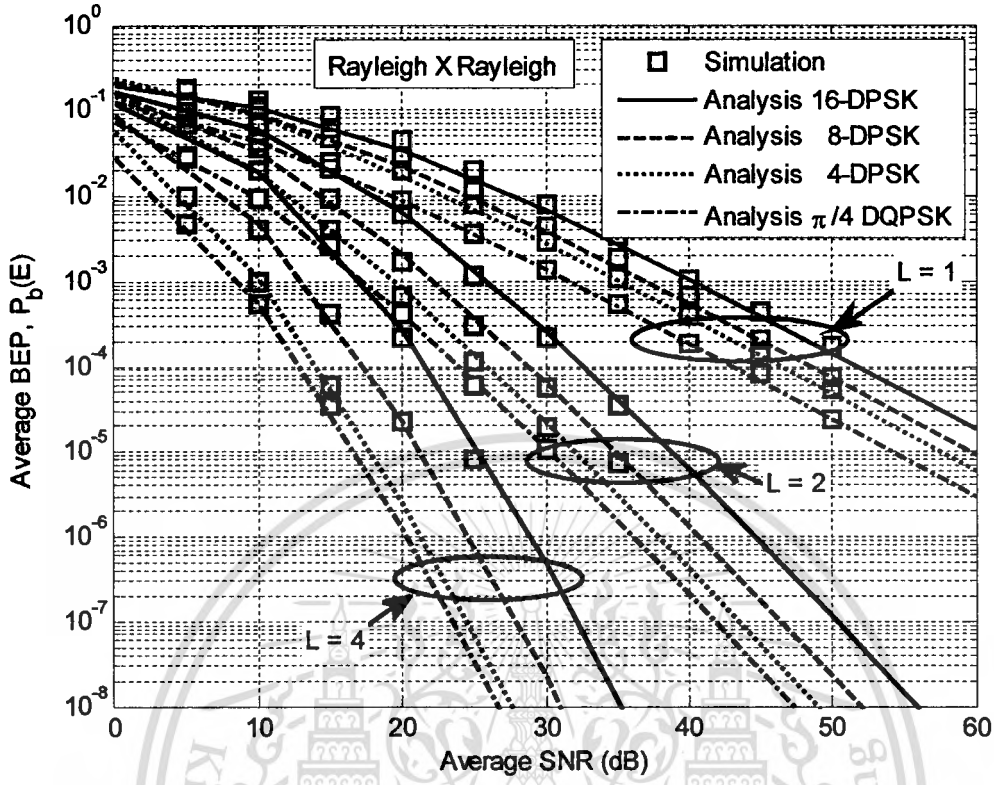

Figure 4.12 Performance comparisons of some differentially coded PSK over combined Rayleigh×Rayleigh fading channel with MRC diversity.

In Figure 4.12, we show the effect of symbol M and L-order diversity on the average BEP for $\pi/4$ DQPSK, 4-DPSK, 8-DPSK, and 16-DPSK in combined Rayleigh×Rayleigh fading channel. As seen in this Figure, an increasing M leads to degrade the average BEP. The modulation with the lowest error probability is $\pi/4$ DQPSK modulation when compared with M-DPSK. The simulation results agree with the numerical results from the derived BEP expression.

Figure 4.13 (a) and (b) show the effects of the number of symbol M and diversity order L on the average BEP of M-PSK and M-QAM over combined Rayleigh×Rayleigh fading channel. Increasing M leads to degraded average BEP.

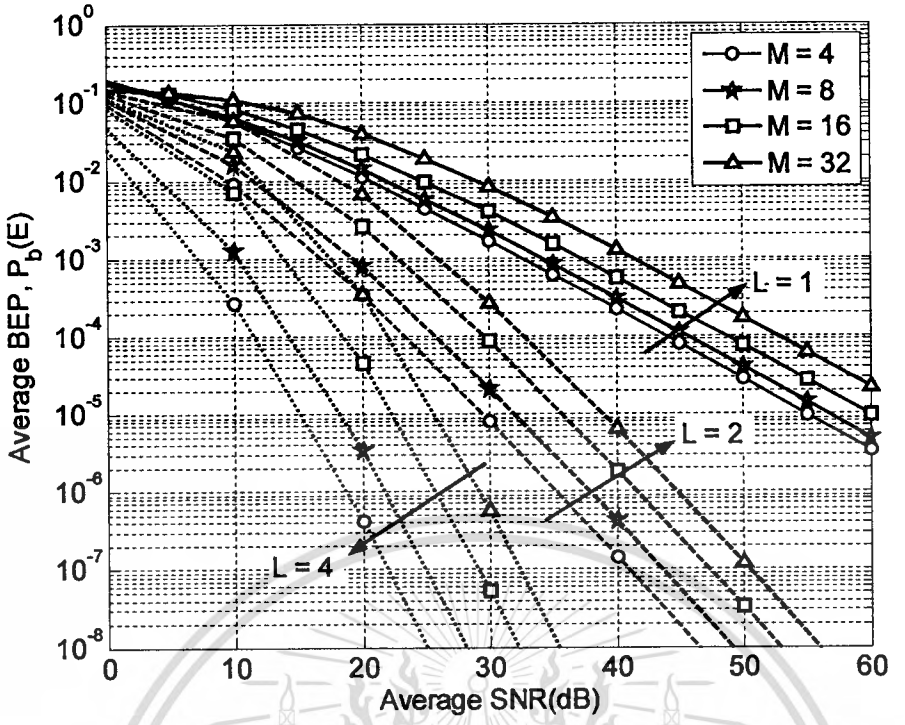

(a) *M*-PSK

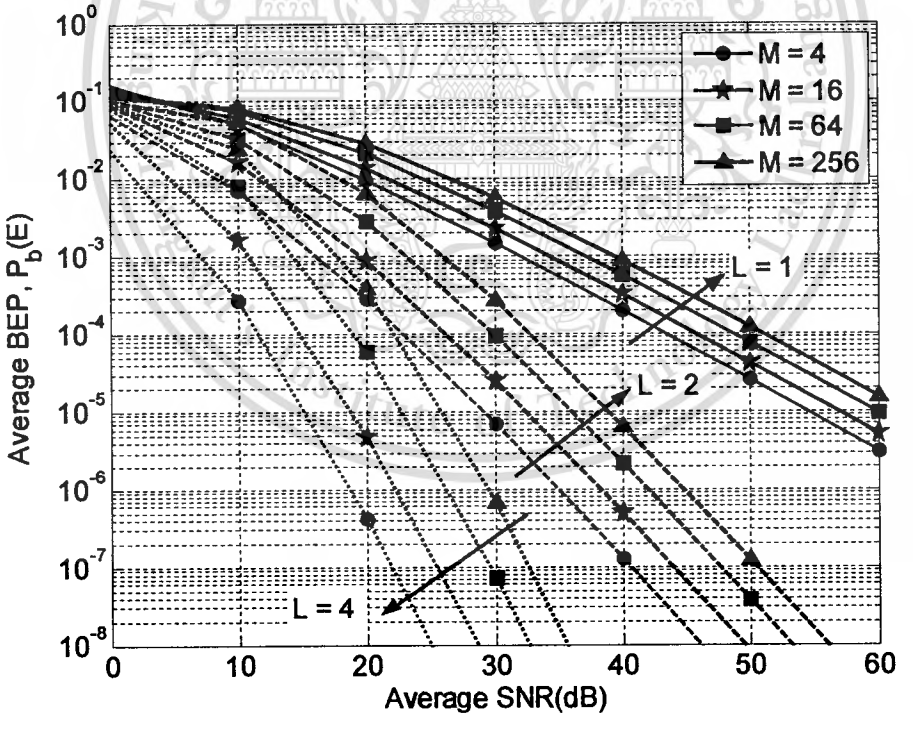

(b) coherent rectangular *M*-QAM

Figure 4.13 The effects of the number of symbol M and diversity order L on average BEP over combined Rayleigh×Rayleigh fading channel.

4.2 Outage Probability

The results of the outage probability performance of MRC receiver diversity over combined fading channel are shown in this Section. The curves are computed by set A=10ln10 in (3.80) and (3.81) to have at most 10^{-10} discretization error. Furthermore, the parameter N and Q are set to be 21 and 15, respectively, to guarantee a truncation error at less than 10^{-10}.

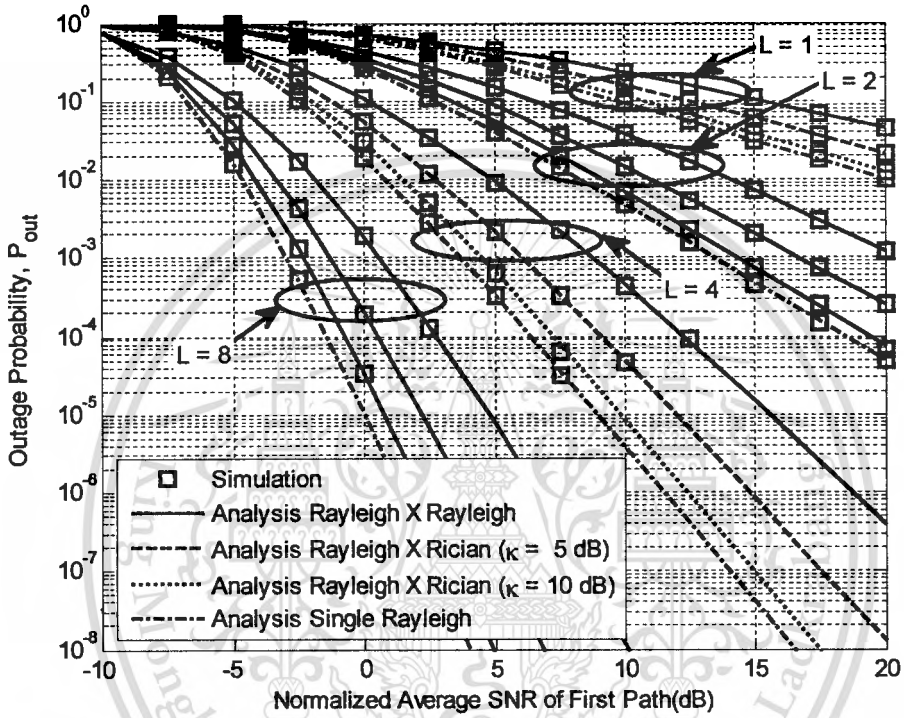

Figure 4.14 The outage probability with MRC versus normalized the average SNR of first path $\bar{\gamma}_1/\gamma_{th}$ over combined Rayleigh×Rician fading channel.

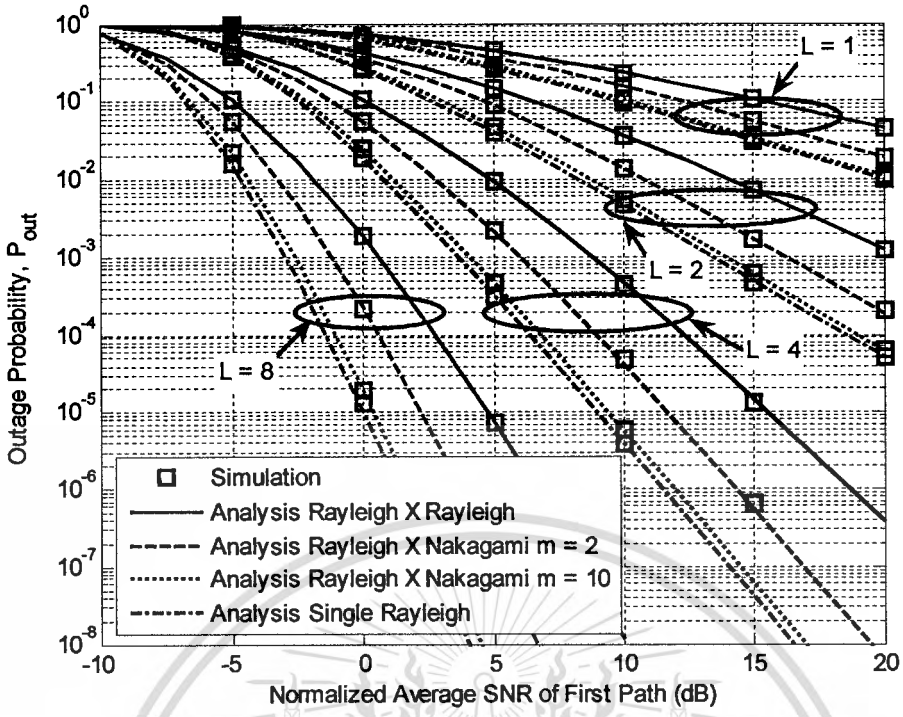

Figure 4.15 The outage probability with MRC versus normalized the average SNR of first path $\bar{\gamma}_1/\gamma_{th}$ over combined Rayleigh×Nakagami-*m* fading channel.

Illustrated in Figure 4.14 are curves for the results of the outage probability performance of MRC receiver diversity over combined Rayleigh×Rician fading channel. While, the results of the outage probability performance of MRC receiver diversity over combined Rayleigh×Nakagami-*m* fading channel are illustrated in Figure 4.15.

We can see that from both Figures the effect of fading severity leads to the more outage probability. With L=1, the result of combined Rayleigh×Rician with κ = 10 and combined Rayleigh×Nakagami-*m* with m=10 are close to that of the single Rayleigh. As L increase, the difference is more evident.

4.3 Conclusions

In this Chapter, we compute the average BEP and the outage probability of various digital modulation schemes over combined scintillation and terrestrial multipath fading channels. In the design of combined fading channel, the performance obtained with combined Rician×Rician fading channel and Nakagami-*m*×Nakagami-*m* fading channel. We observe that the performance is improved as the Rician factor for combined Rician×Rician fading channel or the Nakagami-*m* shape factor for combined Nakagami-*m*×Nakagami-*m* fading channel are increased. When the

combined fading is the combination of Rayleigh×Rayleigh fading, the performance is the most severe. Increasing the diversity order L causes the average BEP decrease as expected.

The closed-form upper bounds of both combined Rician×Rician in (3.70) and combined Nakagami-m×Nakagami-m in (3.72) offer a large improvement in speed when compared with the exact single finite-range integrals as given by (3.68) and (3.71), respectively, when evaluated numerically using MATLAB software.

The performance results from combined Rician×Rician fading channel and Nakagami-m× Nakagami-m fading channel are not equal. When average BEP is small (less than 10^{-2}), the performance results from combined Rician×Rician fading channel required a large average SNR to achieve a prescribed value of average BEP more than the performance results from combined Nakagami-m×Nakagami-m fading channel.

Finally, for the outage probability, the effect of fading severity leads to more outage probability. As L increase, the difference outage probability results are more evident.

CHAPTER 5

CONCLUSIONS

The environment of satellite link system in UHF and lower bands could be degraded by ionospheric scintillation and terrestrial multipath fading effects. With the obtained scintillation data, distribution of Rician PDF, and distribution of Nakagami-*m* PDF. From the measurement result and analysis of probability density of amplitude scintillation, we can simulate the channel when scintillation phenomena occur in the mobile communication system. The simulation of a communication system with scintillation as well as scattering environment due to urban and rural setting can be implemented. Moreover, we can studies the effect of these phenomena for improve performance of the systems.

Combined scintillation and multipath fading channels model the mobile satellite communication channel. These channels are applicable in present wireless communication systems.

The performances of these channels are computed based on the use of MGF. The expressions of MGF for instantaneous SNR in the model of combined Rician×Rician and combined Nakagami-*m*×Nakagami-*m* fading channels are explicitly derived, simplified in a compact form using generalized hypergeometric function ${}_2F_0$ which can be used to describe the characterization of fading whether they are a single, double, or non-fading channel. It is then readily useful for computation of the average BEP with MRC diversity of some common modulation schemes. The MGF formula can also be used to compute the outage probability, considered an important performance criterion of communication system over combined fading channels. The average BEP and the outage probability degrade due to higher scintillation. The performance is the most severe when the combined fading is the combination of Rayleigh×Rayleigh fading. The average BEP can be decreased by an increasing of diversity order *L*.

In addition, we derive an upper bound for the average BEP for some common modulation schemes for a combined Rician×Rician and combined Nakagami-*m*×Nakagami-*m* fading channel with MRC diversity. The expressions are also simplified and formulated in terms of the generalized hypergeometric function, which can be easily computed numerically. Moreover, the

upper bound is faster to compute and less affected by numerical computation error.

Numerical results are obtained using the derived expressions for some common modulation schemes, and compared with simulation results for different fading levels and number of diversity branches. They show that the theoretical and simulation results agree well, while the upper bound is also evaluated and shown to be reasonably tight.

The expressions derived in this thesis are more general than those of the combined Rayleigh×Rayleigh channel found in other systems such as a mobile-to-mobile system and a MIMO key-hole channel with OSTBC receiver.

REFERENCES

[1] Kullstam P. A. and Keskinen M. J. "Ionospheric scintillation effects on UHF satellite communications." **Proc. IEEE Military Commun. Conf. 2000 (MILCOM 2000)**, vol. 2, Oct. 2000. pp. 779-783.

[2] Dresp M. P., Kullstam P. A. and Kumm K. "Statistical propagation models for the mobile user objective system (MUOS)." **Proc. IEEE Military Commun. Conf. 2002 (MILCOM 2002)**, vol.1, Oct. 2002. pp. 328-332.

[3] Pratt T. et. al. **Satellite Communications.** 2nd ed. New Jersey : John Wiley. 2003.

[4] Shaft P. D. "On the relationship between scintillation index and Rician fading." **IEEE Trans. On Commun.,** vol. 22, May 1974. pp. 731-732.

[5] Ye Z.and Satorius E. H. "Channel modelling and simulation for mobile user objective system (MUOS)-Part I: Flat scintillation and fading." **Proc. ICC'03 IEEE International Conferences**, vol.5, May 2003. pp. 3503-3510.

[6] Whitney H. E., Aarons J., Allen R. S., and Seemann D. R. "Estimation of the Cumulative amplitude probability distribution function of ionospheric scintillation." **Radio Sci.**, vol. 7, 1972. pp. 1095-1104.

[7] Basu Sa., MacKenzie E. M., Basu Su., Costa E., Fougere P. F., Carlson H. C., and Whitney H. E. "250 MHz/GHz scintillation parameters in the equatorial, polar, and auroral environments." **IEEE J. Select. Areas Commun.**, vol. SAC-5, Feb. 1987. pp. 102-115.

[8] Fremouw E. J., Livingston R. C., and Miller D. A. "On the statistics of scintillation signals." **J. Atmos. Terr. Phys.**, vol. 42, Aug. 1980. pp. 717-731.

[9] Lindsey W. C. "Error probability for Rician fading multichannel reception of binary and *N*-ary signals." **IEEE Trans. Inform. Theory**, vol. IT-10, Oct. 1964. pp. 339-350.

[10] Proakis J. G., "Probabilities of error for adaptive reception of *M*-phase signals." **IEEE Trans. Commun. Technol.**, vol. COM-16, Feb. 1968. pp. 71-81.

[11] Craig J. W. "A new, simple, and exact result for calculating the probability of error for two-dimensional signal constellations." **Proc. IEEE Military Commun. Conf. (MILCOM'91)**, Oct. 1991. pp. 571-575.

[12] Shayesteh M. and Aghamohammadi A. "On the error probability of linearly modulated signals on frequency-flat Rician, Rayleigh, and AWGN channels." **IEEE Trans. On Commun.**, vol. 43, Feb 1995. pp. 1454-1466.

[13] Simon M. K. and Alouini M.-S. "A unified performance analysis of digital communication with dual selective combining diversity over correlated Rayleigh and Nakagami-*m* fading channels." **IEEE Trans. Commun.**, vol. 47, Jan. 1999. pp. 33-42.

[14] Aalo V. A. and Zhang J. "On the effect of cochannel interference on average error rates in Nakagami-fading channels." **IEEE Commun. Letters**, vol 3, May 1999. pp. 136-138.

[15] Sun J. and Reed I. S. "Performance of MDPSK, MPSK, and noncoherent MFSK in wireless Rician fading channels." **IEEE Trans. Commun.**, vol 47, Jun. 1999. pp. 813-816,

[16] Alouini M.-S. and Goldsmith A. J. "A unified approach for calculating error rates of linearly modulated signals over generalized fading channels." **IEEE Trans. Commun.**, vol. 47, Sep. 1999. pp. 1324-1334.

[17] Annamalai A., Tellambura C., and Bhargava V. K. "Exact evaluation of maximal-ratio and equal-gain diversity receivers for *M*-ary QAM on Nakagami fading channels." **IEEE Trans. Commun.**, vol. 47, Sep. 1999. pp. 1335-1344.

[18] Annamalai A. and Tellambura C. "Error rates for Nakagami-*m* fading multichannel reception of binary and *M*-ary signals." **IEEE Trans. Commun.**, vol. 49, Jan. 2001. pp. 58-68.

[19] Aalo V. A. and Zhang J. "Performance analysis of maximal ratio combining in the presence of multiple equal-power cochannel interferers in a Nakagami fading channel." **IEEE Trans. Commun.**, vol. 50, Mar. 2001. pp. 497-503.

[20] Sun J. and Reed I. S. "Linear diversity analyses for *M*-PSK in Rician fading channels." **IEEE Trans. Commun.**, vol. 51, Jan. 2003. pp. 1749-1753.

[21] Chayawan C.and Aalo V. A. "Average error probability of digital cellular radio system using MRC diversity in the presence of multiple interferers" **IEEE Trans. Wireless Commun.**, vol. 2, Sep. 2003. pp. 860-864.

[22] Zang H.and Gulliver T. A. "Error probability for maximum ratio combining multichannel reception of *M*-ary coherent systems over flat Rician fading channels." **Proc. IEEE WCNC'04**, vol. 1, Mar. 2004. pp. 306-310.

[23] Lim J. S., Hyun K., Yoon D., and Park S. K. "BER performance of rectangular QAM with MRC over Nakagami-*n* fading channels." **IEICE Trans. Commun.**, vol. E88-B, Apr. 2005. pp. 1697-1701.

[24] Annamalai A., Tellambura C. and Bhargava V. K. "A general method for calculating error probabilities over fading channels." **IEEE Trans. Commun.**, vol. 53, May 2005. pp. 841-852.

[25] Efthymoglou G. P., Piboongungon T. and Aalo V. A. "Error rates of *M*-ary signals with multichannel reception in Nakagami-*m* fading channels." **IEEE Commun. Lett.**, vol. 10, Feb. 2006. pp. 100-102.

[26] Uysal M. "Maximum achievable diversity order for cascaded Rayleigh fading channels" **Electron. Lett.**, vol. 41, Nov. 2005. pp. 1289-1290.

[27] Uysal M. "Diversity analysis of space-time coding in cascaded Rayleigh fading channels." **IEEE Commun. Lett.**, vol 10, Mar. 2006. pp. 165-167.

[28] Salo J., El-Sallabi H. M., and Vainikainen P. "Impact of double-Rayleigh fading on system performance." **Proc. 1st Int. Symp. Wireless Pervasive Computing 2006**, Jan. 2006.

[29] Shin H.and Lee J. H. "Effect of keyholes on the symbol error rate of space-time block codes." **IEEE Commun. Lett.**, vol. 7, Jan. 2003. pp. 27-29.

[30] Shin H. and Lee J. H. "Performance analysis of space-time block codes over keyhole Nakagami-*m* fading channels." **IEEE Trans. Veh. Technol.**, vol. 53, Mar. 2004. pp. 351-362.

[31] Gong Y., Letaief K. B. "On the error probability of orthogonal space-time block codes over keyhole MIMO channels." **IEEE Trans. Wireless Commun.**, vol. 6, Sep. 2007. pp. 3402-3409.

[32] Maruyama, T. **Science of Space Environment.** Tadanori Ondoh and Katsushide Marubashi eds. 2001.

[33] Nicholson J. "Status of the mobile user objective system." **Proc. IEEE Military Commun. Conf. 2006. (MILCOM 2006)**, Oct. 2006. pp. 1-4

[34] Fremou E. J. and Bates H. F. "Worldwide behavior of average VHF-UHF scintillation." **Radio Sci.**, vol. 6, Oct. 1971. pp. 863-869.

[35] Crepeau P. J. "Uncoded and coded performance of MFSK and DPSK in Nakagami fading channels." **IEEE Trans. Commun.**, vol. 40, Mar. 1992. pp. 487-493.

[36] Papoulis A. and Pillai S. U. **Probability, Random Variables, and Stochastic Processes.** Boston : McGraw-Hill. 2002.

[37] Gradshteyn I. S. and Rhyzhik I. M. **Table of Integrals, Series, and Products.**New York : Academic Press. 2002.

[38] Simon M. K. **Probability distributions involving Gaussian random variables: A handbook for engineers and scientists.** Boston: Kluwer Academic. 2002.

[39] Abramowitz M. and Stegun I. A. **Handbook of Mathematical functions, Applied Mathematics Series 55.** New York : Nation Bureau of Standards. 1964.

[40] Andrews L. C. **Special function of mathematics for engineers.** New York : McGraw-Hill. 1992.

[41] Wolfram Research, Inc. **The Wolfram functions site.** [Online]. Available : http://functions.wolfram.com/. 2007.

[42] Lebedev N. N. **Special Functions and Their Applications.** New York : Dover Publications. 1972.

[43] Simon M. K. and Alouini, M.-S. **Digital Communication over Fading Channels.** New Jersey : John Wiley. 2005.

[44] Karagiannidis G. K., Sagias N. C., and Mathiopoulos P. T. "*N**Nakagami: A novel stochastic model for cascaded fading channels." **IEEE Trans. Commun.**, vol. 55, no. 8, Aug. 2007. pp. 1453-1458.

[45] Brennan D. G. , "Linear diversity combining techniques," **Proc. IEEE**, vol. 9, no. 2, Feb. 2003, pp. 331-356.

[46] Stüber G. L. **Principles of Mobile Communication.** 2nd ed. Massachusetts: Kluwer Academic publishers. 2001.

[47] Proakis J. G. **Digital Communications.** Boston : McGraw-Hill. 2001.

[48] Abate J. and Whitt W. "Numerical inversion of Laplace transforms of probability distributions." ORSA J. Computing, vol. 7, no. 1, 1995. pp. 36-43.

[49]. Ko Y.-C., Alouini M.-S., and Simon M. K. "Outage probability of diversity system over generalized fading channels." **IEEE Trans. Commun.**, vol. 48, Nov. 2000. pp. 1783-1787.

[50] Tellambura C., Mueller A. J., and bhargava V. K. "BER and outage probability for land mobile satellite channel with maximal ratio combining." **IEE Electron. Lett.**, vol. 31, Arp. 1995. pp. 606-608.

[51] Sung-Chan Ko, Junghwan Kim, and Cheng-Ying Yang. "Practical channel simulation model for the non-GEO land mobile satellite (LMS) communications." **Proc. IEEE 47th Veh. Technol. Conf.**, vol.1, May 1997. pp. 411-415.

[52] Khairy M. M. and Geraniotis E. "BER evaluation of symbol-aided coherent demodulation for Rician and Rayleigh fading channels." **Proc. 3rd IEEE Symp. On Comp. and Commun. (ISCC 1998)**, June 1998. pp. 105-109.

[53] Nakagami M. **The m-distribution - General formula of intensity distribution of fading in Statistical Methods in Radio Wave Propagation.** New York : W.C. Hoffman. 1960.

APPENDICES

APPENDIX A

STATISTICAL DISTRIBUTION OF RANDOM VARIABLES

The objective of this chapter is to provide an overview of statistical distribution of random variables and probability theory used to mathematically describe random signals. The performance analysis in this thesis requires the application of probability theory. Some useful probability distributions for the performance analysis of digital communication systems in combined channels are shown.

A.1 Probability Distributions and Probability Densities of Random Variables

Given an experiment having a sample space S and elements $s \in S$, where s is a number of each possible outcomes of a chance experiment, we define $X(s)$ whose domain is S and whose range is a set of numbers on the real line. The function $X(s)$ is called a *random variable* (RV). In general, a RV can be considered a discrete RV or a continuous RV which are dependent on the appearance of continuity of RV. Throughout the thesis, RVs are denoted by upper case letters while the variables are denoted by lower case letters.

Let us consider the event $\{X \le x\}$ where x is any real number in the interval $(-\infty, \infty)$, the probability of this event can be defined by $P(X \le x)$ and denoted by $F_X(x)$, i.e.,

$$F_X(x) = P(X \le x). \tag{A.1}$$

We note that $F_X(x)$ is called the *cumulative distribution function* (CDF) or *probability distribution function* of the random variable X which has the following properties:[1]

Property 1 : $0 \le F_X(x) \le 1$, with $F_X(-\infty) = 0$ and $F_X(\infty) = 1$.

Property 2 : $F_X(x)$ is continuous from the right; that is, $\lim_{x \to x_{0+}} F_X(x) = F_X(x_0)$.

Property 3 : $F_X(x)$ is a non-decreasing function of x; that is $F_X(x_1) \le F_X(x_2)$ if $x_1 \le x_2$.

The derivative of the CDF $F_X(x)$ is called the *probability density function* (PDF), denoted as $p_X(x)$, of the RVs X can be used for computing statistical averages. Thus, the PDF of a continuous RV of X is defined in terms of the CDF of X by

$$p_X(x) = \frac{dF_X(x)}{dx}, \qquad -\infty < x < \infty, \tag{A.2}$$

or, equivalently,

$$F_X(x) = \int_{-\infty}^{x} p_X(u)du, \qquad -\infty < x < \infty. \tag{A.3}$$

When the RV is a discrete type, the PDF of RV X can be expressed as

$$p_X(x) = \sum_{i=1}^{n} P(X = x_i)\delta(x - x_i), \tag{A.4}$$

where x_i's are the possible discrete values of the RV, $P(X = x_i)$ are the probability, and $\delta(x)$ denotes a dirac impulse at $x = 0$.

From the properties of $F_X(x)$, the PDF $p_X(x)$ has the following properties:

Property 1 : Since $F_X(x)$ is a non-decreasing function and $F_X(-\infty) = 0$, it follows that

$$p_X(x) = \frac{dF_X(x)}{dx} \geq 0. \tag{A.5}$$

Property 2 : From $0 \leq F_X(x) \leq 1$, with $F_X(-\infty) = 0$ and $F_X(\infty) = 1$, hence,

$$\int_{-\infty}^{\infty} p_X(x)dx = 1. \tag{A.6}$$

Property 3 : From (2.6), it follows that

$$P(x_1 < X \leq x_2) = F_X(x_2) - F_X(x_1) = \int_{x_1}^{x_2} p_X(x)dx. \tag{A.7}$$

A.2 Joint Probability Distributions and Probability Densities

Some possible experiments must be characterized by more than one RVs. Multiple RVs are basically multi-dimensional functions which are defined on a sample space of a combined

experiment. For simplicity, we will begin with two RVs X_1 and X_2. The joint CDF of X_1 and X_2 can be expressed as

$$\begin{aligned} F_{X_1X_2}(x_1,x_2) &= P(X_1 \le x_1, X_2 \le x_2) \\ &= \int_{-\infty}^{x_1}\int_{-\infty}^{x_2} p_{X_1X_2}(x_1,x_2)dx_1dx_2, \end{aligned} \tag{A.8}$$

where $p_{X_1X_2}(x_1,x_2)$ is the joint PDF of two RVs X_1 and X_2 which may also be defined by

$$p_{X_1X_2}(x_1,x_2) = \frac{\partial^2 F_{X_1X_2}(x_1,x_2)}{\partial x_1 \partial x_2}. \tag{A.9}$$

The statistics of each RV are marginal functions. Thus, $F_{X_1}(x_1)$ and $F_{X_2}(x_2)$ are referred to as *marginal CDF* which can be computed by the joint CDF $F_{X_1X_2}(x_1,x_2)$ for one of the variable irrespective of the other variable. While *marginal PDF*, we integrate the joint PDF $p_{X_1X_2}(x_1,x_2)$ over one of the variables then we obtain the PDF of the other variable. The marginal CDF and marginal PDF can be expressed as

$$F_{X_1}(x_1) = F_{X_1X_2}(x_1,\infty), \qquad F_{X_2}(x_2) = F_{X_1X_2}(\infty,x_2), \tag{A.10}$$

$$p_{X_1}(x_1) = \int_{-\infty}^{\infty} p_{X_1X_2}(x_1,x_2)dx_2, \qquad p_{X_2}(x_2) = \int_{-\infty}^{\infty} p_{X_1X_2}(x_1,x_2)dx_1. \tag{A.11}$$

Furthermore, if we compute joint CDF $F_{X_1X_2}(x_1,x_2)$ for both variables equal to -∞, we obtain

$$F_{X_1X_2}(-\infty,-\infty) = 0, \quad \text{while} \quad F_{X_1X_2}(\infty,\infty) = 1. \tag{A.12}$$

If we integrate the joint PDF $p_{X_1X_2}(x_1,x_2)$ over both variables, we obtain

$$\int_{-\infty}^{\infty}\int_{-\infty}^{\infty} p_{X_1X_2}(x_1,x_2)dx_1dx_2 = 1. \tag{A.13}$$

Two RVs X_1 and X_2 are called statistically independent if an outcome in X_1 is independent of an outcome in X_2. That is $\{x_1 \in A\}$ and $\{x_2 \in B\}$, where A and B are two arbitrary sets on the x_1

and x_2 axes respectively. The joint CDF and joint PDF are a product of the two probabilities. Hence, the two RVs are statistically independent if and only if

$$F_{X_1X_2}(x_1,x_2)=F_{X_1}(x_1)F_{X_2}(x_2), \tag{A.14}$$

or, alternatively

$$p_{X_1X_2}(x_1,x_2)=p_{X_1}(x_1)p_{X_2}(x_2). \tag{A.15}$$

For the case of multi-dimensional RVs, the joint CDF can be defined as

$$\begin{aligned} F_{X_1X_2\ldots X_n}(x_1,x_2,\ldots,x_n) &= P(X_1\le x_1, X_2\le x_2,\ldots, X_n\le x_n) \\ &= \int_{-\infty}^{x_1}\int_{-\infty}^{x_2}\cdots\int_{-\infty}^{x_n} p_{X_1X_2\ldots X_n}(x_1,x_2,\ldots,x_n)dx_1dx_2\ldots dx_n, \end{aligned} \tag{A.16}$$

where $p_{X_1X_2\ldots X_n}(x_1,x_2,\ldots,x_n)$ is the joint PDF of n RVs which can be computed by taking the partial derivatives of $F_{X_1X_2\ldots X_n}(x_1,x_2,\ldots,x_n)$, i.e.,

$$p_{X_1X_2\ldots X_n}(x_1,x_2,\ldots,x_n)=\frac{\partial^n F_{X_1X_2\ldots X_n}(x_1,x_2,\ldots,x_n)}{\partial x_1\partial x_2\ldots\partial x_n}. \tag{A.17}$$

The concept of multi-dimension statistical independence can be described by an outcome in one experiment that is independent of an outcome in any other experiments. That is, the joint probability of the multi-dimensional independent RV is a product of the probabilities from each outcome, then

$$F_{X_1X_2\ldots X_n}(x_1,x_2,\ldots,x_n)=F_{X_1}(x_1)F_{X_2}(x_2)\ldots F_{X_n}(x_n), \tag{A.18}$$

and

$$p_{X_1X_2\ldots X_n}(x_1,x_2,\ldots,x_n)=p_{X_1}(x_1)p_{X_2}(x_2)\ldots p_{X_n}(x_n). \tag{A.19}$$

A.3 Statistical Average of Random Variables

The significant role in the characterization of the outcomes of experiments and the RVs is the statistical averages. The important statistical averages of a single RV are the first and second moment of RVs. While the particular interest between any pair of RVs in a multi-dimensional set RVs is correlation and the covariance.

A.3.1 Mean of Random Variable

First, we consider a single RV X. The nth moment of the discrete and continuous RV are defined by

$$\text{Discrete:} \quad E\{X^n\} = \sum_{j=1}^{M} x_j^n P_j \tag{A.20}$$

$$\text{Continuous:} \quad E\{X^n\} = \int_{-\infty}^{\infty} x^n p_X(x)dx, \tag{A.21}$$

The *mean* or *expected value* of a discrete RV X is defined as

$$\bar{X} = m_X = E\{X\} = \sum_{j=1}^{M} x_j P_j, \tag{A.22}$$

where $E\{X\}$ denotes expectation, x_j are possible values, and the respective probability $P_j = P(X = x_i)$. While in continuous RV, the sum becomes an integral, hence, the mean value can be computed by

$$\bar{X} = m_X = E\{X\} = \int_{-\infty}^{\infty} x p_X(x)dx, \tag{A.23}$$

A.3.2 Variance and Standard Deviation of Random Variables

The *variance* σ_x^2 of the RV X provides a measure of the dispersion. A useful relation for obtaining σ_x^2 is the mean of the RV $\left(X - E\{X\}\right)^2$, thus,

$$\sigma_x^2 = E\left\{\left(X - m_X\right)^2\right\} = E\left\{X^2 - 2Xm_X + m_X^2\right\} = E\left\{X^2\right\} - 2m_X^2 + m_X^2. \tag{A.24}$$

Hence,

$$\sigma_x^2 = E\{X^2\} - m_X^2, \tag{A.25}$$

where σ_x is called the *standard deviation* of the RV X.

A.4 Some Useful Probability Distribution

In this Section, we consider some probability distributions which are related and used in this research.

A.4.1 Gaussian (Normal) Distribution

The **normal distribution**, also called the **Gaussian distribution**, is an important PDF applicable in many fields. A Gaussian vector X is a vector whose components are statistically independent and identically distributed Gaussian RVs with different statistical mean and equal variance σ_x^2, are obtained from

$$X = \begin{bmatrix} X_1 \\ X_2 \\ \vdots \\ X_n \end{bmatrix}, \quad m_X = \begin{bmatrix} m_{X_1} \\ m_{X_2} \\ \vdots \\ m_{X_n} \end{bmatrix}, \quad \sigma_x^2 = \sigma_{x_i}^2, i = 1,2,...n, \tag{A.26}$$

where a variable with a boldface type, X, will be used to denote a matrix or vector which always assumed to be in a column format.

The class of Gaussian vectors is described by two parameters: mean m_X (or location) and variance σ_x^2 (or scale), which shall be denoted by $N_n(m_X, \sigma_x^2)$. The **standard normal distribution** is the normal distribution with a zero mean and a unit variance. The PDF of a Gaussian distribution RV is

$$p_X(x) = \frac{1}{\sqrt{2\pi\sigma_x^2}} \exp\left[-\frac{(x-m_X)^2}{2\sigma_x^2}\right]. \tag{A.27}$$

The CDF of RV X is

$$
\begin{aligned}
F_X(x) &= \int_{-\infty}^{x} p_X(u)du \\
&= \frac{1}{\sqrt{2\pi\sigma_x^2}} \int_{-\infty}^{x} \exp\left[-\frac{(u-m_X)^2}{2\sigma_x^2}\right]du \\
&= \frac{1}{\sqrt{\pi}} \int_{-\infty}^{(x-m_X)/\sqrt{2\sigma_x^2}} \exp\left(-t^2\right)dt \\
&= \frac{1}{2} + \frac{1}{2} erf\left(\frac{x-m_X}{\sqrt{2\sigma_x^2}}\right).
\end{aligned}
\tag{A.28}
$$

where $erf(x)$ is the error function, defined as

$$
erf(x) = \frac{2}{\sqrt{\pi}} \int_{0}^{x} \exp\left(-t^2\right)dt. \tag{A.29}
$$

Moreover, it may also be expressed in terms of the complementary error function as

$$
\begin{aligned}
F_X(x) &= 1 - \frac{1}{2} erfc\left(\frac{x-m_X}{\sqrt{2\sigma_x^2}}\right), \\
&= 1 - Q\left(\frac{m_X}{\sigma_x}\right),
\end{aligned}
\tag{A.30}
$$

where $erfc(x)$ is the complementary error function which is defined by

$$
\begin{aligned}
erfc(x) &= \frac{2}{\sqrt{\pi}} \int_{x}^{\infty} \exp\left(-t^2\right)dt \\
&= 1 - erf(x),
\end{aligned}
\tag{A.31}
$$

and $Q(x)$ is the Gaussian Q function which can be defined as

$$
\begin{aligned}
Q(x) &= \frac{1}{\sqrt{2\pi}} \int_{x}^{\infty} \exp\left(-\frac{t^2}{2}\right)dt, \qquad x \geq 0 \\
&= \frac{1}{2} erfc\left(\frac{x}{\sqrt{2}}\right),
\end{aligned}
\tag{A.32}
$$

The moments of a Gaussian RV X are

$$E\{X^k\} = \sum_{i=0}^{k} \binom{k}{i} m_X^i \mu_{k-i}, \tag{A.33}$$

where

$$\mu_k = E\{(X - m_X)^k\} = \begin{cases} 1 \cdot 3 \cdot \ldots \cdot (k-1)\sigma^k & \text{(even } k\text{)} \\ 0 & \text{(odd } k\text{)} \end{cases} \tag{A.34}$$

The PDF and CDF are shown in Figure A.1.

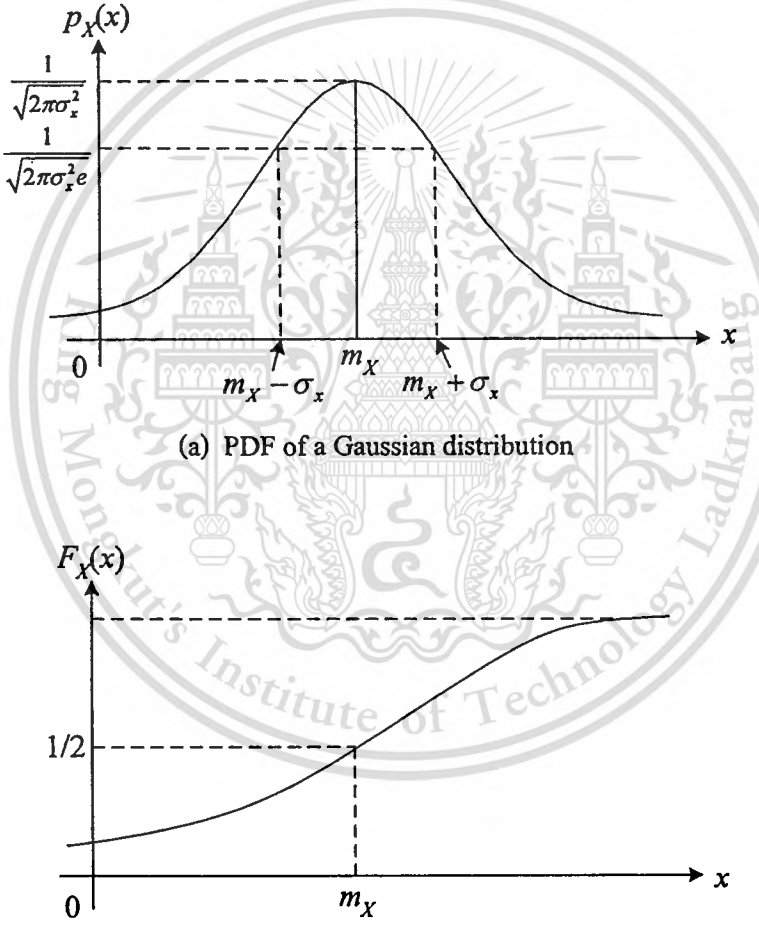

(a) PDF of a Gaussian distribution

(b) CDF of a Gaussian distribution

Figure A.1 A Gaussian PDF and CDF with mean m_X and variance σ_x^2.

A.4.2 Rayleigh Distribution

The Rayleigh distribution is a special case of the joint Gaussian PDF which $R^2 = X_1^2 + X_2^2$ where X_1 and X_2 are statistically independent Gaussian RVs. Each RV has a zero mean and a variance σ^2. Hence, the joint PDF can be written as

$$p_{X_1X_2}(x_1, x_2) = p_{X_1}(x_1)p_{X_2}(x_2) = \frac{1}{2\pi\sigma^2}\exp\left[-\frac{x_1^2 + x_2^2}{2\sigma^2}\right]. \tag{A.35}$$

By using the polar coordinates R and θ which are defined by

$$R = \sqrt{X_1^2 + X_2^2}, \quad \text{and} \quad \theta = \tan^{-1}\left(\frac{X_2}{X_1}\right), \tag{A.36}$$

so that

$$\begin{aligned} X_1 &= R\cos\theta, \\ X_2 &= R\sin\theta, \end{aligned} \tag{A.37}$$

where $0 \le \theta < 2\pi$ and $0 \le R < \infty$.

Under the transformation, the area dx_1dx_2 in the x_1x_2 plane transform to the area $rdrd\theta$ in the $r\theta$ plane by using the Jacobian transform as

$$\frac{\partial(x_1, x_2)}{\partial(r, \theta)} = \begin{vmatrix} \frac{\partial x_1}{\partial r} & \frac{\partial x_1}{\partial \theta} \\ \frac{\partial x_2}{\partial r} & \frac{\partial x_2}{\partial \theta} \end{vmatrix} = \begin{vmatrix} \cos\theta & -r\sin\theta \\ \sin\theta & r\cos\theta \end{vmatrix} = r. \tag{A.38}$$

Thus, the Rayleigh PDF of R and θ is

$$p_{R\theta}(r, \theta) = rp_{X_1X_2}(x_1, x_2)\Big|_{x_1 = r\cos\theta, x_2 = r\sin\theta} = \frac{r}{2\pi\sigma^2}\exp\left(-\frac{r^2}{2\sigma^2}\right), \quad 0 \le \theta < 2\pi, \ 0 \le r < \infty. \tag{A.39}$$

If we integrate $p_{R\theta}(r, \theta)$ over θ to get the PDF in terms of R alone as shown in (A.11), we obtain

$$p_R(r) = \frac{r}{\sigma^2}\exp\left(-\frac{r^2}{2\sigma^2}\right), \qquad 0 \le r < \infty. \tag{A.40}$$

The average envelope power is $E\{R^2\} = \Omega = 2\sigma^2$. The PDF in (A.40) can thus be written as

$$p_R(r) = \frac{2r}{\Omega}\exp\left(-\frac{r^2}{\Omega}\right), \tag{A.41}$$

The CDF of Rayleigh distribution is

$$\begin{aligned} F_R(r) &= \int_0^r \frac{u}{\sigma^2}\exp\left(-\frac{u^2}{2\sigma^2}\right)du \\ &= 1-\exp\left(-\frac{r^2}{2\sigma^2}\right), \quad r \geq 0. \end{aligned} \tag{A.42}$$

The plot of the Rayleigh PDF is given in Figure A.2

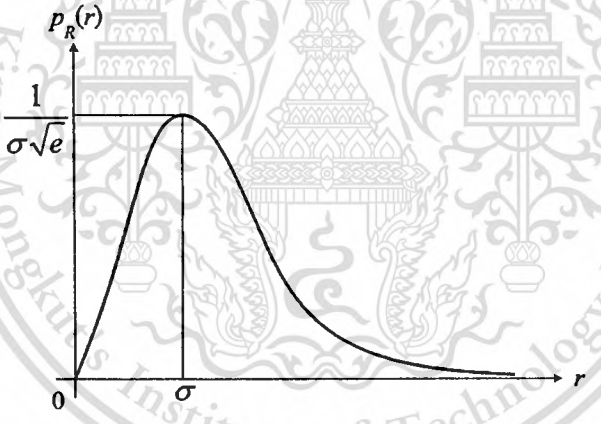

Figure A.2 The Rayleigh PDF.

This Rayleigh distribution is often used to model the statistic of signals transmitted through radio channels such as cellular radio.

A.4.3 Rician Distribution

The Rician distribution is a special case of the joint Gaussian PDF similar to the Rayleigh distribution with X_1 and X_2 in (A.36) being statistically independent Gaussian RVs with non-zero means m_{X_1} and m_{X_2}, respectively. The Rician PDF can be derived by using the summation of sinusoidal signal with the joint Gaussian RVs, i.e.,

$$y = s\cos(\omega t + \phi) + n, \tag{A.43}$$

where

$$n = n_c \cos(\omega t + \phi) + n_s \sin(\omega t + \phi). \tag{A.44}$$

Hence,

$$\begin{aligned} y &= (s + n_c)\cos(\omega t + \phi) + n_s \sin(\omega t + \phi), \\ &= r\cos(\omega t + \theta + \phi), \end{aligned} \tag{A.45}$$

where

$$r = \sqrt{(s + n_c)^2 + n_s^2}, \text{ with } r \geq 0 \quad \text{and} \quad \theta = -\tan^{-1}\left(\frac{n_s}{s + n_c}\right). \tag{A.46}$$

The joint PDF of n_c and n_s can be derived same as the Rayleigh PDF of R and θ in (A.39) with non-zero means as

$$p_{R\theta}(r, \theta) = \frac{r}{2\pi\sigma^2}\exp\left(-\frac{n_c^2 + n_s^2}{2\sigma^2}\right), \tag{A.47}$$

where

$$\begin{aligned} r^2 &= (s + n_c)^2 + n_s^2, \\ &= s^2 + 2sn_c + n_c^2 + n_s^2, \end{aligned} \tag{A.48}$$

so that

$$\begin{aligned} n_c^2 + n_s^2 &= r^2 - s^2 - 2sn_c, \\ &= r^2 - 2s(s + n_c) + s^2, \\ &= r^2 - 2sr\cos\theta + s^2, \end{aligned} \tag{A.49}$$

where $\cos\theta = (s + n_c)/r$. Therefore, the PDF in (A.47) can be written as

$$p_{R\theta}(r,\theta)=\frac{r}{2\pi\sigma^2}\exp\left(-\frac{r^2-2sr\cos\theta+s^2}{2\sigma^2}\right). \tag{A.50}$$

If we integrate $p_{R\theta}(r,\theta)$ over θ to get the PDF in terms of R alone as shown in (A.50), we obtain

$$\begin{aligned} p_R(r) &= \int_0^{2\pi}\frac{r}{2\pi\sigma^2}\exp\left(-\frac{r^2-2sr\cos\theta+s^2}{2\sigma^2}\right)d\theta, \\ &= \frac{r}{2\pi\sigma^2}\exp\left(-\frac{r^2+s^2}{2\sigma^2}\right)\int_0^{2\pi}\exp\left(\frac{2sr\cos\theta}{2\sigma^2}\right)d\theta, \\ &= \frac{r}{\sigma^2}\exp\left(-\frac{r^2+s^2}{2\sigma^2}\right)I_0\left\{\frac{rs}{\sigma^2}\right\}, \end{aligned} \tag{A.51}$$

where the v-th order modified Bessel function of the first kind $I_v\{z\}$ can be computed by using integral representation as

$$I_v\{z\}=\frac{1}{2\pi}\int_0^{2\pi}\exp(z\cos\theta)\cos(v\theta)d\theta. \tag{A.52}$$

Moreover, this PDF can be written in terms of Rician factor κ, where the Rician factor κ is defined by the ratio of the specular power s^2 to the scatted power $2\sigma^2$, i.e.,

$$\kappa=\frac{s^2}{2\sigma^2}. \tag{A.53}$$

The average envelope of the Rician distribution can be computed by

$$E\{R^2\}=\Omega=s^2+2\sigma^2. \tag{A.54}$$

From (A.53) and (A.54), the relation between the specular power s^2, the scatted power $2\sigma^2$, and Rician factor κ can be written as

$$s^2=\frac{\kappa\Omega}{\kappa+1}, \tag{A.55}$$

and

$$2\sigma^2 = \frac{\Omega}{\kappa+1}. \tag{A.56}$$

Accordingly, the PDF in (A.51) can be written in terms of Rician factor κ as

$$p_R(r) = \frac{2r(\kappa+1)}{\Omega}\exp\left(-\kappa - \frac{r^2(\kappa+1)}{\Omega}\right) I_0\left\{2r\sqrt{\frac{\kappa(\kappa+1)}{\Omega}}\right\}. \tag{A.57}$$

When $\kappa = 0$, the distribution reduces to the Rayleigh distribution, and when $\kappa = \infty$, the distribution becomes Gaussian distribution.

The CDF of the Rician distribution can thus be computed from

$$F_R(r) = 1 - Q_1\left(\frac{s}{\sigma}, \frac{r}{\sigma}\right), \qquad r \geq 0, \tag{A.58}$$

where $Q_1(a,b)$ is defined by

$$Q_m(a,b) = \int_b^\infty x\left(\frac{x}{a}\right)^{m-1} \exp\left(-\frac{x^2+a}{2}\right) I_{m-1}\{ax\}\,dx. \tag{A.59}$$

.

The plot of the Rician PDF is given in Figure A.3

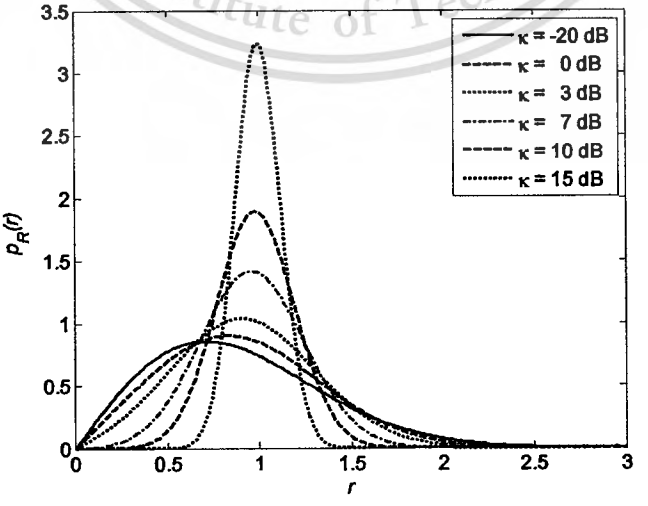

Figure A.3 The Rician PDF for various Rician factor κ.

The Rician distribution is also used to model the statistical fluctuations of the signal transmitted through some radio channels.

A.4.4 Nakagami-*m* Distribution

Distribution that characterizes the statistics of signals received from a multipath fading channel is the Nakagami-*m* distribution. The Nakagami-*m* distribution, introduced by Nakagami [53], is often used due to its fit to experimental data which is known to provide a closer match to some experimental data than either the Rayleigh or Rician distribution [46]. The Nakagami-*m* distribution is of such interest because it allows for modelling of a wide range of fading from one-sided Gaussian fading to non-fading environments by varying the shaping factor *m*, while yielding closed-form expressions for many interesting features of the channel. This distribution is in essence a central chi-square distribution given by

$$p_R(r) = \frac{2m^m r^{2m-1}}{\Omega^m \Gamma(m)} \exp\left(-\frac{mr^2}{\Omega}\right), \qquad r \geq 0, \tag{A.60}$$

where the variable $\Omega = E\{r^2\}$ is average envelope power. The parameter *m* is the Nakagami-*m* shape factor defined by Ω^2/σ^2, which ranges from 0.5 to ∞. By varying the shape factor *m*, various distribution may be obtained. For example, when *m* = 0.5, the distribution is a one-sided Gaussian distribution, when *m* = 1, the distribution becomes Rayleigh, and the distribution becomes non-fading when *m* goes to infinite.

The Rician distribution is related to the Nakagami-*m* distribution by

$$m = \frac{(\kappa+1)^2}{2\kappa+1}, \qquad \kappa \geq 0, \tag{A.61}$$

and

$$\kappa = \frac{\sqrt{m^2-m}}{m-\sqrt{m^2-m}}, \qquad m \geq 1. \tag{A.62}$$

In addition, the Nakagami-*m* distribution offers features of analytical convenience in comparison to the Rician distribution because the Nakagami-*m* distribution is a central distribution and does

not contains a Bessel function. As a result of this distinction, the Nakagami-*m* distribution often leads to mathematical simplicity unseen in the Rician distribution.

The plot of the Nakagami-*m* PDF is given in Figure A.4.

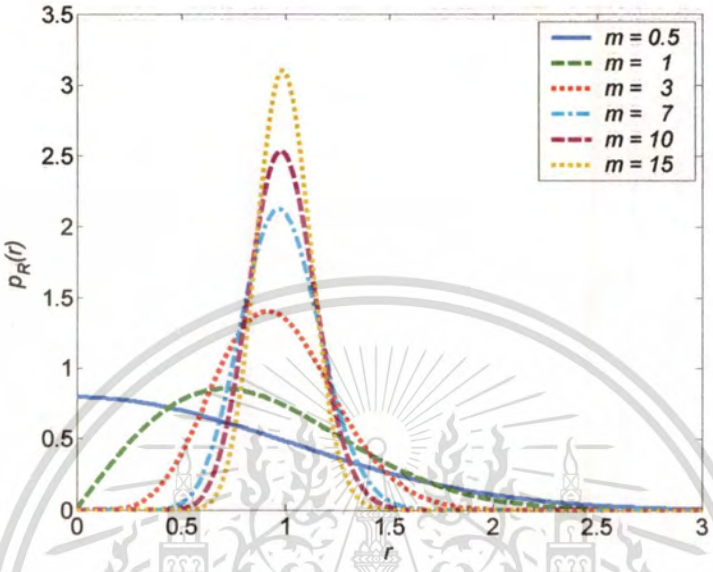

Figure A.4 The Nakagami-*m* PDF for various Nakagami shape factor *m*.

APPENDIX B

PROBABILITY DENSITY OF AMPLITUDE SCINTILLATION

The comparison between the experimental S_4 index distribution and Rician distribution for some example in S-band and VHF are presented in this Section. (Note that Rician factor κ_{sc} is calculated from equation (2.8) in Chapter 2).

Scintillation phenomenon affecting S-band satellite signals has been observed from January 2002 to April 2002. By receiving carrier wave from Geostationary Meteorological Satellite-5 (GMS-5) at King Mongkut's Institute of Technology Ladkrabang (KMITL), Bangkok, Thailand. The data of amplitude scintillation is obtained every 0.02 seconds or 50 Hz. The details of experimental setup are given in Table B.1.

Table B.1 Satellite receiving system parameters of S-band

Satellite	GMS-5
Receiver Position	100.8°E ,13.7° N
Receiver Frequency	1.694 GHz
Elevation angle	42.40°
Azimuth angle	106.2°
Received Antenna	1.8 diameter parabolic antenna

Figure B.1 shows the probability density of amplitude scintillation, it presents the comparison between the experimental S_4 index distribution and Rician distribution in S-band. Data of three S_4 level are obtained.

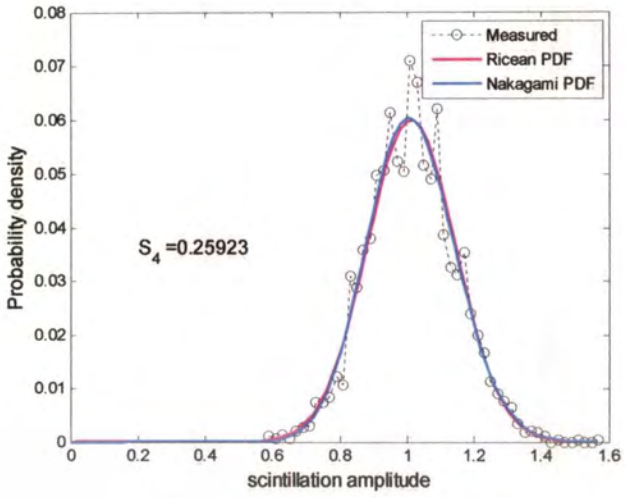

(a) 09/02/2002 13:42-13:45LT

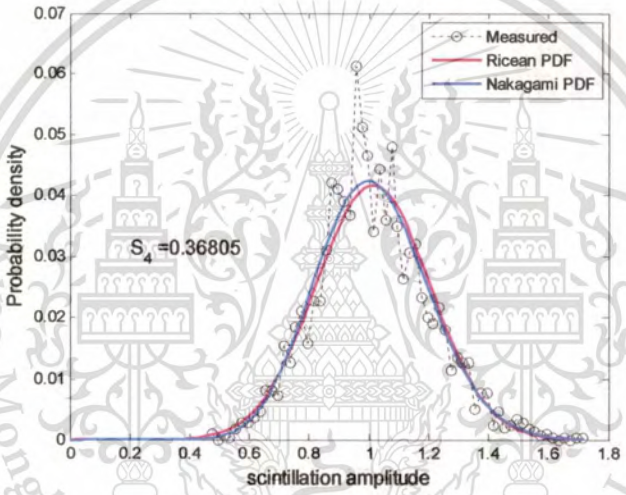

(b) 09/04/2002 15:14-15:17LT

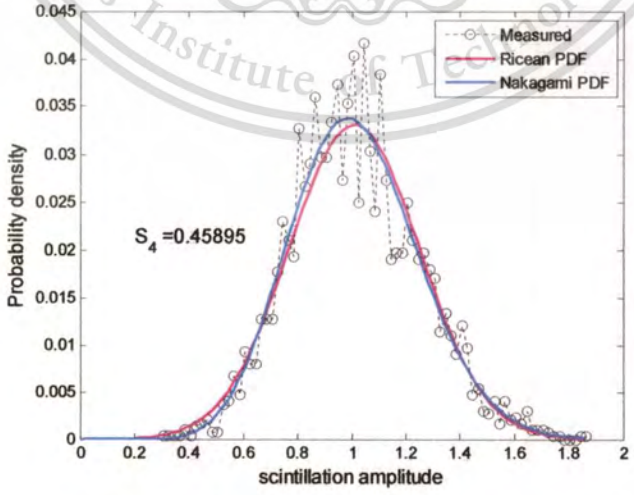

(c) 09/04/2002 15:20-15:23LT

Figure B.1 Probability density functions of amplitude scintillation in S-band.

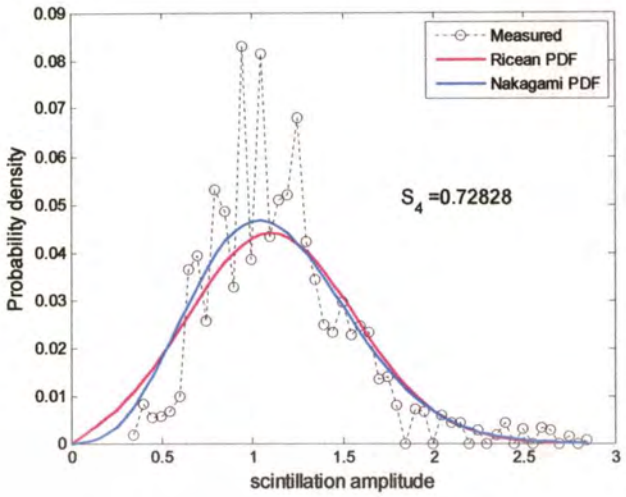

(a) 20/10/2002 13:50-13:53 LT

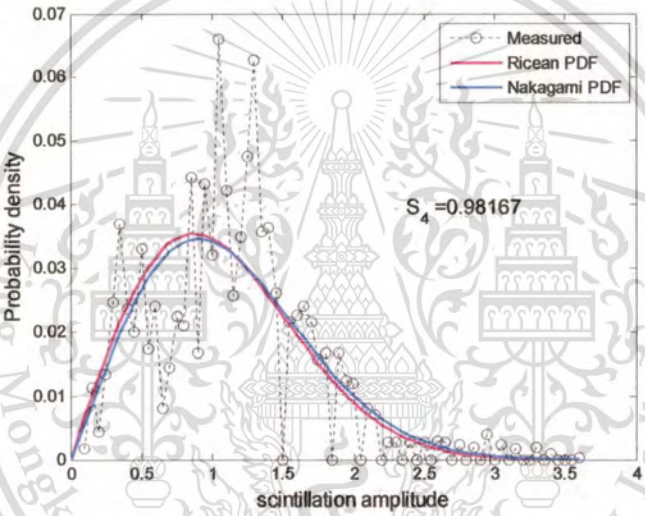

(b) 20/10/2002 13:58-14:01LT

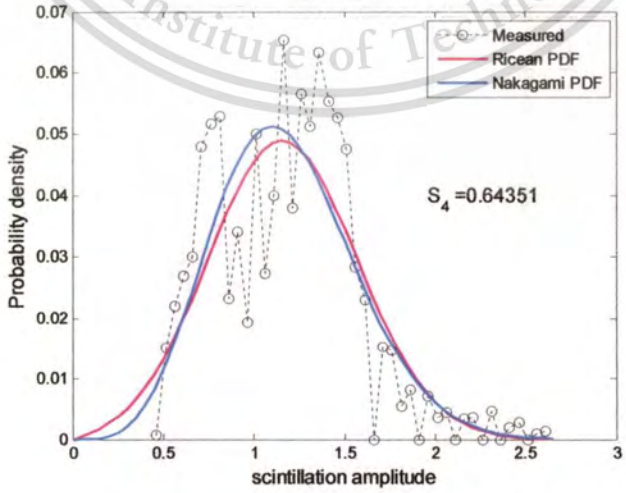

(c) 10/08/2003 13:48-13:51LT

Figure B.2 Probability density functions of amplitude scintillation in VHF.

Scintillation phenomenon affecting VHF satellite signals has been observed from October 2002 to August 2003. By receiving carrier wave from Fleet Satellite Communication (FLTSATCOM) at King Mongkut's Institute of Technology Ladkrabang (KMITL), Bangkok, Thailand. The details of experimental system are given in Table B.2.

Table B.2: Satellite receiving system parameters of VHF

Satellite	FLTSATCOM
Receiver Position	100.8°E ,13.7° N
Receiver Frequency	244.165 MHz
Elevation angle	51.15°
Azimuth angle	247.53°
Received Antenna	Yagi Antenna, 10 element
Antenna Gain	13.2 dBi

The comparison of the probability density of amplitude scintillation between the experimental S_4 index distribution and Rician distribution in VHF are illustrated in Figure B.2.

According to the results, the experimental S_4 index distribution agrees well with Rician distribution [4].

APPENDIX C

CHANNEL MODELING OF SATELLITE MOBILE COMMUNICATION SYSTEM

This chapter addresses the modeling and simulation of flat ionospheric scintillation. Specify analytical channel modeling is provided, with the emphasis on narrowband waveform. There are several important factors to consider for channel modeling of satellite mobile communication systems. Specifically, the effects of signal fading, signal decorrelation time, power spectral density, and level crossing rate. Measured data of ionospheric scintillation can be characterized by only small-scale fading [2]. Amplitude scintillation is statistically modeled as Rayleigh, Rician and/or Nakagami-*m* fading with finite signal decorrelation time and limited coherent bandwidth of the transmission channel[1] where depending on the severity of ionopheric scintillation (or scintillation index, S_4). While the phase statistics distribution is similar in shape to a Gaussian distribution.

C.1 Observed Statistics

The scintillation coefficient $\alpha_{sc}(t)$ is statistically modeled as a non-zero mean and complex Gaussian random process which can be written as

$$\alpha_{sc}(t) = \sqrt{a_{sc}}e^{j\phi} + b_{sc}(t), \tag{C.1}$$

where a_{sc} is proportional to the signal power via the specular signal component (LOS path), ϕ is uniform random phase shift distribution over the interval $[-\pi, \pi]$, and $b_{sc}(t)$ is a complex Gaussian random process over scattered path (NLOS path). Consequently, the signal power over scattered path can be computed by

$$2\sigma_{sc}^2 \equiv E\left[b_{sc}(t)\right]^2. \tag{C.2}$$

As a result, the average envelope power is given by

$$E\left[\alpha_{sc}^2\right]=\Omega_{sc}=a_{sc}+2\sigma_{sc}^2. \quad \text{(C.3)}$$

The envelope PDF of scintillation coefficient $r_{sc}=|\alpha_{sc}(t)|$ has a Rician distribution where the Rician factor can be computed by

$$\kappa_{sc}=\frac{a_{sc}}{2\sigma_{sc}^2}. \quad \text{(C.4)}$$

Given that the average envelope power Ω_{sc} = 1, then the power of specular and scattered signal can be defined by

$$a_{sc}=\frac{\kappa_{sc}}{\kappa_{sc}+1}, \quad \text{(C.5)}$$

$$2\sigma_{sc}^2=\frac{1}{\kappa_{sc}+1}. \quad \text{(C.6)}$$

Moreover, the phase distribution of the random signal propagation path in ionopheric scintillation phenomena is approximately Gaussian distribution [1].

C.2 Simulation Model

For simulation, we employ the model as shown in Figure C.1 to simulate scintillation coefficients. The autocorrelation function of $n_{sc}(t)$ must be specified by [5]

$$R_{sc}(\tau)\equiv E\left[n_{sc}(t)\cdot n_{sc}^{*}(t-\tau)\right]=2\sigma_{sc}^2\cdot e^{-(\tau/\tau_0)^2}, \quad \text{(C.7)}$$

where τ_0 is the signal decorrelation time interval.

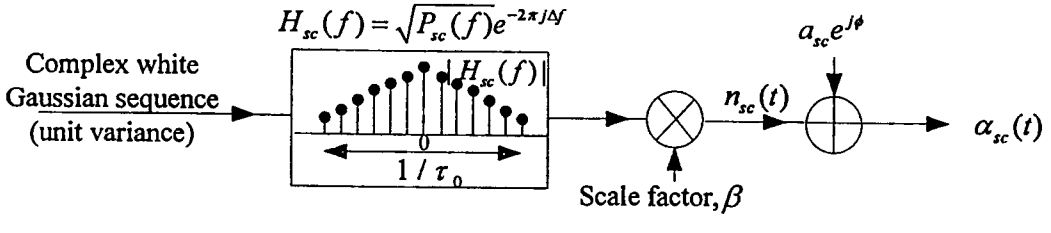

Figure C.1 Simulation model of scintillation coefficient

The power spectral density $P_{sc}(f)$ of the scintillation is used to generate the scattered component $n_{sc}(t)$ due to ionospheric scintillation effect in time or frequency domain that can be written as [1],[2],[5]

$$\begin{aligned} P_{sc}(f) = |H_{sc}(f)|^2 &= \int_{-\infty}^{\infty} R_{sc}(\tau)\cdot e^{-j2\pi f\tau} d\tau \\ &= \int_{-\infty}^{\infty} 2\sigma_{sc}^2 e^{-(\tau/\tau_0)^2}\cdot e^{-2\pi jf\tau} d\tau \\ &= 2\sigma_{sc}^2\tau_0\sqrt{\pi}\cdot e^{-(\pi\tau_0 f)^2}. \end{aligned} \tag{C.8}$$

The scale factor is a constant which chosen to yield the desired output variance $2\sigma_{sc}^2$, defined by

$$\beta = \sqrt{\frac{2\sigma_{sc}^2}{\sum_{l=0}^{2N-1}\left|H_{sc}(l)^2\right|/2N}}, \tag{C.9}$$

where N is the number of points computed.

The sample scattered component $n_{sc}(t)$ can be generated as follows [5]

$$\begin{aligned} n_{sc}(t) &= \frac{1}{2N}\beta\sum_{l=0}^{2N-1}\xi(l)H_{sc}(l)e^{2j\pi tl/2N} \\ &= \frac{1}{2N}\sqrt{\frac{2\sigma_{sc}^2}{\sum_{l=0}^{2N-1}\left|H_{sc}(l)^2\right|/2N}}\cdot\sum_{l=0}^{2N-1}\xi(l)H_{sc}(l)e^{2j\pi tl/2N}, \end{aligned} \tag{C.10}$$

where $0\le t\le N-1$, and $\xi(l)$ denotes samples of a white, unit variance complex Gaussian sequence.

The level crossing rate or fade rate is the expected number of crossings of the fade threshold level which normalized by mean-square envelope $\hat{T}$. It can be expressed in terms of the signal decorrelation time interval τ_0, Rician factor κ_{sc}, and fade threshold level $\hat{T}$, i.e., [5],[46]

$$L_R = \sqrt{2\pi(\kappa_{sc}+1)\hat{T}}\,\frac{1}{\tau_0}\exp\left(-\kappa_{sc}-(\kappa_{sc}+1)\hat{T}\right)I_0\left\{2\sqrt{\kappa_{sc}(\kappa_{sc}+1)\hat{T}}\right\}. \tag{C.11}$$

This level crossing rate is inversely proportional to the decorrelation time. Moreover, as the Rician factor increases, i.e., a larger specular component, the level crossing rate decreases exponentially for a given τ_0 in the envelope density function.

APPENDIX D

ANOTHER APPLICATIONS IN EXISTING WIRELESS SYSTEMS OVER COMBINED FADING CHANNEL

The derived MGF results of combined Rician×Rician and Nakagami-*m*×Nakagami-*m* fading channel expressions find applications in existing wireless systems such as satellite mobile communication system, mobile-to-mobile communication system, and MIMO wireless communication system. In this appendix, we propose the charactistic of mobile-to-mobile communication system and MIMO wireless communication system over combined fading channel.

D.1 Mobile-to-Mobile Communication System

The mobile-to-mobile communication system, such as the mobile ad hoc networks is distinct due to the motion of both transmitter and receiver. The narrow-band impulse response of radio channels after multiple scattering can be modeled as

$$\alpha_N = \xi_0 C + \xi_1 \alpha_0 + \xi_2 \alpha_1 \alpha_2 + \xi_3 \alpha_3 \alpha_4 \alpha_5 + ..., \tag{D.1}$$

where C is the deterministic LOS component with constant magnitude, α_is are independent identically distributed (i.i.d.) isotropic zero-mean Gaussian random variables, and the weights $\{\xi_n\}_{n=0}^{N}$ are positive real constant. Conventionally, only the first-order scattering ($\alpha_i = 0$ for all $i \geq 1$) is assumed, which the magnitude signal is Rayleigh fading (or Rician, if $|C| > 0$) and the weight parameter ξ_0 and $\xi_1 = 1$.

For NLOS double scattering, where $\xi_2 = 1$, $\alpha_i = 0$ for all $i \neq 1,2$ and $C = 0$, the magnitude signal can be defined by double Rayleigh distribution (or combined Rayleigh×Rayleigh) which is often used to model multipath fading in mobile-to-mobile communication channel.

D.2 MIMO Wireless Communication System

We use the following notations throughout this Section. A variable with a boldface type will be used to denote a matrix or vector. $N_u(m,R)$ denotes the circularly symmetric complex u-variate

Gaussian distribution with the mean m and the variance R. $\mathbf{I}_n$ denotes the $n \times n$ identity matrix. $\|\mathbf{H}\|_F^2$ is the squared Frobenius norm of matrix and $\|\mathbf{h}\|^2$ will be used to denote the squared Euclidean norm of vector h. $E\{\cdot\}$ denoting expectation is the mean-square envelope. The superscript ^{T}, *, and ^{H} will be employed to denote transpose, complex conjugate, and complex conjugate transpose, respectively. The subscript $_T$ and $_R$ will be used to denote transmit and receive array, respectively. Finally, $p(\cdot)$ denotes a PDF.

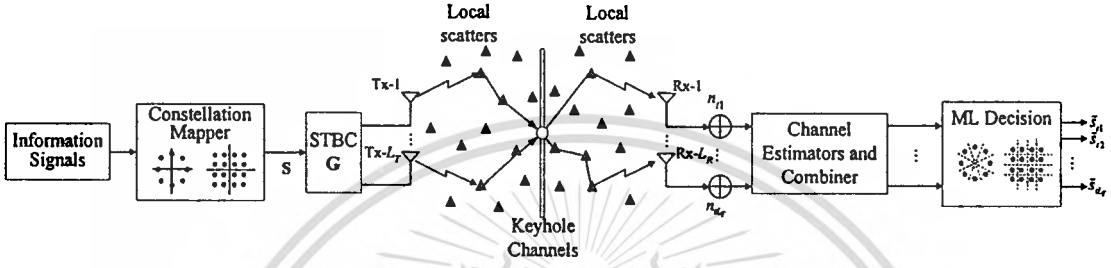

Figure D.1 Spec-time block-coded MIMO system over keyhole channels.

This Section commences by a considering the degeneracy transpired by the occurrence of the keyhole flat fading effects in a MIMO wireless communication system as shown in Figure D.1, which consists of L_T transmit and L_R receive antennas. The received signals can be given by

$$\mathbf{R} = \mathbf{ZS} + \mathbf{n}, \tag{D.2}$$

where $\mathbf{R}$ is an $L_R \times 1$ matrix representing the received signal, $\mathbf{S} = \left[s_1, s_2, ..., s_{L_T} \right]^T$ that is the L_T signals which are transmitted simultaneously through L_T transmit antennas. The $\mathbf{n}$ denotes $L_R \times 1$ noise samples which are the independent and identically distributed (i.i.d.) complex AWGN with zero mean and variance $N_0/2$ per dimension, i.e., $\mathbf{n} \sim N_{L_R}\left(0, N_0 \cdot \mathbf{I}_{L_R}\right)$. The $\mathbf{Z}$ is the $L_R \times L_T$ channel matrix for keyhole MIMO channel which is given by

$$\mathbf{Z} = \boldsymbol{\beta}\boldsymbol{\alpha}^T = \begin{bmatrix} \alpha_1\beta_1 & \alpha_2\beta_1 & \cdots & \alpha_{L_T}\beta_1 \\ \alpha_1\beta_2 & \alpha_2\beta_2 & \cdots & \alpha_{L_T}\beta_2 \\ \vdots & \vdots & \ddots & \vdots \\ \alpha_1\beta_{L_R} & \alpha_2\beta_{L_R} & \cdots & \alpha_{L_T}\beta_{L_R} \end{bmatrix}, \tag{D.3}$$

where each element of the $\{\alpha_i\}_{i=1}^{L_T}$ and $\{\beta_j\}_{j=1}^{L_R}$ are i.i.d. Rician random variable with fading severity parameters at the transmit and receive arrays, respectively. Both elements are with probability density function (PDF) given by

$$p_T(\alpha) = \frac{2\alpha^{L_T}(\kappa_T+1)}{\Omega_T}\sqrt{\frac{\kappa_T+1}{\kappa_T L_T \Omega_T}}^{L_T-1} \exp\left(-\frac{\alpha^2(\kappa_T+1)}{\Omega_T} - L_T\kappa_T\right) \cdot I_{L_T-1}\left\{2\alpha\sqrt{\frac{\kappa_T L_T(\kappa_T+1)}{\Omega_T}}\right\}, \tag{D.4}$$

$$p_R(\beta) = \frac{2\beta^{L_R}(\kappa_R+1)}{\Omega_R}\sqrt{\frac{\kappa_R+1}{\kappa_R L_R \Omega_R}}^{L_R-1} \exp\left(-\frac{\beta^2(\kappa_R+1)}{\Omega_R} - L_R\kappa_R\right) \cdot I_{L_R-1}\left\{2\beta\sqrt{\frac{\kappa_R L_R(\kappa_R+1)}{\Omega_R}}\right\}, \tag{D.5}$$

where the Rician factor κ_T and κ_R are defined as the ratio of the specular power to scattered power of transmit and receive array, respectively. $\Omega_T = E[\alpha_i^2]$, and $\Omega_R = E[\beta_j^2]$. We assume that the average envelope power in transmit and receive scatterers are equal to 1, that is, $E[|z_{i,j}|^2] = \Omega_T \cdot \Omega_R = 1$ where $|z_{i,j}|^2$ denotes the square magnitude of $z_{i,j}$. Moreover, all entries of the channel matrix **Z** are uncorrelated but rank (**Z**) = 1.

Let us consider a space-time block-coded (STBC) designed for L_T transmit antennas in keyhole MIMO channel. In general, STBC is defined by p time slots and L_T transmit antennas in $p \times L_T$ transmission matrix **G**

$$\mathbf{G} = \begin{bmatrix} g_{11} & g_{12} & \cdots & g_{1L_T} \\ g_{21} & g_{22} & \cdots & g_{2L_T} \\ \vdots & \vdots & \ddots & \vdots \\ g_{p1} & g_{p2} & \cdots & g_{pL_T} \end{bmatrix}, \tag{D.6}$$

where each element of g_{ij} in each row and each column is a signal point selected from a signal constellation with $M=2^b$ signal points. Therefore, 2^b data bits are mapped into L_T signal point in each time slot. Each element in matrix **G** is formed by complex and complex conjugates linear combinations of $s_1, s_2, \ldots, s_M$ such that the rows or columns are orthogonal with each other. The rate of STBC is defined as $R = M/p$ which the possible rate of diversity STBC is $R \leq 1$.

The received signal after STBC over p time slots can be given by

$$\mathbf{Y} = \mathbf{ZG} + \mathbf{n}, \tag{D.7}$$

where $\mathbf{Y}$ is an $L_R \times p$ vector.

It should be noted that in the STBC, the total transmission power over t-th time slot is pE_s. Moreover, the STBCs encoding and decoding can effectively transform a MIMO fading channel into the parallel SISO channels from the orthogonality property [30]:

$$\mathbf{y} = \sqrt{\frac{\|\mathbf{Z}\|_F^2}{L_T}}\mathbf{g} + \mathbf{n} = \sqrt{\frac{\|\boldsymbol{\alpha}\|^2 \|\boldsymbol{\beta}\|^2}{L_T}}\mathbf{g} + \mathbf{n}, \tag{D.8}$$

where $\mathbf{y}$ represents a m×1 received signal vector at L_R received antennas and $\mathbf{g} = [g_{t1}, g_{t2}, \ldots, g_{tL_T}]^T$. From the equivalent above, STBC channel in (D.8) shows that the spectral efficiency and becomes $R\log_2 M$ bits/s/Hz. This is because there is a bandwidth loss by a factor R and the rate loss of STBC has already been reimbursed by the energy combining gain of STBC. Consequently, the instantaneous SNR per symbol γ_{STBC} after STBC decoding is defined by

$$\gamma_{\text{STBC}} = \frac{E_s}{N_0} \cdot \frac{\|\boldsymbol{\alpha}\|^2 \|\boldsymbol{\beta}\|^2}{L_T R}. \tag{D.9}$$

After that, the received signals $\mathbf{y}$ are then passed through to the ML detector which is employed for recovering the transmitted data symbol in MIMO system. With perfect channel-state information by the ML detector that is assumed to know the channel matrix $\mathbf{H}$, the decoder then searches the closest Square Euclidean distance between the hypothesized received sequence and the actual received sequence. Thus the decoder output is

$$\tilde{\mathbf{S}} = agr \min \|\mathbf{Y} - \mathbf{ZS}\|_F^2. \tag{D.10}$$

D.2.1 PDF of keyhole Rician fading channels

From (D.3), each entry of the fading coefficient for a keyhole flat Rician fading MIMO channel is the product of two i.i.d. complex Rician random variables which has the PDF

$$p_{T,R}(\alpha,\beta) = p_T(\alpha)\cdot p_R(\beta). \tag{D.11}$$

The probability of z where $z = \alpha\times\beta$ can be found from

$$\begin{aligned} p_Z^{keyhole}(z)dz &= \iint_D p_T(\alpha)\,p_R(\beta)d\alpha d\beta \\ &= \int_{-\infty}^{\infty} p_T(\alpha)\,p_R\left(\frac{z}{\alpha}\right)\frac{dz}{\alpha}d\alpha \\ \therefore p_Z^{keyhole}(z) &= \int_{-\infty}^{\infty}\frac{1}{\alpha}p_T(\alpha)\,p_R\left(\frac{z}{\alpha}\right)d\alpha. \end{aligned} \tag{D.12}$$

Substituting (D.4)-(D.5) into (D.12) and using the series representation of the modified Bessel function in (2.24). The envelope PDF of keyhole flat Rician fading MIMO channel, $p_Z^{keyhole}(z)$, can be expressed as

$$\begin{aligned} p_Z^{keyhole}(z) &= \int_{\infty}^{\infty}\frac{1}{\alpha}p_T(\alpha)p_R\left(\frac{z}{\alpha}\right)d\alpha \\ &= 4z^{L_R}(\kappa_T+1)(\kappa_R+1)\sqrt{\frac{\kappa_T+1}{\kappa_T L_T}}^{L_T-1}\sqrt{\frac{\kappa_R+1}{\kappa_R L_R}}^{L_R-1}\exp\left(-L_T\kappa_T - L_R\kappa_R\right) \\ &\quad\cdot\sum_{l=0}^{\infty}\sum_{j=0}^{\infty}\frac{\left(\sqrt{\kappa_T L_T(\kappa_T+1)}\right)^{L_T-1+2l}\left(z\sqrt{\kappa_R L_R(\kappa_R+1)}\right)^{L_R-1+2j}}{i!\,j!\,\Gamma(L_T+i)\Gamma(L_R+j)} \\ &\quad\cdot\int_{\infty}^{\infty}\alpha^{2L_T-2L_R+2l-2j-1}\exp\left(-\alpha^2(\kappa_T+1)-\frac{z^2(\kappa_R+1)}{\alpha^2}\right)d\alpha. \end{aligned} \tag{D.13}$$

Using the relation (2.26), the envelope PDF of keyhole Rician fading channel, $p_Z^{keyhole}(z)$, can be written as

$$p_Z^{keyhole}(z)=\frac{4}{z}\left(\sqrt{z^2(\kappa_T+1)(\kappa_R+1)}\right)^{L_T+L_R}\exp(-L_T\kappa_T-L_R\kappa_R)$$
$$\cdot\sum_{i=0}^{\infty}\sum_{j=0}^{\infty}\frac{(L_T\kappa_T)^i(L_R\kappa_R)^j\left(\sqrt{z^2(\kappa_T+1)(\kappa_R+1)}\right)^{i+j}}{i!j!\Gamma(L_T+i)\Gamma(L_R+j)} \quad \text{(D.14)}$$
$$\cdot K_{L_T-L_R+i-j}\left\{2\sqrt{z^2(\kappa_T+1)(\kappa_R+1)}\right\}.$$

To obtain the PDF of instantaneous SNR $p_\Gamma^{keyhole}(\gamma)$, where we determine the density of $\gamma=z^2$ thus the envelope PDF with change-of-variable as shown in (2.35) and (2.36) are used to obtain

$$p_\Gamma^{keyhole}(\gamma)=\frac{1}{\frac{d}{dz}z^2}\left[p_Z^{keyhole}(z)+p_Z^{keyhole}(-z)\right]$$
$$=\frac{1}{2\sqrt{\gamma}}\left[p_Z^{keyhole}\left(\sqrt{\gamma}\right)+p_Z^{keyhole}\left(-\sqrt{\gamma}\right)\right]. \quad \text{(D.15)}$$

However, every possible z is non-negative, hence,

$$p_\Gamma^{keyhole}(\gamma)=\frac{p_Z^{keyhole}\left(\sqrt{\gamma}\right)}{2\sqrt{\gamma}}, \quad \text{(D.16)}$$

and the instantaneous SNR of the square Frobenius norm of the channel matrix is

$$\Gamma=\|\mathbf{Z}\|_F^2=\|\boldsymbol{\alpha}\|^2\|\boldsymbol{\beta}\|^2=\sum_{j=1}^{L_R}\sum_{i=1}^{L_T}\alpha_i^2\beta_j^2=\sum_{i=1}^{L_T}\alpha_i^2\cdot\sum_{j=1}^{L_R}\beta_j^2=A\cdot B. \quad \text{(D.17)}$$

where $A=\sum_{i=1}^{L_T}\alpha_i^2$ and $B=\sum_{j=1}^{L_R}\beta_i^2$.

Consequently, the PDF of instantaneous SNR can be computed by substituting (D.14) into (D.15) to produce

$$p_\Gamma^{keyhole}(\gamma)=\frac{2}{\gamma}\left(\sqrt{\gamma(\kappa_T+1)(\kappa_R+1)}\right)^{L_T+L_R}\exp(-L_T\kappa_T-L_R\kappa_R)$$
$$\cdot\sum_{i=0}^{\infty}\sum_{j=0}^{\infty}\frac{(L_T\kappa_T)^i(L_R\kappa_R)^j\left(\sqrt{\gamma(\kappa_T+1)(\kappa_R+1)}\right)^{i+j}}{i!j!\Gamma(L_T+i)\Gamma(L_R+j)} \quad \text{(D.18)}$$
$$\cdot K_{L_T-L_R+i-j}\left\{2\sqrt{\gamma(\kappa_T+1)(\kappa_R+1)}\right\}.$$

D.2.2 MGF of keyhole Rician fading channels

In this subsection, we derive the MGF of instantaneous SNR per symbol of keyhole flat Rician fading MIMO channel where this MGF $\Phi_{\gamma}^{keyhole}(-s)$ is defined from the keyhole fading $p_{\Gamma}^{keyhole}(\gamma)$ as following

$$\Phi_{\gamma}^{keyhole}(-s)=\int_{0}^{\infty}\exp(-s\gamma)\,p_{\Gamma}^{keyhole}(\gamma)\,d\gamma, \tag{D.19}$$

where s is a complex variable. Replacing the PDF $p_{\Gamma}^{keyhole}(\gamma)$ in (D.18) into (D.19), then using the relation (3.3), (3.5) and (3.8). A final result of the MGF can consequently be expressed in terms of a generalized hypergeometric function ${}_2F_0(a,b;;z)$ as

$$\begin{aligned}\Phi_{\gamma}^{keyhole}(-s)&=\exp\left(-L_T\kappa_T-L_R\kappa_R\right)\\&\cdot\sum_{i=0}^{\infty}\sum_{j=0}^{\infty}\frac{\left(L_T\kappa_T\right)^i\left(L_R\kappa_R\right)^j}{i!\,j!}\,{}_2F_0\left(L_T+i,L_R+j;;-\frac{s}{\left(\kappa_T+1\right)\left(\kappa_R+1\right)}\right).\end{aligned} \tag{D.20}$$

From the STBC decoding condition in (D.10), the MGF of γ_{STBC} of keyhole MIMO Rician fading channel can be readily written as

$$\begin{aligned}\Phi_{\gamma_{\text{STBC}}}^{keyhole}(-s)&=\Phi_{\gamma}^{keyhole}\left(-s\frac{\frac{E_s}{N_0}}{L_TR}\right)\\&=\exp\left(-L_T\kappa_T-L_R\kappa_R\right)\sum_{i=0}^{\infty}\sum_{j=0}^{\infty}\frac{\left(L_T\kappa_T\right)^i\left(L_R\kappa_R\right)^j}{i!\,j!}\\&\cdot{}_2F_0\left(L_T+i,L_R+j;;-\frac{s\frac{E_s}{N_0}}{\left(\kappa_T+1\right)\left(\kappa_R+1\right)L_TR}\right).\end{aligned} \tag{D.21}$$

In the limit when either Rician factor goes to zero, the MGF reduces to a single sum, e.g., when κ_R becomes 0

$$\Phi_{\gamma_{\text{STBC}}}^{keyhole}(-s)=\exp\left(-L_T\kappa_T\right)\sum_{i=0}^{\infty}\frac{\left(L_T\kappa_T\right)^i}{i!}\,{}_2F_0\left(L_T+i,L_R;;-\frac{s\frac{E_s}{N_0}}{\left(\kappa_T+1\right)L_TR}\right). \tag{D.22}$$

In the limit when both Rician factors become zero, the MGF reduces to

$$\Phi_{\gamma_{STBC}}^{keyhole}(-s) = {}_2F_0\left(L_T, L_R; ; -\frac{s\frac{E_s}{N_0}}{L_T R}\right). \tag{D.23}$$

D.2.3 Performance analysis

The average SEP, $P_s(E)$, can be obtained by averaging the conditional SEP given the instantaneous SNR per bit in (3.60). Throughout this paper, we define the conditional SEP for some common modulation schemes depending on the parameter a and g as (3.61). Substituting the MGF $\Phi_{\gamma_{STBC}}^{keyhole}(-s)$ in (D.21) into (3.60), the average SEP becomes

$$P_s(E) = \frac{a}{\pi}\exp\left(-L_T\kappa_T - L_R\kappa_R\right)\sum_{i=0}^{\infty}\sum_{j=0}^{\infty}\frac{\left(L_T\kappa_T\right)^i\left(L_R\kappa_R\right)^j}{i!j!} \cdot \int_0^{\pi/2} {}_2F_0\left(L_T+i, L_R+j; ; -\frac{s\frac{E_s}{N_0}}{\left(\kappa_T+1\right)\left(\kappa_R+1\right)L_T R}\right)d\theta, \tag{D.24}$$

where s is defined by $g/\sin^2\theta$.

In the limit when either Rician factor goes to zero, the average SEP becomes

$$P_s(E) = \frac{a}{\pi}\exp\left(-L_T\kappa_T\right)\sum_{l=0}^{\infty}\frac{\left(L_T\kappa_T\right)^l}{l!}\int_0^{\pi/2} {}_2F_0\left(L_T+i, L_R; ; -\frac{s\frac{E_s}{N_0}}{\left(\kappa_T+1\right)L_T R}\right)d\theta. \tag{D.25}$$

In the limit when both Rician factors become zero, the average SEP becomes

$$P_s(E) = \frac{a}{\pi}\int_0^{\pi/2} {}_2F_0\left(L_T, L_R; ; -\frac{s\frac{E_s}{N_0}}{L_T R}\right)d\theta. \tag{D.26}$$

The resulting average SEP equations can therefore be expressed in a compact form and is a function of Rician factor (κ_T and κ_R), L_T transmit, and L_R receive antennas.

D.2.4 Numerical Results and Discussions

In this Subsection, some PDFs of the output SNR of MIMO keyhole channels are illustrated from the derived results in Subsection D.2.1. Moreover, some theoretical and simulation results of the average SEP for some modulation types over keyhole flat Rician fading MIMO channel

with STBC decoding are presented. The performance from theoretical results is numerically computed from the corresponding expression derived in Subsection D.2.3.

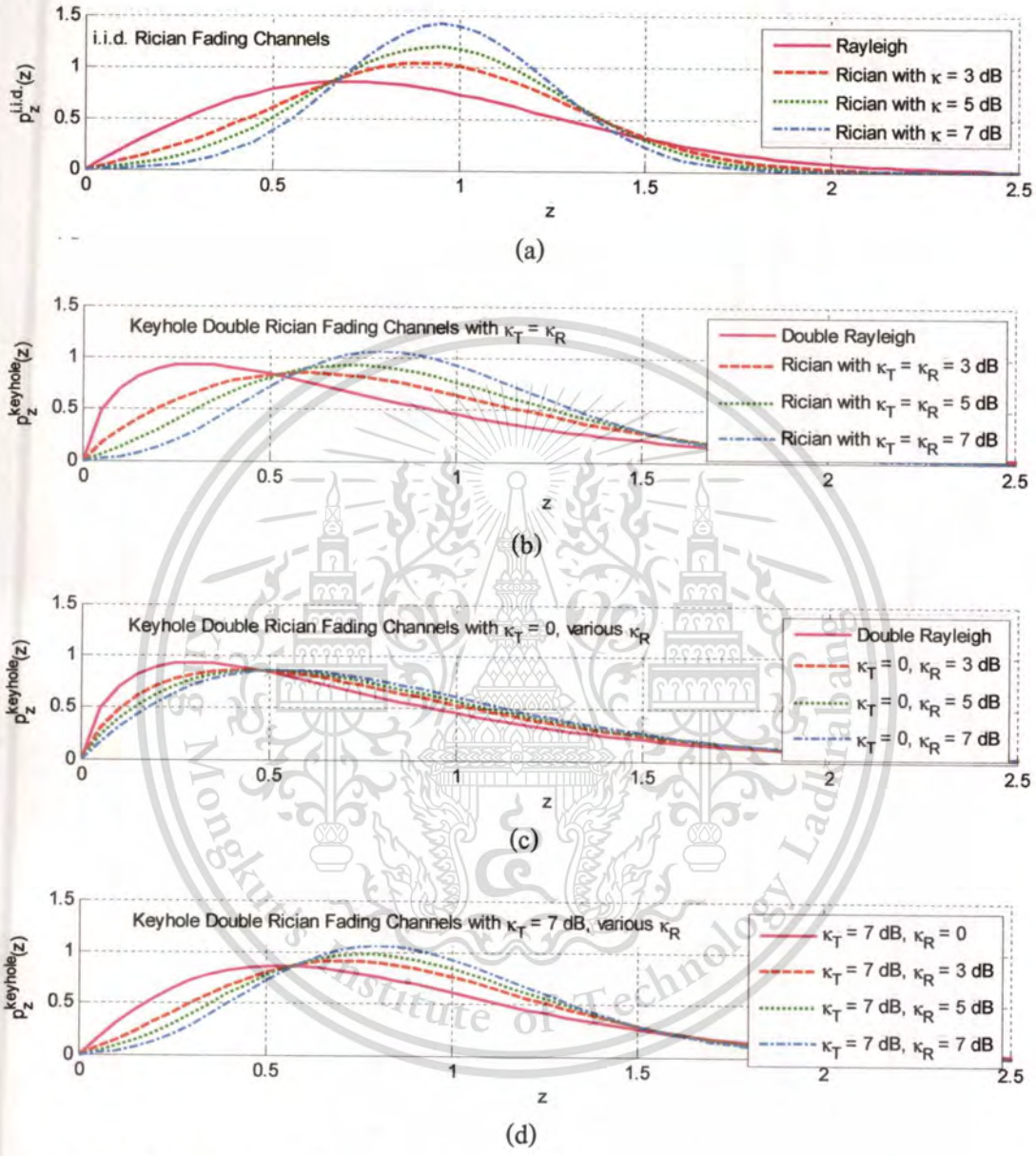

Figure D.2 Probability density functions (PDF) of i.i.d. and keyhole flat Rician fading channels with various Rician factor κ_T and κ_R.

Figure D.2 (a)-(d) shows the PDFs of the output SNR of MIMO keyhole channels with various Rician factor from (D.14). As seen from this Figure, in i.i.d Rician fading channel, the distribution in each case of Rician factor κ have a large difference. While the distribution differences of keyhole double Rician fading channel are less than that i.i.d. Rician fading channel.

Moreover, we can see the part of z less than 1 in keyhole double Rician fading channel are more than the the part of z less than 1 in i.i.d. Rician fading channel. This means the keyhole double Rician fading channel have severe fade signal more than i.i.d. Rician fading channel.

In Figure D.3, we illustrated the average SEP versus the average SNR per antenna defined by SNR = E_s/N_0, where E_s is the average power of each antenna transmitted symbol, and $\sigma^2 = N_0/2$ is the noise variance for the one-rate STBC $\mathbf{G}_2$ (Alamouti code) with 8-PSK modulation. The average SEP for STBC $\mathbf{G}_2$ with 8-PSK over i.i.d. Rician in comparison with the results in keyhole double Rician fading channels for various values of Rician factor (κ_T and κ_R) by using two transmit and two receive antennas are shown in this figure. The numerically results are agreed exactly with the results from the simulation. As we can see from this figure, the error performance results in keyhole Rician fading are worse than the error performance of i.i.d. Rician, particularly in channels with the severance of fading, i.e., small values of the Rician factor.

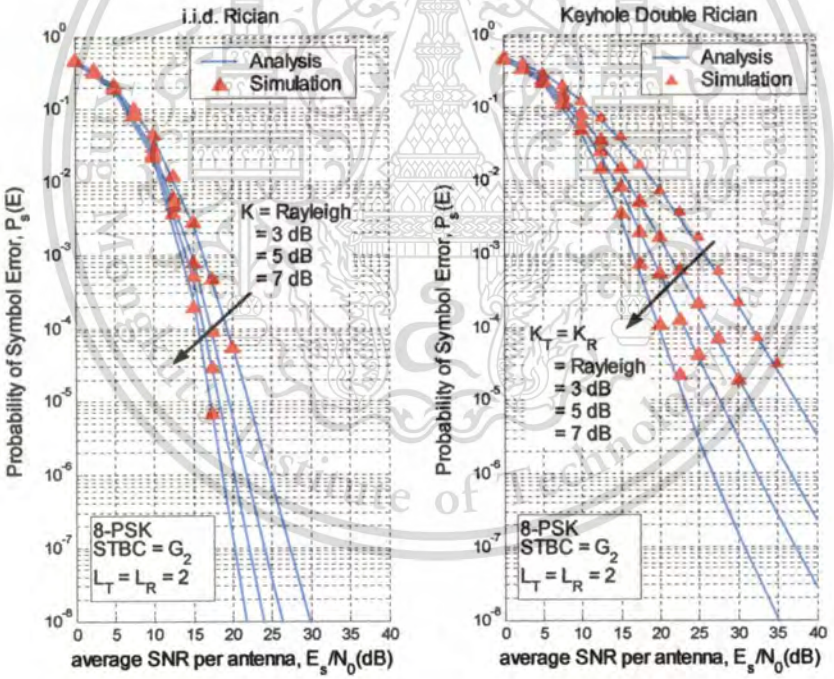

Figure D.3 The average SEP versus average SNR per antenna for the STBC $\mathbf{G}_2$ with 8-PSK over i.i.d. and keyhole flat Rician fading channels with various Rician factor $\kappa_T = \kappa_R = 0$(Rayleigh), 3, 5, 7 dB and $L_T = L_R = 2$.

AUTHOR BIOGRAPHY

Author : Miss Wannaree Wongtrairat

Date of Birth : March 19, 1979

Bechelor Degree : Bachelor of Engineering Program in Telecommunications Engineering

Institute : Department of Telecommunications Engineering

Faculty of Engineering

King Mongkut's Institute of Technology Ladkrabang (KMITL)

Year of Graduation : 2001

Master Degree : Master of Engineering Program in Telecommunications Engineering

Institute : Department of Telecommunications Engineering

Faculty of Engineering

King Mongkut's Institute of Technology Ladkrabang (KMITL)

Year of Graduation : 2004

Interested Researches : Effect of ionospheric scintillation, Mobile satellite communication, Wireless communication system

Related Publication

[1] Pornchai Supnithi, Wannaree Wongtrairat, and Sawasd Tantaratana, "Performance of *M*-PSK in Mobile Satellite Communication over Combined Ionospheric Scintillation and Flat Fading Channels with MRC Diversity." **IEEE Trans. Wireless Commun.**, *Accepted Feb. 15, 2009.*

[2] Wannaree WONGTRAIRAT, Pornchai SUPNITHI, "Performance of Digital Modulation in Double Nakagami-*m* Fading Channels with MRC Diversity." **IEICE Trans. Commun.**, Vol. E92-B, No. 2, Feb. 2009, pp. 559-566.

[3] Wannaree Wongtrairat, Pornchai Supnithi, and Sawasd Tantaratana, "Performance of *M*-PSK modulation in double Rician fading channels with MRC diversity." **Proc. 2008 Electrical Engineering/Electronics, Computer, Telecommunications and Information Technology (ECTI) International Conference (ECTI-CON 2008)** [CD-ROM], Krabi, Thailand. Vol. 1, 14-17 May 2008, pp. I-321 to I-324.

[4] W. Wongtrairat and P. Supnithi, "Performance of Digital Modulation in Double Nakagami Fading Channels with MRC Diversity." **International Workshop on Smart Info-Media Systems in Bangkok (SISB 2007)**, Bangkok, Thailand, 1-2 Nov. 2007.

[5] W. Wongtrairat, P. Supnithi, "Average Probability of Bit Error of MPSK in Combined Flat Ionospheric Scintillation and Flat Fading Channels." **2006 IEEE Region 10 Conference (TENCON 2006)**, Hong Kong, 14-17 Nov. 2006, pp. 1-4.

[6] W. Wongtrairat, P. Supnithi, and etc., "Performance of MPSK in Satellite Mobile Channels with Combined Ionospheric Scintillation and Flat Fading Channels." **10th International Conference on Ionospheric Radio System and Techniques (IRST 2006)**, London, UK, 18-21 July 2006, pp. 217-221.

[7] W. Wongtrairat, P. Supnithi, "Wavelet-based MC-CDMA Communication System under Scintillation Channels." **IASTED International Conference on Networks and Communication Systems (NCS 2005)**, Krabi, Thailand, 18-20 Apr. 2005, pp. 335-340.

[8] W. Wongtrairat, P. Supnithi, "Statistical Modeling of Ionospheric Scintillation for System Modeling." **International Symposium on Earth's Atmosphere (ISEA 2004)**, Chiang Mai, Thailand, 16-17 Dec. 2004, pp 16.